High-temperature superconductivity with *d*-wave symmetry of the order parameter (Review Article)

G. G. Sergeeva, Yu. P. Stepanovskiĭ, and A. V. Chechkin

National Science Center Kharkov Physicotechnical Institute, 310108 Kharkov, Ukraine
(Submitted June 17, 1998; revised July 15, 1998)
Fiz. Nizk. Temp. **24**, 1029–1042 (November 1998)

It has been established as a result of successful direct experimental studies of the symmetry of the superconducting order parameter that the pairing symmetry in the compounds YBCO, GdBCO, Tl2201, and Bi2212 is of the *d*-wave type. In this paper, experimental and theoretical results concerning the *d*-wave superconducting state and the peculiarities of magnetic properties of the *d*-type superconductor such as pseudogap, charge ordering, and unusual structure of vortex excitations differing from that for *s*-states are analyzed. Several mechanisms of *d*-pairing and related microscopic theories are discussed and possible experiments for their verification are proposed. © *1998 American Institute of Physics.* [S1063-777X(98)00111-X]

1. INTRODUCTION

In spite of the fact that the experimental results obtained for low-temperature superconductors with the *s*-wave pairing (*s*-type HTSC) are in accord with the BCS theory, some facts such as the Knight shift in NMR for Hg, Sn, and Va (see Ref. 1 and the literature cited therein) contradict this theory and are of considerable interest. Starting from 1960, these facts stimulated a large number of investigations[1–6] (see also the review by Suhl[7]) devoted to a peculiar (other than *s*-wave) symmetry of the superconducting (or superfluid[8]) order parameters and nonphonon pairing mechanisms. It was predicted that *p*-pairing of electrons with the orbital angular momentum $l=1$ may be associated with peculiarities such as vanishing of the gap $\Delta(k)$ for certain values of the wave vector $\mathbf{k}$ and a nonexponential temperature dependence of heat capacity.[4,8] Balian and Werthamer[1] noted that, in the case of *d*- ($l=2$) and *p*-pairing, magnetic impurities suppress the superconducting transition temperature T_c approximately to the same extent as in the case of *s*-type HTSC, but the same concentration of nonmagnetic impurities must reduce the value of T_c much more strongly. These results are in contradiction both with the BCS theory and with the available experimental data.

The interest in the existence of a state with a peculiar symmetry of the superconducting order parameter (SOP) increased after the discovery of superconductivity in compounds with heavy fermions.[9] A number of important publications[10–12] were devoted to an analysis of possible types of SOP symmetry depending on the symmetry of the crystal lattice. This made it possible to obtain generalized Ginzburg–Landau equations in the mean-field approximation near T_c, irrespective of the microscopic mechanism of superconductivity. Numerical calculations of the Hubbard model[13] based on the Monte Carlo method revealed the possibility of pairing of electrons with an even orbital angular momentum without a suppression of pairing by repulsion at short distances.[14] The conclusion concerning the possibility of *d*-pairing in compounds with heavy fermions was drawn by Miyake *et al.*[15] who, like Privorotski,[5] proved that exchange by fluctuational antiferromagnetic (AFM) excitations suppresses *s*-type HTSC.

The discovery of HTSC (1986) with a phase diagram with a large number of different states led to various hypotheses on pairing mechanisms and SOP symmetry. It became clear by 1990 following the observation of the Shapiro steps[16] and magnetic flux quantum Φ_0 in the study of the vortex lattice of Y-based superconductors[17] that superconductivity is associated with pairing of electrons. The results of measurements of the temperature dependence of the Knight shift[18,19] indicate a singlet state of paired electrons with even orbital angular momenta, i.e., *s*- or *d*-wave symmetry of the SOP. The knowledge of the symmetry is essential for the development of the microscopic theory of HTSC as well as for applications of these materials in electronics and technology. This is due to the fact that the presence of excitations with zero energy in a system with *d*-pairing leads to a power temperature dependence of various physical quantities and to a considerable effect of impurities on the behavior of the superconductor. For example, the surface impedance acquires a finite value which sets a limit on the *q*-factor of microwave loops with HTSC.

Such ''anomalous'' properties of HTSC (e.g., temperature dependences of the longitudinal and transverse nuclear relaxation time,[20–22] heat capacity,[23] and magnetic field penetration depth[24]) were first indirect experimental evidences of a peculiar SOP symmetry. The following two circumstances played a decisive role in determining the SOP symmetry. The first is associated with a number of theoretical publications[25,26] in which the possibility of existence of high-temperature superconductivity with *d*-pairing (*d*-type HTSC) was proved and with the methods of direct determination of the SOP symmetry, which were proposed in 1992.[27] The second circumstance is that such measurements were made successfully in 1993–1996.[28–35] This led to a consensus on the *d*-wave symmetry of SOP for the compounds $Tl_2Ba_2CuO_{6+x}$(Tl2201), $GdBa_2Cu_3O_{7-x}$(GdBCO),

$Bi_2Sr_2CaCu_2O_{8+x}$(Bi2212), $YBa_2Cu_3O_{7-x}$(YBCO). which was reached on the 5th International Conference on HTSC Mechanisms and Materials in 1997.[36]

This problem was discussed in a number of brilliant reviews,[37–42] but the present review has at least one advantage: we do not have to convince the reader that superconductivity with *d*-pairing does exist. Our aim is to show how this was done and to consider the most crucial question at present concerning the consequences of this phenomenon, since the properties of *d*-type HTSC differ considerably from those of *s*-type HTSC. The structure of the review is as follows. Without aiming at a complete discussion and citation of the results of theoretical and experimental publications in the field of pairing symmetry in HTSC, we consider in Secs. 2 and 3 of this review only those results which are essential for understanding *d*-pairing (in our opinion). Section 4 is devoted to a brief analysis of peculiarities in magnetic properties of *d*-type HTSC, such as strong AFM fluctuations, phase separation, and unusual properties of the vortex state. Some mechanisms of pairing and related microscopic theories are discussed in Conclusion.

2. PHENOMENOLOGICAL THEORY OF *D*-TYPE SUPERCONDUCTORS

The possibility of existence of superconductivity with *d*-pairing was demonstrated in Refs. 13–15 and 25: the exchange of fluctuational AFM excitations in the Hubbard model leads to pairing of electrons with even orbital angular momentum $l=2$ in the *d*-channel with the $d_{x^2-y^2}$ component. However, this mechanism did not attract special attention of the researchers at that time since it did not explain the high values of T_c. A more comprehensive approach developed later in the phenomenological and self-consistent models[26] using parameters from NMR measurements[22] proved that this pairing mechanism leads to the $d_{x^2-y^2}$ symmetry of the SOP with the coupling constant sufficient for high values of T_c. Van Harlingen, who was one of the authors of the first direct experimental evidence of the $d_{x^2-y^2}$ symmetry,[28] wrote: ''From an experimental viewpoint, the prediction of the $d_{x^2-y^2}$ symmetry was a significant step, since it put on the table a testable hypothesis that has motivated a tremendous wave of experiments designed to determine the pairing symmetry.'' [40] These experiments are based on the dependence of the tunnel current sensitivity in a Josephson junction on the phase of the wave function for a Cooper pair, which depends on the direction of the vector **k** in the case of *d*-wave SOP. The generalized Ginzburg–Landau theory that makes the classification of symmetries of superconducting states possible, has played a decisive role in determining the SOP symmetry.

2.1. Generalized Ginzburg–Landau equations

The generalized Ginzburg–Landau theory in the mean-field approximation for a superconductor near T_c is based on general symmetry properties[10–12] and does not depend on the microscopic superconductivity mechanism (see reviews in Refs. 37, 43 and 44). The Ginzburg–Landau functional near T_c is an expansion of the free energy F in even powers of the SOP and must remain scalar under transformations with a complete symmetry group. If the spin–orbit coupling is taken into account in the case of *d*-type HTSC, one-particle states are no longer eigenstates of spinor operators. The inclusion of spin–orbit coupling in the adiabatic approximation allows us to go over to a pseudospin representation with formally identical transformations, whose application is justified when separate transformations of the spin and orbital space are not required.

The complete symmetry group for an idealized tetragonal lattice consists of the crystallographic group D_{4h}, the time inversion group K, and the gradient-invariant group $U(1)$. In subsequent analysis, in this section we shall use the tables from the review by Sigrist and Ueda.[37] The D_{4h} group has ten irreducible representations five of which $\Gamma_1^+,\Gamma_2^+,\Gamma_3^+,\Gamma_4^+,\Gamma_5^+$ correspond to even basis functions. In the general case, the gap $\Delta(\mathbf{k},\mathbf{r})$ (whose symmetry coincides with the symmetry of the paired wave function) for nondegenerate singlet *s*- and *d*-wave states with corresponding irreducible representations Γ_1^+ and Γ_3^+ is a function of the wave vector **k** and the coordinate **r** of the center of mass of the paired electron state:

$$\Delta(\mathbf{k},\mathbf{r})=\eta_{s-i}(\mathbf{r},\Gamma_1^+)\Delta_{s-i}(\Gamma_1^+,\mathbf{k})+\eta_{s-ex}(\mathbf{r},\Gamma_1^+)\times\Delta_{s-ex}(\Gamma_1^+,\mathbf{k})+\eta_d(\mathbf{r},\Gamma_3^+)\Delta(\Gamma_3^+,\mathbf{k}), \quad (1)$$

where η_{s-i} and η_{s-ex} are complex SOP of the *s*-wave isotropic and extended states, respectively, η_d is the SOP of the *d*-wave state, and $\Delta_{s-i}(\Gamma_1^+,\mathbf{k})$, $\Delta_{s-ex}(\Gamma_1^+,\mathbf{k})$, $\Delta(\Gamma_3^+,\mathbf{k})$ are the basis functions of the representations Γ_1^+ and Γ_3^+:

$$\Delta_{s-i}(\Gamma_1^+,\mathbf{k})=1;$$

$$\Delta_{s-ex}(\Gamma_1^+,\mathbf{k})=\Delta_s(k_x^2+k_y^2);\quad \Delta_s=\Delta_{s-ex}(\Gamma_1^+,0);$$

$$\Delta(\Gamma_3^+,\mathbf{k})=\Delta_d(k_x^2-k_y^2);\quad \Delta_d=\Delta(\Gamma_3^+,0).$$

The simultaneous inclusion of *s*- and *d*-wave states is necessary if their superconducting transition temperatures are close,[37] while for heterogeneous superconductors with structural or topological defects this is associated with the dependence of the SOP on **r**.[45] The general form of the expression for free energy in a magnetic field **H** taking into account the coupling between η_d and η_s (which is equal to η_{s-i} or η_{s-ex}) is

$$F(\eta_s,\eta_d)=F_s(\eta_s)+F_d(\eta_d)+F_{sd}(\eta_s,\eta_d)+\frac{1}{8\pi}|\mathbf{h}|^2, \quad (2)$$

where all the terms must satisfy the conditions of invariance under transformations with the complete symmetry group

$$F_s(\eta_s)=\alpha_s|\eta_s|^2+\beta_s|\eta_s|^4+K_{s1}(|D_x\eta_s|^2+|D_y\eta_s|^2)+K_{s2}|D_z\eta_s|^2; \quad (3)$$

$$F_d(\eta_d)=\alpha_d|\eta_d|^2+\beta_d|\eta_d|^4+K_{d1}(|D_x\eta_d|^2+|D_y\eta_d|^2)+K_{d2}|D_z\eta_d|^2; \quad (4)$$

$$F_{sd}(\eta_s,\eta_d)=\beta_{sd}|\eta_s|^2|\eta_d|^2+\beta_4(\eta_s^{*2}\eta_d^2+\eta_s^2\eta_d^{*2})+K_{sd}\times[(D_x\eta_s)^*(D_x\eta_d)-(D_y\eta_s)^*(D_y\eta_d)+\text{c.c.}]. \quad (5)$$

Here $D_i=\partial/\partial x_i-2ieA_i/c$; $\mathbf{h}=\nabla\times\mathbf{A}$, $\mathbf{A}$ is the vector potential. The necessity for taking into account the last term in (5), viz., mixed gradient terms, was noted by Joynt[46] and was confirmed by the microscopic derivation of generalized Ginzburg–Landau equations with the effective two-particle interaction potential.[47] It will be proved below (see Sec. 4.2) that the effect of induction of the s-wave state in a heterogeneous d-type HTSC is associated with these terms which are linear in η_s.

It should be noted that Eq. (2) for d-type HTSC must be supplemented with the term taking into account the interaction of uniform strains with η_d, which leads to spontaneous anisotropic deformation of the crystal lattice with $\sim|\eta_d|^2 \sim|T-T_c|$[37] which is equal to zero in the case of s-pairing.

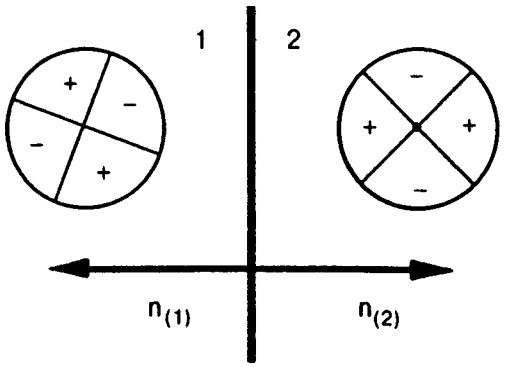

FIG. 1. Josephson π junction between two d-type HTSC (the orientation of the crystal lattice and the sign of $\Delta_d(k)$ on both sides of the junction are shown in the circles) (from Ref. 41).

2.2. Josephson effect in *d*-type HTSC

Electrons moving at right angles to the surface of a Josephson junction make the main contribution to the current, and the tunneling is sensitive to the orientation relative to the surface of the junction and to the direction of crystallographic axes on both sides of the junction. In the Ginzburg–Landau theory, the free energy of the surface of a junction with SOP η_1 and η_2 on both sides of the junction is given by[37,41]

$$F_{12}=t_0\int dS\chi_1(\mathbf{n}_1)\chi_2(\mathbf{n}_2)[\eta_1^*\eta_2+\eta_1\eta_2^*], \tag{6}$$

where t_0 is the magnitude of coupling and $\mathbf{n}_i$ the vector perpendicular to the surface on the ith side of the junction whose symmetry function $\chi_i(\mathbf{n}_i)$ coincides with the symmetry of the SOP η_i. The variation of the total free energy $F=F_d+F_{12}$ in η_1 and η_2 leads to the boundary conditions at the surface:

$$[K_{d1}(n_{1x}D_x+n_{1xy}D_y)+K_{d2}n_{1z}D_z]\eta_1 = -t_0\chi_1(\mathbf{n}_1)\chi_2(\mathbf{n}_2)\eta_2. \tag{7}$$

The second equation can be obtained by the transposition of the indices ''1'' and ''2.'' The current density J perpendicular to the surface can be determined from the condition

$$\mathbf{n}\times\mathbf{J}=c\mathbf{n}\times\frac{\partial F}{\partial\mathbf{A}} \tag{8}$$

and has the form

$$J=\frac{4\pi ct_0}{\Phi_0}\chi_1(\mathbf{n}_1)\chi_2(\mathbf{n}_2)|\eta_1||\eta_2|\sin(\varphi_1-\sigma_2). \tag{9}$$

Here φ_i is the phase of the ith SOP. The Josephson current is a function of the phase of the paired wave function and can have any sign depending on the direction of $\mathbf{n}$ if at least one of the superconductors has the $d_{x^2-y^2}$-symmetry of the SOP (Fig. 1). A negative critical current is equivalent to a phase shift by π in the junction and leads to spontaneous current generating the magnetic flux $\Phi_0/2$ in zero magnetic field.

Silver and Zimmerman[48] who observed for the first time the flux $\Phi_0/2$ in a Josephson junction in 1967 proposed a hypothesis on scattering on a magnetic impurity, which was substantiated theoretically by Bulaevskii *et al.*[49] The assumption concerning the relation of the flux $\Phi_0/2$-vortices with zeros of the superfluid order parameter was put forth for the first time by Volovik and Mineev.[50] Later, attempts were made to study the Josephson effect in compounds with heavy fermions both experimentally[51] and theoretically.[52] Geshkenbein *et al.*[52] were the first to note that tunnel current vanishes when the normal to the surface is oriented along the direction in which the gap in the excitation spectrum vanishes. Sigrist and Rice[27] suggested in 1992 that the sensitivity of the Josephson effect to the phase jump in the SOP be used for testing the $d_{x^2-y^2}$-symmetry in HTSC.

3. EXPERIMENTAL EVIDENCE OF THE $D_{X^2-Y^2}$-PAIRING

Even in first publications on peculiar superconductivity[4,6,8,10,11] it was proved that, in the presence of zeros in the gap, the excitation spectrum starts with zero energy, and various physical quantities must have power temperature dependences. The zero line in the gap of d-type HTSC leads to power temperature dependences of heat capacity (which were predicted by Volovik and Gor'kov[11] and measured by Hardy *et al.*[24]) and of magnetic field penetration depth.[23,53] Figure 2 shows the results of calculations and measurements of temperature dependences of ''transverse'' [20,54] and ''longitudinal'' nuclear relaxation rates.[18,55] These and other ''indirect'' measurements (tunneling of quasiparticles and photoemission spectroscopy[56]) in 1993 established reliably the gap anisotropy which could be interpreted from the viewpoint of the d- and s-symmetry of SOP: the measurements of the modulus $|\Delta(\mathbf{k})|$, its anisotropy, and even the presence of zeros do not allow to distinguish the $d_{x^2-y^2}$-symmetry from the s-symmetry of SOP, which takes into account anisotropy and orthorhombic crystal lattice distortions of HTSC.[57] The dependences $\Delta_d(\mathbf{k})$, $\Delta_{\text{anis}}(\mathbf{k})$ and $\Delta_{\text{gen}}(\mathbf{k})$ presented in Fig. 3 show that only the measurements of phase anisotropy of the gap make it possible to determine the symmetry of pairing.

Direct observations of the d-wave SOP were carried out in three modifications of experiments with Josephson junctions. In experiments of the first type, the phase shift by π was determined by using interference effects,[28,58] while in experiments of the second type the modulation of critical current by magnetic field was used.[31,32] A significant disad-

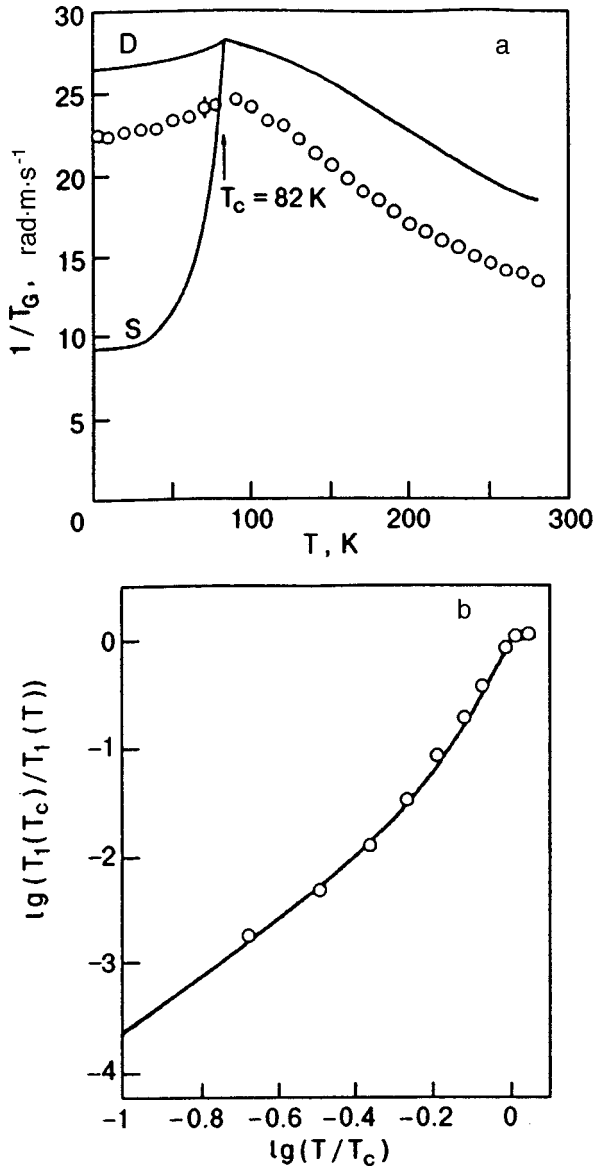

FIG. 2. Temperature dependence of the reciprocal time T_G of transverse (*a*) and T_1 of longitudinal (*b*) relaxation for the ^{63}Cu nucleus for YBCO. The solid curves are the results of calculations (*D* for *d*- and *S* for *s*-symmetries of SOP. Circles correspond to the results of measurements (from Refs. 18, 54, 55).

vantage of these two methods was the high quality of single crystals required for measurements. The third technique based on three-crystal magnetometry of rings made of superconducting epitaxial films makes it possible to observe the effect of quantization of magnetic flux with $\Phi_0/2$ in measurements with YBCO, GdBCO, Tl2201, and Bi2212 films.[29,30,36]

First observations of the phase shift by π were made at temperatures 2–4 K on superconducting quantum interference devices (SQUID) consisting of two Josephson junctions (YBCO single crystal–gold barrier–thin Pb film).[28] Figure 4 shows the arrangement of junctions in the angular and planar configurations. The phase shift and the magnetic flux quantum $\Phi_0/2$ were observed in the angular configuration in which Josephson junctions lie in two orthogonal planes *ac* and *bc* and form a bimetallic ring. Figure 5a illustrates the modulation of critical current by a magnetic field for SQUIDs with single crystals of *s*-type low-temperature and *d*-type high-temperature superconductors. It can be seen that in contrast to *d*-type HTSC, the angular configuration for *s*-type LTSC for $H=0$ displays a single unsplit peak. A comparison of the dependence $J_c(\Phi/\Phi_0)$ for circulation current (Fig. 5b) shows that $J_c=0$ for integral values of Φ/Φ_0 for *s*-type LTSC and for half-integral values of this ratio for *d*-type HTSC. Figure 6 shows the results of measurements of critical current as a function of magnetic field for a YBCO single crystal:[31] a split peak typical of *d*-type HTSC is observed in the angular configuration. Similar measurements for a planar configuration of junctions reveal the absence of a phase shift, and a single unsplit peak is observed in zero field. The important remark made by Klemm[59] that the angular configuration can lead to a current singularity or to trapped magnetic moment was analyzed by Wollmann *et al.*[28] The measurements with Nb-SQUID proved that ''angular'' effects are insignificant.[40]

The method of three-crystal magnetometry of rings made of superconducting epitaxial films was used as a systematic test of the SOP symmetry. The geometry of measurements of spontaneous magnetization of rings made of YBCO epitaxial film deposited on a three-crystal $SrTiO_3$ (100) substrate using a scanning SQUID microscope is shown in Fig. 7.[29] The angles of orientation of *a*,*b* axes in the superconducting rings and of the boundaries of three crystals of the substrate were chosen so that three rings have an even number of junctions with a phase shift by π and an odd number of junctions in one ring at the center (left part of Fig. 7). The even number of junction does not lead to a phase jump by π, while the odd number leads to such a shift. The measurements of magnetic flux quantum by a SQUID microscope at 4.2 K gives $\Phi_0/2$ only for the ring with the odd number of junction. If the angles in a reference sample with the same number of junction are changed, measurements do not lead to the observation of the $\Phi_0/2$ quanta (right part of Fig. 7), which means that the assumption on another mechanism of the phase shift by π (say a magnetic impurity in the junction), which does not depend on the SOP symmetry, is incorrect. The same group of authors[36] carried out three-crystal magnetometric experiments in a special geometry that rules out mixing of *s* and *d*-symmetries. Thus, direct observations of $\Phi_0/2$ quantum in yttrium samples of various shapes[28–30] and in GdBCO, Tl2201, and Bi2212 films[32–36] indicate[36] the *d*-symmetry of SOP. It should be noted that attempts to explain the same experiments from the position of the *s*-wave symmetry are still being continued. However, the number of direct and indirect evidences in favor of the *d*-wave symmetry of SOP increases, the most convincing of these being the coexistence of superconductivity and antiferromagnetism (see Sec. 4.1).

4. MAGNETIC PROPERTIES OF *D*-TYPE HTSC

The conclusion about the decisive role of fluctuational spin excitations in the formation of the Fermi surface in HTSC has been substantiated reliably by now (see reviews in Refs. 42 and 60 and the literature cited therein). This should

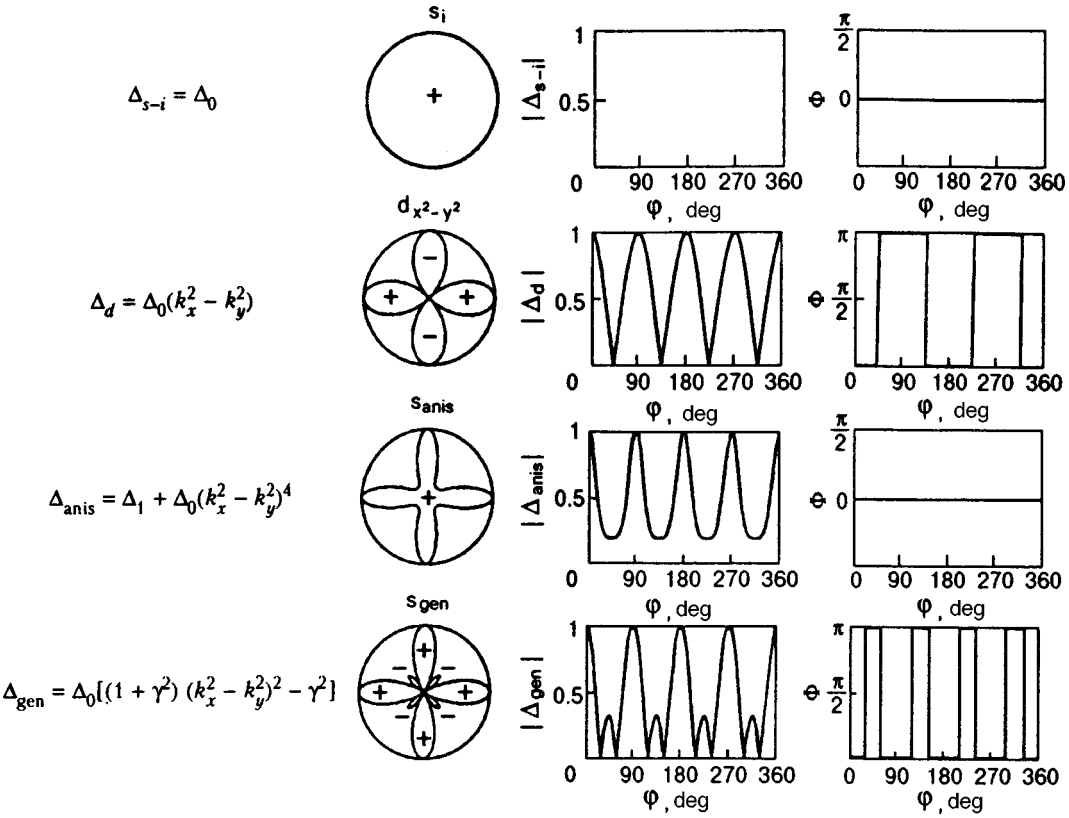

FIG. 3. Dependences of $\Delta(\mathbf{k})$, the modulus $|\Delta(\mathbf{k})|$, and phase Φ on the direction of the CuO_2 plane for d- and s-pairing ($|\Delta_{s-i}|$ is independent of $\mathbf{k}$) (from Ref. 40).

apparently explain peculiarities in the magnetic properties of d-type HTSC, such as the observed pseudogap, a dynamic analog of phase separation (charge ordering), and a peculiar structure of vortex excitations.

The existence of fluctuational AFM excitations in $La_{2-x}Sr_xCuO_4$,[61] YBCO,[62,63] and Bi2212 compounds[64–66] in the entire interval of doping is well known. Photoemission spectroscopy (ARPES) of Bi2212 proved[64] that AFM excitations double the period of the Fermi surface and are responsible for the emergence of a low-intensity photoelectron line associated with this doubling. Such ''shadow'' states were predicted earlier in the phenomenological model[67] and were attributed to U-processes with $|\mathbf{k}'-\mathbf{k}-\mathbf{Q}|<1/\zeta$, where ζ is the length of strong AFM correlations and $\mathbf{Q}=(\pi,\pi)$ is the AFM vector (the dimensionless quantity k is normalized to the reciprocal lattice constant a). The density of states near the Fermi level ε_F, which was calculated under the assumption on the spin susceptibility peak in the vicinity of the vector $\mathbf{Q}$, indicates the presence of a spin pseudogap (a valley at ε_F and peaks on the right and on the left). Dispersion relations obtained for Bi2212 by the ARPES method[65] directly indicate the opening of a gap on the Fermi surface along the line $(\pi,0)$–(π,π) upon a decrease in the hole concentration. At the same time, an analysis of the pseudogap in Bi2212 with the help of tunneling spectroscopy[66] confirmed the independence of the origin and symmetry of the superconducting state of the degree of doping. The results of NMR measurements and observations of infrared spectra[68] indicate the formation of a pseudogap for weakly doped (at $T^*>T_c$) and optimally doped (at $T^*=T_c$) compounds.

At the present time, several different hypothesis concerning the origin of the pseudogap have been proposed (see, for example, the article by Abrikosov[69] and the literature cited therein). Ovchinnikov[60] proposed in his review that the formation of the pseudogap is associated with charge ordering (dynamic analog of phase separation) resulting from segregation of holes doped into conducting regions[70] (e.g., in Nagaev conducting drops[70]) and from the formation of insulating local domains with a short-range AFM order.[64,67] A similar model formed the basis of the microscopic theory of high-temperature superconductivity, which was formulated by Emery *et al.*[71] (see below). These hypotheses,[69–71] as well as the assumptions about the role of the SOP phase fluctuations in strongly anisotropic HTSC in the formation of the pseudogap, which were put forth in the review by Loktev and Sharapov,[72] do not clarify completely the origin of the pseudogap.

4.1. Charge ordering

Starting from the first assumptions on possible segregation of holes doped in an AFM insulator and on the formation of regions free of excess holes and ''enriched'' by them,[70] as well as experimental observations of phase separation in La-based cuprates,[73] this problem remains an object of intense studies. The relation between superconductivity and phase separation associated with charge ordering was confirmed by Zakharov *et al.*:[74] no phase separation was observed in a high-quality La_2CuO_{4+x} crystal for $x=0.03$, for

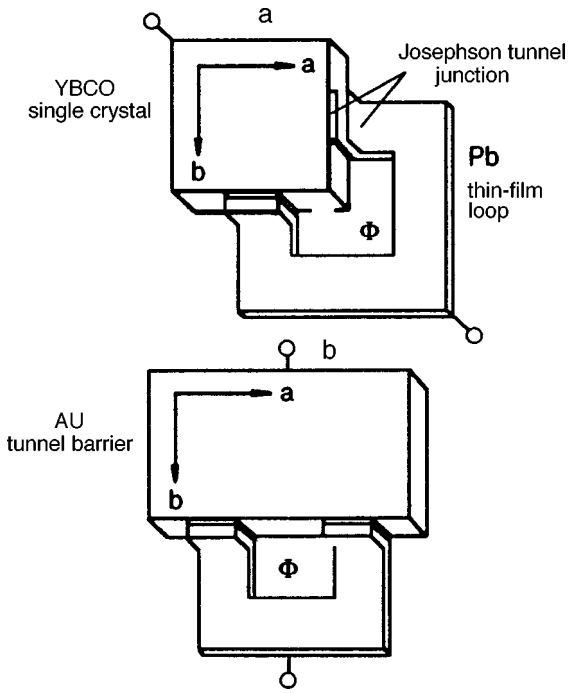

FIG. 4. Arrangement of contacts in superconducting quantum interference devices (SQUID): angular configuration (*a*) and planar configuration used for reference (*b*) (from Ref. 40).

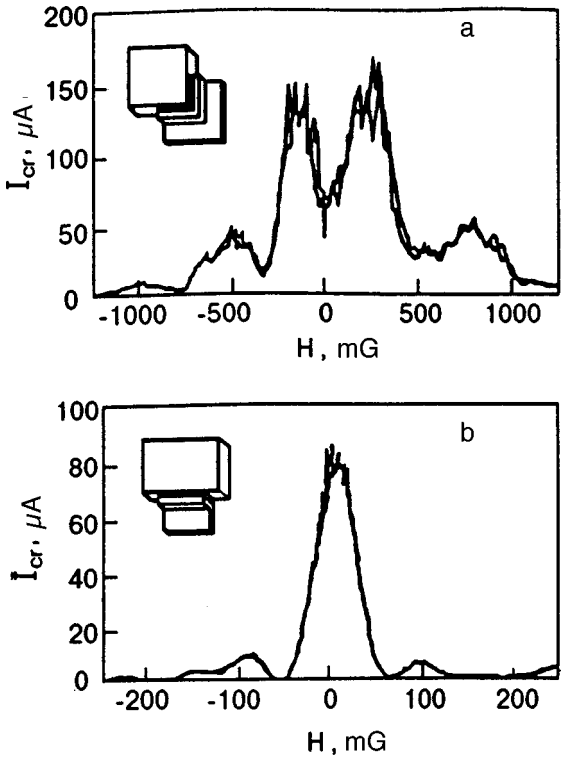

FIG. 6. Modulation of critical current by a magnetic field in measurements using SQUID devices with two Josephson junctions (YBCO single crystal–gold barrier–thin Pb film)[31] in the angular (*a*) and planar (*b*) configurations.

which $T_c \simeq 12$ K, while in a sample with a larger number of defects phase separation is observed even for $x = 0.04$, and $T_c \simeq 40$ K.

The analysis of the effect of doping on charge ordering is of considerable interest: metallic stripes (met-stripes) and insulating stripes with a period ~ 11 Å were observed in the La_2CuO_{4+x} system doped with copper at room temperature.[75] The relation between stripe phases and superconductivity was studied in the same system doped with Nd and Sr: it was found that the value of T_c increases from 4 to 15 K upon an increase in the Sr concentration from 0.12 to 0.20,

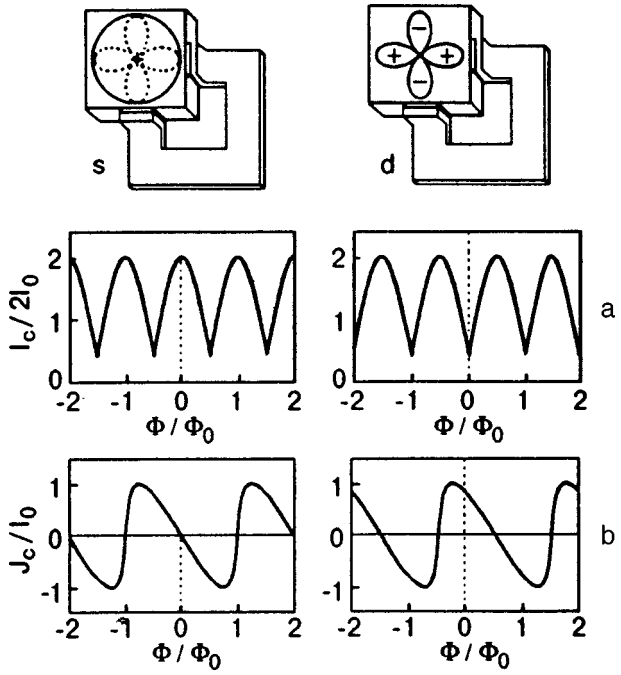

FIG. 5. Modulation of critical (*a*) and circulation (*b*) currents by a magnetic field in SQUID devices with *d*-type HTSC and *s*-type LTSC in the angular configuration (I_0 is the normalization factor) (from Ref. 40).

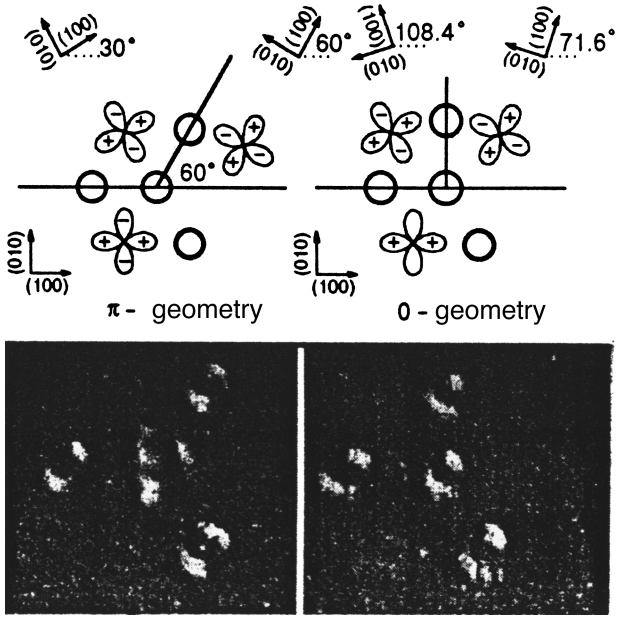

FIG. 7. Geometry and images obtained by using a scanning SQUID microscope on two three-crystal YBCO samples: with one π-contact (left) and without π-contacts (right). The samples are cooled in a field $H < 5$ mG and scanned at 4.2 K (from Ref. 30).

i.e., upon a decrease in the width of insulating stripes.[76] The results of recent measurements[77] convincingly prove that the temperature of charge ordering in La-based systems ($T_{ch} \simeq 217$ K) is much higher than the temperature of spin ordering ($T_{sp} \simeq 110$,K), and fluctuations of stripe phases are observed at $T > T_{ch}$.

The observation of long-range fine structure of x-ray absorption and electron diffraction[78] in Bi2212 in the ab plane reveals met-stripes with an orthorhombic structure alternating with the stripes of the insulating tetragonal phase, the widths of the stripes being $5.3a$ and $9.3a$, respectively (see Fig. 25 in the review by Ovchinnikov.[60]). An analysis of the results of ARPES measurements in Bi2212 leads to the same conclusion.[79] The existence of stripes of the tetragonal phase can be associated with the peak of low-frequency acoustic energy absorption observed at $T < T_c$ in Bi-base samples containing the 2212 phase (see Ref. 80 and the literature cited therein), resulting from the contribution to free energy from the interaction of uniform strain with η_d (see Sec. 2.1).

An analysis of neutron scattering in YBCO[81] points to the existence of similar (but disordered) structures. The results of spectral analysis of nuclear Raman scattering[82] in $TmBa_2Cu_4O_8$ on the basis of the ''spin ladder'' model[83] also lead to the conclusion about charge ordering. The origin of charge ordering and its obvious relation with the superconductivity of copper oxides has not been established and remains an object of heated discussions.[71,84] In Ref. 84, two different approaches to the interesting hypothesis about the existence of two spatially separated components (one of which contains localized and the other collectivized electrons) in the electron subsystems are proposed.

Some important regularities of spin ordering in $La_{2-x}Sr_xCuO_4$ (La Sr-214 with a single CuO_2 plane) and $Y_{1-x}Ca_xBa_2Cu_3O_{6.02}$ (Y Ca-123 with two CuO_2 planes) were obtained recently from the analysis of muon spin rotation.[85] The measurements of muon spin polarization made it possible to estimate the size of nonmagnetic regions; it was found that these regions are smaller than 20 Å. Figure 8 shows magnetic phase diagrams for different concentrations p_{sh} of holes in the CuO_2 plane, exhibiting three different modes of magnetic behavior. In the region of low p_{sh} (mode I), the spins of Cu^{2+} ions and holes are ordered independently: the former spins are ordered in the $3D$ AFM state at the Néel temperature T_N, while the latter ''freeze'' at T_f. As the value of p_{sh} increases, a phase transition to a state with strong magnetic correlations (mode II) similar to the spin glass state occurs at $T_N(p_{sh}) = T_f(p_{sh}) = T_g$ (Niedermayer *et al.*[85] used the term ''cluster spin glass'' for this state). The absence of a long-range AFM order can be explained by the limited size $L(p_{sh}) \approx p_{sh}^{-1/2}$ of the AFM regions formed during charge ordering. A state of ''cluster spin glass'' coexists with the superconducting state in mode III (the authors noted only a slight difference of the $T_g(p_{sh})$ dependence from the similar dependence for nonsuperconducting samples). The identical magnetic behavior of La Sr-214 and Y Ca-123 compounds suggests that the coexistence of the AFM and superconducting states is a property inherent in CuO_2 planes.

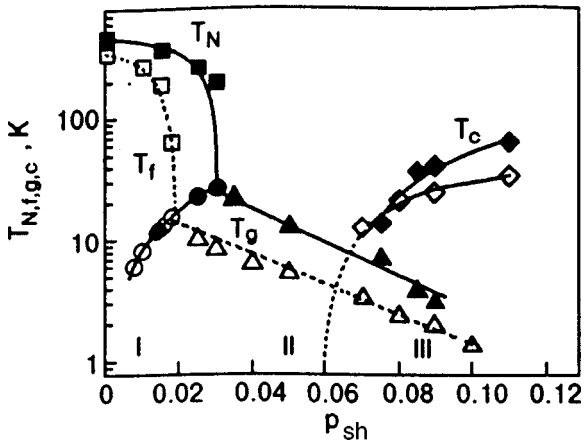

FIG. 8. Magnetic phase diagram as a function of hole concentration p_{sh} on the CuO_2 plane for compounds $La_{2-x}Sr_xCuO_4$ (light symbols) and $Y_{1-x}Ca_xBa_2Cu_3O_{6.02}$ (dark symbols). Spin ordering mode (mode I): squares denote dependences of the Néel temperature $T_N(p_{sh})$ for spins of Cu^{2+} in the $3D$ AFM state, while circles denote the temperature $T_f(p_{sh})$ of spin freezing for doped holes. Charge ordering mode (mode II): triangles denote the transition to the cluster spin glass state $T_g(p_{sh})$, which coexists with superconductivity in mode III (from Ref. 85).

4.2. Vortices

The properties of the vortex state with the d-wave symmetry of the SOP differ significantly from the properties of s-type LTSC. The effect of charge ordering on the vortex lattice is a question of prime importance. Niedermayer *et al.*[85] noted that the vortex lattice depends on phase separation: the vortex lattice exists in the entire volume of the sample in the case of microscopic sizes of stripe phases and only in met-stripes for stripes of macroscopic size (~ 3000 Å).

The main contribution to the density of states $N(0)$ in s-type LTSC comes from the states localized by the flux line:[86] $N(0) \propto N_F \xi^2$ (where N_F is the density of states in a normal metal and ξ the coherence length). Such states also exist for SOP with a zero line, but according to Volovik,[45] their contribution is smaller than that from delocalized states, i.e.,

$$N(0) \sim N_F \sqrt{H/H_{c2}},$$

where H_{c2} is the upper critical field. The magnetic field dependence of the density of states gives a contribution to heat capacity proportional to $H^{1/2}$, which was observed in Refs. 24. Such delocalized states lead to a singularity in the vortex density of states and to peculiar laws of similitude of thermodynamic and kinetic properties of d-type HTSC at low temperatures in weak fields $B \ll H_{c2}$.[87]

The states localized by a flux line for ultrapure d-type HTSC at low temperatures ($T \ll T_c$) strongly affect vortex dynamics for $B/H_{c2} \ll T/T_c$: finite dissipation of flux appears due to an analog of Landau damping on modes in the vortex core.[88] The formation of such modes can be explained by the presence of a minigap in the spectrum of localized states (which is equal to zero in the case of s-pairing). The existence of this gap in Bi2212 is confirmed by measurements.[88]

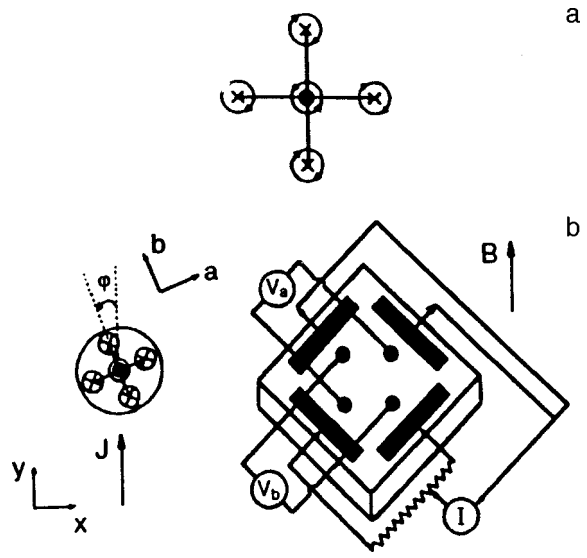

FIG. 9. (*a*) Structure of a block of vortices: (*d*-vortex (at the center) and four *s*-vortices along the axes *a* and *b*. The arrows show the direction of circulations of superfluid velocity in vortices (from Ref. 91). (*b*) Mutual orientation of *s*- and *d*-vortices, crystallographic axes, and current; φ is the angle between the direction of current and the *b*-axis (left). Experimental block diagram for measurements of the Hall effect as a function of the angle φ (from Ref. 93).

TABLE I. Basic characteristics of *s*-wave state of an isotropic low-temperature superconductor and a *d*-type HTSC.

s-Symmetry of SOP	*d*-symmetry of SOP
Electron state	
singlet	singlet
Pairing mechanism	
Phonon exchange	not established
Gap function $\Delta(\mathbf{k},\mathbf{r})$	
has no zeros	has a zero line for $k_x=k_y$
Excitation spectrum	
no excitations with $E<\Delta_0$	excitations with $E\geqslant 0$
Temperature dependence of physical quantities	
$\sim\exp(-\Delta/T)$	$\sim T^{\alpha}$
Magnetic flux quantum ($\Phi_0=hc/2e$)	
Φ_0	$\Phi_0/2$, Φ_0
Nonmagnetic defects	
weakly affect the value of T_c	Strongly suppress T_c
Magnetic defects	
suppress T_c and lead to depairing	influence depends on their solubility
Coexistence with the AFM state	
impossible	established experimentally

An important peculiarity of the flux line in *d*-type HTSC is associated with topological instability of the SOP zero line:[89] the vortex core contains a region in which the total function $\Delta(k)$ has no zeros, and the vortex core must contain all possible symmetry elements Γ_1^+ and Γ_3^+, i.e., both *s*- and *d*-wave states with opposite signs of the order parameter phase.[45] Ren *et al.*[90] proved that if mixed gradient terms F_{sd} are taken into account in the generalized Ginzburg–Landau equations (2) and (5), the superconducting state in a magnetic field can be regarded as a pure *d*-wave state only in homogeneous samples, while in heterogeneous samples this is true only on scales larger than the penetration depth λ. Mixed gradient terms in a heterogeneous superconductor induce *s*-wave states both in the vortex core (with the phase of the *s*-wave SOP equal to $-\theta$, which is opposite to the phase θ of the *d*-wave SOP) and outside the core at distances $\xi\ll r\ll\lambda$ (with the phase of the *s*-wave SOP equal to $+3\theta$) with the order parameter decreasing with increasing distance from the *d*-vortex in proportion to r^{-2}.[47,90,91] This leads to the emergence of four *s*-vortices near a *d*-vortex, which lie along the axes *a* and *b* (Fig. 9a, anisotropy in the vortex shape, and the stability of the skew vortex lattice. Such a lattice was observed in YBCO.[92]

In a magnetic field perpendicular to the interface between regions with *s*- and *d*-wave states, the symmetry of rotations about the *z*-axis is lowered to a four-fold degenerate symmetry, but neither structural nor topological heterogeneity of the sample leads to a local symmetry breaking in time inversion since the phase difference for *s*- and *d*-wave SOP is equal to zero or π.[47]

Breaking of symmetry of rotations about the *z*-axis and anisotropy in the shape of *s*- and *d*-vortices change the transport properties also: an analysis of time-dependent generalized Ginzburg–Landau equations revealed a considerable nonlinear dependence of the Hall effect on the magnitude and direction of current.[93] Figure 9b shows the orientations of vortices and current as well as the schematic diagram for measuring the angular dependence of the Hall effect.

5. CONCLUSIONS

Thus, we can state that the *d*-symmetry of SOP has been established for YBCO, GdBCO, Tl2201, and Bi2212 compounds.[28–37] The experimental studies convincingly indicate charge ordering in YBCO and Bi2212 compounds as well as in some other HTSC (such as lanthanum cuprates and nickelates and $TmBa_2Cu_4O_8$) and a close relation between charge ordering and superconductivity.[73–83] The existence of collective excitations with a spectral function peak near AFM vector has been established in YBCO and Bi2212 compounds over a wide range of energies Q.[94,95]

The characteristics of the *s*-wave state of an isotropic low-temperature superconductor are compared with those for a *d*-type superconductor in Table I.

The knowledge of the SOP symmetry is the first important step in determining the pairing mechanism and in subsequent development of the microscopic theory of HTSC. It is quite possible that the next step towards the understanding of the mechanism has already been taken, and it remains for us only to verify this. Almost all pairing mechanisms can be classified into the following two groups (see the review by Loktev[96]): the mechanisms described by the generalized BCS theory, in which electron pairing results from the exchange by elementary excitations belong to the first group, while the second group includes all mechanisms that do not fit into the BCS theory. By way of an example, let us con-

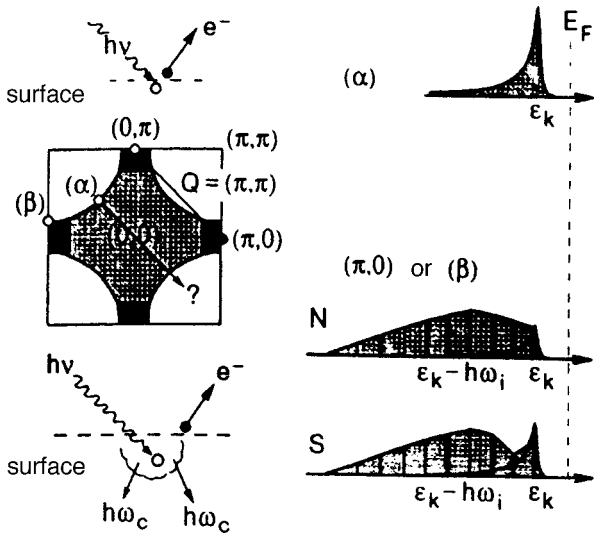

FIG. 10. Illustration of the process of photoemission and spectral density in regions of Fermi surface with a strong (β) and weak (α) coupling (from Ref. 94).

sider the mechanisms that can lead to superconductivity with the d-wave SOP.

One of the well-known models in the generalized BCS theory (see the review in Ref. 97 and the literature cited therein) is the model of a nearly AFM Fermi liquid (NAFMFL) with a magnetic mechanism of pairing, which was proposed in 1990.[26] In this model, the pairing (similar to Cooper pairing) is due to the interaction between the electron subsystem and fluctuational spin excitations whose properties can be determined from NMR measurements.[22] Calculations according to Eliashberg's scheme proved that electron pairing in the $d_{x^2-y^2}$-channel leads to superconductivity with high values of T_c. The consistency of this model, a rapid increase in SOP with decreasing temperature at $T \leqslant T_c$, and a quite substantiated $2D\sigma$ model for describing the magnetic state[98] attracted attention of experimenters and led to the development of a special technique for direct measurements of the SOP phase (see Sec. 3). The achievements of the NAFMFL model include a qualitative agreement between its results and the results of measurements of inelastic neutron scattering, experimental dependence of longitudinal and Hall conductivity as well as optical investigations (see Ref. 99 and the literature cited therein). Recent calculations taking into account higher approximations in the Eliashberg approach proved the enhancement of interactions between electrons and spin fluctuations with the momentum equal to the AFM vector $\mathbf{Q}=(\pi,\pi)$.[100] The most serious critical remarks concerning this model were made by Anderson[101] and were associated with the application of the Fermi liquid description to the normal state of a superconductor.

The results of measurements and analysis of ARPES spectra in weakly doped Bi2212 in the superconducting and normal states obtained by Shen and Schrieffer[94] can serve as an indirect confirmation of the NAFMFL model (Fig. 10). These authors consider the peak observed in the photoemission spectrum in the superconducting state as evidence of the existence of collective excitations whose spectral function has a peak in the vicinity of the vector **Q**. Figure 10 shows that a hole on the Fermi surface near the point $(0,\pi)$ [(β) regions with a strong coupling] can emit a collective excitation with a wave vector $\sim\mathbf{Q}$ and remain on the Fermi surface near the point $(\pi,0)$. For holes at other points on the Fermi surface [(α) regions with a weak coupling], the emission of excitations with $\mathbf{k}'\sim\mathbf{Q}$ indicates a transition to a state with the wave vector $\mathbf{k}-\mathbf{Q}$ far away from the Fermi surface. Neutron scattering data for other copper oxides[95] suggest that the collective mode has a fairly wide energy distribution, but final conclusions can be drawn only on the basis of similar measurements for Bi2212 in a wide energy range. Comparing the results obtained in Ref. 94 with the rapid decrease in the superconducting gap width upon an increase in the density of charge carriers (i.e., an increase in doping) observed in Ref. 102, the authors came to the conclusion that these collective excitations are responsible for pairing. However, the origin of such excitations and their spectral function are yet to be determined.

Pairing mechanisms that cannot be explained by the BCS theory and the reason behind the interest in such mechanisms were discussed by many authors (see the review in Ref. 96). Emery, Kivelson, and Zachar proposed recently a new pairing (EKZ) mechanism which is a spin analog of the superconducting proximity effect.[71] The EKZ mechanism is closely related with the results of recent investigations of HTSC and can be formulated as follows.

(1) The process of expulsion of doped holes by an antiferromagnet leads to charge ordering, i.e., to the formation of metallic and nonconducting stripe phases.[70–72]
(2) In metallic quasi-one-dimensional stripes, the charge and spin of holes are separated into ''spinons'' and ''holons'' predicted in 1968[103,104] and observed recently in $1D$ $SrCuO_2$.[105]
(3) The pseudogap appears as a consequence of local pairing of ''spinons,'' i.e., neutral excitations with spin 1/2, leading to strong fluctuations of SOP in individual stripes.
(4) The superconducting transition occurs after the establishment of global phase coherence as a result of Josephson coupling between the stripe phases and CuO_2 planes.

This mechanism is a realization of several ideas put forth earlier, such as Anderson's idea concerning spin liquid and its versions[106] and the idea proposed by Kivelson *et al.*[107] on BCS-like pairing of spinons, leading to superconductivity.[108] Emery and Kivelson[109] predicted earlier a close connection of the average separation between stripes with the value of T_c whose observation was reported earlier.[76] The authors of Ref. 71 proposed an extensive list of existing experimental evidences of the EKZ mechanism and a new qualitative test involving the artificial construction of such a system of spin ladders[83] and a sample with copper–oxygen chains. The compound $1D-SrCuO_2$ can be proposed as a reservoir of holons and spinons.[105] In our opinion, the experimental observation of ''spinons'' and ''holons'' in met-stripes of HTSC compounds at $T>T_c$ with the help of ARPES measurements similar to those made in Ref. 105 is very important for testing the EKZ mechanism.

In conclusion of this review, we must also mention the hypothesis proposed by Zhang[110] and combining the theory of superconductivity and antiferromagnetism: In the framework of the SO-5 symmetry, there exists a ''superspin,'' viz., a vector with five components two of which are SOP while the remaining three form the AFM order parameter. The instantaneous critical response to this hypothesis[111] is an indication of its novelty.

[1]R. Balian and N. R. Werthamer, Phys. Rev. **131**, 1553 (1963).
[2]D. J. Thouless, Ann. Phys. **10**, 553 (1960).
[3]B. V. Karpenko, Fiz. Met. Metalloved. **9**, 794 (1960).
[4]P. W. Anderson and P. Morel, Phys. Rev. **123**, 1911 (1961).
[5]A. I. Akhiezer and I. A. Akhiezer, Zh. Éksp. Teor. Fiz. **43**, 2208 (1962) [Sov. Phys. JETP **16**, 1560 (1962).
[6]I. A. Privorotskiĭ, Zh. Éksp. Teor. Fiz. **43**, 2255 (1962) [Sov. Phys. JETP **16**, 1593 (1962).
[7]H. Suhl, in Low Temperature Physics (ed. by C. DeWitt, B. Dreyfus, and P. G. de Gennes), Gordon and Breach, New York (1962).
[8]K. A. Bruekner, T. Soda, P. W. Anderson, and P. Morel, Phys. Rev. **118**, 1442 (1960); V. J. Emery and A. M. Sessler, Phys. Rev. **119**, 42 (1960).
[9]F. Steglich, J. Aarts, C. D. Bredl *et al.*, Phys. Rev. Lett. **43**, 1892 (1979).
[10]E. I. Blount, Phys. Rev. B **32**, 2935 (1985).
[11]G. E. Volovik and L. P. Gor'kov, Zh. Éksp. Teor. Fiz. **88**, 1412 (1985) [Sov. Phys. JETP **61**, 843 (1985).
[12]D. Sahu, A. Langner, and T. F. George, Phys. Rev. B **38**, 2466 (1988).
[13]J. E. Hirsch, Phys. Rev. Lett. **54**, 1317 (1985).
[14]S. J. Scalapino, E. Loh, and J. E. Hirsch, Phys. Rev. B **34**, 8190 (1986).
[15]K. Miyake, S. Schmitt-Rink, and C. V. Varma, Phys. Rev. B **34**, 6554 (1986).
[16]D. Esteve, Europhys. Lett. **3**, 1237 (1987).
[17]P. Gammel, D. J. Bishop, G. J. Dolan *et al.*, Phys. Rev. Lett. **59**, 2592 (1987).
[18]M. Takigava, P. C. Hammel, R. H. Heffner, and Z. Fisk, Phys. Rev. B **39**, 737 (1989).
[19]S. E. Barret, J. A. Martindale, D. J. Durand *et al.*, Phys. Rev. Lett. **66**, 108 (1991).
[20]A. V. Bondar', D. L. Lyfar', and I. G. Mikhaĭlov, in *Physical Problems in HTSC* [in Russian] (ed. by V. M. Loktev), Naukova Dumka, Kiev (1990), p. 5.
[21]Y. Itoh, H. Yasuoka, Y. Fujiwara *et al.*, J. Phys. Soc. Jpn. **61**, 1287 (1992).
[22]C. P. Slichter, in *Strongly Correlated Electron Systems* (ed. by K. S. Bedell), Addison-Wesley, New York (1994).
[23]K. A. Moler, D. J. Baar, J. S. Urbach *et al.*, Phys. Rev. Lett. **73**, 2744 (1994); A. Junod, M. Roulin, D. Revaz *et al.*, Physica C **282–287**, 1399 (1997).
[24]W. N. Hardy, D. A. Bonn, D. C. Morgan *et al.*, Phys. Rev. Lett. **7O**, 3999 (1993).
[25]C. Gros, R. Joynt, and T. M. Rice, Z. Phys. B **68**, 425 (1987); N. E. Bickers, D. J. Scalapino, and R. T. Scaleter, Int. J. Mod. Phys. B **1**, 687 (1987); Z. Y. Weng, T. K. Lee, and C. S. Ting, Phys. Rev. B **38**, 6561 (1988); N. E. Bickers, D. J. Scalapino, and S. R. White, Phys. Rev. Lett. **66**, 108 (1989).
[26]A. Millis, P. Monthoux, and D. Pines, Phys. Rev. **42**, 167 (1990); P. Monthoux, A. Balatsky, and D. Pines, Phys. Rev. B **46**, 14 803 (1992); P. Monthoux, and D. Pines, Phys. Rev. B **49**, 4261 (1994); K. Ueda, T. Moriya, and Y. Takahashi, J. Phys. Chem. Solids **53**, 1515 (1992).
[27]M. Sigrist and T. M. Rice, J. Phys. Soc. Jpn. **61**, 4283 (1992).
[28]D. A. Wollmann, D. J. Van Harlingen, W. C. Lee *et al.*, Phys. Rev. Lett. **71**, 2134 (1993); D. A. Wollmann, D. J. Van Harlingen, and A. J. Leggett, Phys. Rev. Lett. **73**, 1872 (1994).
[29]C. C. Tsuei, J. R. Kirtley, C. C. Chi *et al.*, Phys. Rev. Lett. **73**, 593 (1994).
[30]J. R. Kirtley, M. B. Ketchen, and K. G. Stawiasz, Appl. Phys. Lett. **66**, 1138 (1995); Nature (London) **373**, 225 (1995).
[31]D. A. Wollmann, D. J. van Harlingen, J. Giapintzanis, and D. M. Ginsberg, Phys. Rev. Lett. **74**, 797 (1995).
[32]J. H. Miller, Q. Y. Ying, Z. G. Zou *et al.*, Phys. Rev. Lett. **74**, 2347 (1995).
[33]C. C. Tsuei, J. R. Kirtley, C. C. Chi *et al.*, J. Phys. Chem. Solids **56**, 1787 (1995).
[34]J. R. Kirtley, C. C. Tsuei, M. Rupp *et al.*, Phys. Rev. Lett. **76**, 1336 (1996).
[35]J. R. Kirtley, C. C. Tsuei, and K. A. Moler, Czech. J. Phys. **46**, Suppl. 6, 3169 (1996): J. R. Kirtley, C. C. Tsuei, H. Raffy *et al.*, Europhys. Lett. **36**, 707 (1996).
[36]T. M. Rice, in *Proceedings of the Fifth M^2T–HTS Conference*, Physica **C282–287**, part 1, xix (1997); C. C. Tsuei and J. R. Kirtley, *ibid.*, 4 (1997).
[37]M. Sigrist and K. Ueda, Rev. Mod. Phys. **63**, 239 (1991).
[38]D. Pines and P. Monthoux, J. Phys. Chem. Solids **56**, 1651 (1995).
[39]D. J. Scalapino, Phys. Rep. **250**, 331 (1995).
[40]D. J. Van Harlingen, Rev. Mod. Phys. **67**, 515 (1995).
[41]M. Sigrist and T. M. Rice, Rev. Mod. Phys. **67**, 503 (1995).
[42]V. Barzykin and D. Pines, Phys. Rev. B **52**, 13 585 (1995).
[43]L. P. Gorkov, Sov. Sci. Rev., Sect. A **9**, 1 (1987).
[44]J. F. Annett, Adv. Phys. **39**, 83 (1990).
[45]G. E. Volovik, Pis'ma Zh. Éksp. Teor. Fiz. **58**, 457 (1993) [JETP Lett. **58**, 469 (1993)].
[46]R. Joynt, Phys. Rev. B **41**, 4271 (1990).
[47]J.-H. Xu, Y. Ren, and C. S. Ting, Phys. Rev. B **52**, 7663 (1995).
[48]A. H. Silver and J. E. Zimmerman, Phys. Rev. **157**, 317 (1967).
[49]L. N. Bulaevskii, V. V. Kuzii, and A. A. Sobyanin, JETP Lett. **25**, 290 (1977).
[50]G. E. Volovik and V. P. Mineev, Pis'ma Zh. Éksp. Teor. Fiz. **24**, 605 (1976) [JETP Lett. **24**, 561 (1976)].
[51]F. Steglish, U. Rauchschwalbe, U. Gottwick *et al.*, J. Appl. Phys. **57**, 3054 (1985).
[52]V. B. Geschkenbein and A. I. Larkin, Pis'ma Éksp. Teor. fiz. **43**, 306 (1986) [JETP Lett. **43**, 395 (1986)]; V. B. Geschkenbein, A. I. Larkin, and A. Barone, Phys. Rev. B **36**, 235 (1987).
[53]J. F. Annett, F. N. Goldenfeld, and S. R. Renn, Phys. Rev. B **43**, 2778 (1991).
[54]Y. Kitaoka, J. Phys. Soc. Jpn. **62**, 2803 (1993); N. Bulut and D. J. Scalapino, Phys. Rev. Lett. **67**, 2898 (1991).
[55]N. Bulut and D. J. Scalapino, Phys. Rev. Lett. **68**, 706 (1992).
[56]Z.-X. Shen, D. S. Dessau, B. O. Wells *et al.*, Phys. Rev. Lett. **70**, 1553 (1993); J. Ma, Science **267**, 862 (1996).
[57]S. A. Chakraverty, A. Sudbo, P. W. Anderson, and S. Dtrong, Science **261**, 337 (1993); P. Chaudhari and S.-Y. Lin, Phys. Rev. Lett. **72**, 1084 (1994); J. Chen, J. F. Zasadzinski, K. E. Gray *et al.*, Phys. Rev. B **49**, 3683 (1994).
[58]D. A. Brawner and H. R. Ott, Phys. Rev. B **50**, 6530 (1994).
[59]R. A. Klemm, Phys. Rev. Lett. **73**, 1871 (1994).
[60]S. G. Ovchinnikov, Usp. Fiz. Nauk **167**, 1042 (1997) [sic].
[61]R. J. Birgeneau, D. R. Gable, H. P. Jensen *et al.*, Phys. Rev. B **38**, 6614 (1988).
[62]J. M. Tranquada, P. M. Gehring, G. Shirane *et al.*, Phys. Rev. B **46**, 5561 (1992).
[63]J. Rossat-Mignod, L. P. Regnault, C. Vettier *et al.*, Physica C **185–189**, 86 (1991).
[64]P. Aebi, J. Osterwalder, P. Schwaller *et al.*, Phys. Rev. Lett. **72**, 2757 (1994).
[65]D. S. Marshall, D. S. Dessau, and A. G. Loeser, Phys. Rev. Lett. **76**, 4841 (1996).
[66]Ch. Renner, B. Revaz, and J.-Y. Genoud, Phys. Rev. Lett. **80**, 149 (1998).
[67]A. P. Kampf and J. R. Schrieffer, Phys. Rev. B **42**, 7967 (1990).
[68]A. V. Pushkov, D. N. Basov, and T. J. Timusk, J. Phys.: Condens. Matter **8**, 10 049 (1996).
[69]A. A. Abrikosov, Phys. Rev. B **54**, 6708 (1996).
[70]É. L. Nagaev, JETP Lett. **6**, 484 (1967); J. R. Schrieffer, S. C. Zhang, and X. G. Wen, Phys. Rev. Lett. **60**, 944 (1988); V. J. Emery, S. A. Kivelson, and H. Lin, Phys. Rev. Lett. **64**, 475 (1990).
[71]V. J. Emery, S. A. Kivelson, and O. Zachar, Physica C **282–287**, 1, 174 (1997); Phys. Rev. B **56**, 6120 (1997).
[72]V. M. Loktev and S. G. Sharapov, Condens. Matter Phys. **11**, 131 (1997).
[73]É. L. Nagaev, Usp. Fiz. Nauk **165**, 529 (1995) [Phys. Usp. **38**, 497 (1995)]; J. M. Tranquada, B. J. Sternlieb, J. D. Axe *et al.*, Nature (London) **375**, 561 (1995); *International Workshop on Phase Separation in HTS*, J. Supercond. **9**, No. 4 (1996).
[74]A. A. Zakharov, A. A. Nikonov, O. E. Parfionov *et al.*, Physica C **223**, 157 (1994).
[75]X. L. Dong, B. R. Zhao, Z. X. Zhao *et al.*, Physica C **282–287**, 1877 (1997).

[76]J. M. Tranquada, J. D. Axe and N. Ichikawa, Phys. Rev. Lett. **78**, 338 (1997).
[77]G. Blumberg, M. V. Klein, and S. V. Cheong, Phys. Rev. Lett. **80**, 564 (1998); Y. Murakami, H. Kawada, H. Kawata *et al.*, Phys. Rev. Lett. **80**, 1932 (1998).
[78]K. A. Muller (Ed.), *Phase Separation in Cuprate Superconductors*, World Scientific, Singapore (1992); A. Bianconi and M. Missori, J. Phys. (Paris) **4**, 361 (1994).
[79]M. Salkola, V. J. Emery, and S. A. Kivelson, Phys. Rev. Lett. **76**, 155 (1996).
[80]G. G. Sergeeva, Fiz. Nizk. Temp. **24**, 1003 (1998) [Low Temp. Phys. **24**, 757 (1998)].
[81]B. Sternlieb, J. M. Tranquada, G. Shirane *et al.*, Phys. Rev. B **50**, 12 915 (1994); J. M. Tranquada, Physica C **282–287**, 166 (1997); H. Dai, H. A. Mook, and F. Dogan, Cond. Mat. 9707112.
[82]O. N. Bakharev, M. V. Eremin, and M. A. Teplov, Pis'ma Zh. Éksp. Teor. Fiz. **61**, 499 (1995) [JETP Lett. **61**, 515 (1995)]; M. A. Teplov, E. V. Kryukov, A. V. Duglav *et al.*, Pis'ma Zh. Éksp. Teor. Fiz. **63**, 233 (1996) [JETP Lett. **63**, 227 (1996)].
[83]S. Gopalan, T. M. Rice and M. Sigrist, Phys. Rev. B **49**, 8901 (1994); E. Dagotto and T. M. Rice, Science **271**, 618 (1996).
[84]A. Bianconi and M. Misssori, J. Supercond. **8**, 545 (1995); J. S. Zhou and J. B. Goodenough, Phys. Rev. B **56**, 6288 (1997); C. Castellani, C. Di Castro, and M. Grilli, Phys. Rev. Lett. **75**, 4650 (1995); Phys. Rev. B **54**, 16 216 (1996).
[85]Ch. Niedermayer, C. Bernhard, T. Blasius *et al.*, Phys. Rev. Lett. **80**, 3843 (1998).
[86]C. Caroli, P. G. de Gennes, and J. Matricon, Phys. Lett. **9**, 307 (1964).
[87]N. B. Kopnin and G. E. Volovik, Pis'ma Zh. Eksp. Teor. Fiz. **64**, 641 (1996) [JETP Lett. **64**, 690 (1996)]; G. E. Volovik, Pis'ma Zh. Éksp. Teor. Fiz. **65**, 491 (1997) [JETP Lett. **65**, 522 (1997)].
[88]N. B. Kopnin and G. E. Volovik, Phys. Rev. Lett. **79**, 1377 (1997); Ch. Renner, B. Revaz, K. Kadowaki *et al.*, Phys. Rev. Lett. **80**, 3606 (1998).
[89]P. G. Grinevich and G. E. Volovik, J. Low Temp. Phys. **72**, 371 (1988).
[90]Y. Ren, J. H. Xu, and C. S. Ting, Phys. Rev. Lett. **74**, 3680 (1995).
[91]A. J. Berlinsky, A. L. Fetter, M. Franz *et al.*, Phys. Rev. Lett. **75**, 2200 (1995); M. Franz, Phys. Rev. B **53**, 5795 (1996).
[92]B. Keimer, J. W. Lynn, R. W. Erwin *et al.*, J. Appl. Phys. **76**, 6788 (1994); I. Maggio-Aprile, Phys. Rev. Lett. **75**, 2754 (1995).
[93]J. J. Vicente Alvarez, D. Dominguez, and C. A. Balseiro, Phys. Rev. Lett. **79**, 1373 (1997).
[94]Z.-X. Shen and J. R. Schrieffer, Phys. Rev. Lett. **78**, 1771 (1997).
[95]N. F. Fong, Phys. Rev. Lett. **75**, 316 (1995); S. M. Hayden, Phys. Rev. Lett. **76**, 1344 (1996).
[96]V. M. Loktev, Fiz. Nizk. Temp. **22**, 3 (1996) [Low Temp. Phys. **22**, 3 (1996)].
[97]A. V. Chubukov and D. K. Morr, Phys. Rep. **288**, 355 (1997).
[98]T. N. Antsygina and V. A. Slyusarev, Fiz. Nizk. Temp. **21**, 127 (1995) [Low Temp. Phys. **21**, 93 (1995)].
[99]D. P. Stojkovic and D. Pines, Phys. Rev. B **56**, 11 931 (1997).
[100]P. Monthoux, Phys. Rev. B **55**, 16 261 (1997).
[101]P. W. Anderson, Phys. Today **No. 2**, 11 (1994).
[102]P. J. White, Z.-X. Shen, C. Kim *et al.*, Phys. Rev. B **54**, 15 669 (1996).
[103]E. H. Lieb and F. Y. Wu, Phys. Rev. Lett. **20**, 1445 (1968).
[104]A. Luther and V. J. Emery, Phys. Rev. Lett. **33**, 589 (1974).
[105]C. Kim, Z.-X. Shen, and N. Motoyama, Phys. Rev. B **56**, 15 589 (1997); Phys. Rev. Lett. **77**, 4054 (1996).
[106]P. W. Anderson, Science **235**, 1196 (1987); Mater. Res. Bull. **8**, 153 (1973); V. Kalmeyer and R. B. Laughlin, Phys. Rev. Lett. **59**, 2095 (1987).
[107]S. A. Kivelson, D. S. Rokhsar, and J. P. Sethna, Phys. Rev. B **35**, 8865 (1987); S. A. Kivelson, Phys. Rev. B **36**, 7237 (1987); C. Gros, Phys. Rev. B **38**, 931 (1988).
[108]D. S. Rokhsar and S. A. Kivelson, Phys. Rev. Lett. **61**, 2376 (1988).
[109]V. J. Emery and S. A. Kivelson, in *Proc Tenth Anniversary HTS Workshop*, Houston (1996) (Ed. by B. Battlogg, C. W. Chu, D. V. Gubser, and K. A. Muller), World Scientific, Singapore (1996).
[110]S. C. Zhang, Science **275**, 1089 (1997); S. Meixner, W. Hanke, E. Demler, and S. C. Zhang, Phys. Rev. Lett. **79**, 4902 (1997).
[111]M. Greiter, Phys. Rev. Lett. **79**, 4898 (1997).

Translated by R. S. Wadhwa

SUPERCONDUCTIVITY, HIGH-TEMPERATURE SUPERCONDUCTIVITY

Correlated redistribution of optical conductivity spectra of HTSC: contribution of interband excitations to the formation of the metal state of $La_{2-x}Sr_xCuO_4$ and $YBa_2Cu_3O_{6+x}$

V. N. Samovarov

B. Verkin Institute for Low Temperature Physics and Engineering, National Academy of Sciences of the Ukraine, 310164 Kharkov, Ukraine[*)]

(Submitted May 22, 1998; revised July 2, 1998)
Fiz. Nizk. Temp. **24**, 1043–1057 (November 1998)

A phenomenological model is proposed for the transformation of interband conductivity caused by electron transitions through the optical (dielectric) gap $\hbar\omega_g$ into the intraband conductivity of hole carriers in high-temperature superconductors under chemical doping. The interrelation between the interband and intraband conductivity components is analyzed in terms of the spectral function $N(\omega)\sim\int\sigma(\omega)d\omega$ for integral conductivity of the normal phase. Two groups of coexisting charge carries of the p- and d-types with different relations with interband transitions are singled out. The integral conductivity of narrow-band d-carriers is determined by interband excitations with the gap attenuation $\Gamma\propto\omega_g$. The integral conductivity of wide-band p-carriers is not connected with interband excitations and is determined by the standard Drude spectrum. The obtained spectral functions are compared with the available data for $La_{2-x}Sr_xCuO_4$ and $YBa_2Cu_3O_{6+x}$ in the doping range from the beginning of metallization up to loss of superconductivity. The good agreement with the experimental data leads to the following conclusions: (i) the integral interband conductivity at the doping stage with increasing temperature of superconducting transition is mainly determined by the d-component to which interband excitations are ''pumped;'' (ii) as soon as one of the planes CuO_2 or CuO_x goes over to a predominantly p-metal state, a noncorrelated metal with loss of superconductivity is formed.
[S1063-777X(98)00211-4]

INTRODUCTION

The electron spectrum of high-temperature superconductors has an interesting peculiarity manifested in correlated redistribution of optical conductivity spectra. The optical correlation effect observed in HTSC by Uchida *et al.*[1] remains an object of experimental and theoretical investigations.[2–5] Apart from the observed peculiar frequency dependence of optical conductivity $\sigma(\omega)\sim 1/\omega$,[6] the sensitivity of optical spectra to the superconducting transition,[7,8] and photoinduced superconductivity,[9,10] optical correlation effect reflects peculiarities of the electron structure of HTSC and has no analogs in traditional BCS materials. The effect can be described as follows.

In the dielectric phase of the HTSC, the entire spectrum $\sigma(\omega)$ of conductivity and optical absorption proportional to $\sigma(\omega)$ is concentrated in the interband transition region for $\hbar\omega\geqslant E_g$, where $E_g\simeq 1.5-2$ eV is the optical gap separating the valence (filled) band and the upper (empty) band. These interband transitions cause electron transfer from oxygen to copper in the CuO_2 plane. In the case of chemical doping as a result of which mobile holes appear in the valence band at the Fermi level and a hole band is formed, the interband conductivity decreases, while the intraband conductivity component extending up to $\hbar\omega=0$ increases in the frequency range $\hbar\omega<E_g$. In classical materials, the suppression of interband transition under hole doping is observed near the threshold energy $\hbar\omega_g$ due to electron depletion of states near the Fermi level. The intensity of interband transitions originating deep under the Fermi level in traditional materials changes insignificantly. The result according to which the integral interband conductivity in HTSC decreases in the entire spectral range $\hbar\omega\geqslant E_g$, i.e., even for transitions from deep levels in the valence band, appeared as quite unexpected. A strong (by tens of percents) decrease in the interband conductivity is observed for a very low hole occupancy of the valence band, amounting only to a few percent (the occupancy can be estimated from the ratio ε_F/ω, where $\varepsilon_F\simeq 10^{-1}$ eV is the width of the hole band and $\omega\simeq 3$ eV the width of the valence band). The main idea in the explanation of the effect is that the emergence of holes in the valence band leads to a decrease in the number of free states in the upper band.[4] As a result, the intensity of all interband transitions (including those from deep levels of the valence band) must decrease. A more detailed analysis shows that free states of the upper bands are transferred to the optical gap (mainly, to the peripheral region), where a high-intensity

correlation peak appears in the density of states.[11] Such a situation when intraband conductivity increases upon a decrease in the interband conductivity is possible in strongly correlated systems in which oscillator forces of electron excitations of the interband and intraband origin are interrelated.

The optical correlation effect is observed not only under chemical doping. Experimental and theoretical proofs have been obtained for the existence of this effect under cooling[11,12] and photoirradiation of $YBa_2Cu_3O_{6+x}$.[12] For example, the absorption of $YBa_2Cu_3O_{6+x}$ films cooled to low temperatures decreases in the entire visible spectral region during transitions with charge transfer, while the absorption in the IR region increases.[8,12] Taking into account what has been said above, we can say that such a temperature behavior of the spectra indicates the formation of a temperature-induced doping channel. At the present time, we can speak of the correlated redistribution of optical spectra of HTSC due to chemical, low-temperature, and photoinduced doping. Considerable interest in the problem of interrelation of interband and intraband oscillators is based on possible participation of electron excitations with charge transfer in the mechanism of high-temperature superconductivity (see, for example, the reviews in Refs. 13 and 14).

In the present paper, the interrelation between the inter- and intraband components of conductivity is studied for the case of chemical doping of the metal phase of HTSC using the integral characteristic $N(\omega)\sim\int\sigma(\omega)d\omega$. Two groups of mobile charge carriers of the p- and d-types with different couplings with interband transitions are singled out. The integral intraband spectrum $N(\omega)$ for more localized d-carriers is determined by correlated interaction with interband transitions. A model conductivity spectrum $\sigma(\omega)$ is proposed for determining this integral d-component with the gap attenuation of interband excitations $\Gamma\sim\omega_g$. The integral conductivity of more delocalized p-carriers is not associated with interband transitions with charge transfer and is determined by the conventional Drude conductivity mechanism. The obtained frequency dependences $N(\omega)$ are compared in the second part of this paper with the available data for $La_{2-x}Sr_xCuO_4$ and $YBa_2Cu_3O_{6-x}$ in the doping range from the beginning of metallization up to the loss of superconductivity. A good agreement with experimental results obtained in a wide frequency range from $\sim$0.1 to $\sim$1.5 eV leads to the following basic conclusions.

At the doping stage during which the superconducting transition temperature increases, the integral intraband conductivity is mainly determined by the d-component emerging due to integral pumping of ''over-the-gap'' excitations with charge transfer to the hole band; the enhancement of integral conductivity of the p-component under doping slows down the increase in the superconducting transition temperature and ultimately leads to the formation of a noncorrelated metal and the loss of superconducting properties.

The main result of this research is the establishment of the decisive role of electron excitations with charge transfer in the formation of the metallic phase of HTSC with high values of the superconducting transition temperature.

PHENOMENOLOGICAL MODEL

Optical conductivity $\sigma(\omega)$ characterizes the relation between the average current in a crystal and the electric field of a light wave: $\mathbf{j}(\omega)=\sigma(\omega)\mathbf{E}(\omega)$. Optical conductivity spectra can be obtained from an analysis of the frequency dependences of the reflection coefficient $R(\omega)$ by the Kramers–Kronig method. The most extensive data on the behavior of $\sigma(\omega)$ in HTSC can be obtained from the results of polarization measurements of $R(\omega)$ in perfect single crystals. For the polarization of light perpendicular to the c-axis of the crystal ($\mathbf{E}\perp c$), the light wave determines the conductivity of the ab-plane containing CuO_2 planes of HTSC cuprates and the impurity-doped structure, viz., CuO_x chains, in the case of Y–Ba–Cu–O. In the case of $La_{2-x}Sr_xCuO_4$ and similar compounds, the unit cell contains only one CuO_2 plane. For this reason, measurements for the polarization $\mathbf{E}\perp c$ give the optical conductivity of this single copper–oxygen structure, i.e., $\Sigma_{ab}^{\text{meas}}(\omega)=\sigma(CuO_2)$. The unit cell of $YBa_2Cu_3O_{6+x}$ contains two CuO_2 planes and a CuO_x chain which is doubled in the region of existence of the ortho–I phase for $x>0.65$. The results for $YBa_2Cu_3O_{6+x}$ crystals are obtained from measurements in the a- and b directions. The CuO_x chains formed as a result of introduction of oxygen are aligned along the b-axis. A light wave with the a-polarization ($\mathbf{E}\|a$) does not excite the chains, and hence the conductivity of only one CuO_2 plane [$\Sigma_a^{\text{meas}}(\omega)=\sigma(CuO_2)$] is measured for this polarization (the light wave excites current in two a-directions, one from each CuO_2 plane). For the polarization $\mathbf{E}\|b$, the values of $\Sigma_b^{\text{meas}}(\omega)=\sigma(CuO_2)+\sigma(CuO_x)$ are measured, and the conductivity of the chain structure can be determined from the difference spectrum: $\Sigma_b^{\text{meas}}(\omega)-\Sigma_a^{\text{meas}}(\omega)=\sigma(CuO_x)$. Obviously, the total conductivity of the unit cell of $YBa_2Cu_3O_{6+x}$ is equal to $\Sigma_{ab}^{\text{meas}}(\omega)=\Sigma_a^{\text{meas}}+\Sigma_b^{\text{meas}}=2\sigma(CuO_2)+\sigma(CuO_x)$. The relation between $\sigma(CuO_2)$ and $\sigma(CuO_x)$ depends on the doping level and the degree of perfection of the crystal.

The most comprehensive analysis of optical conductivity of La-based single crystals at 300 K as a function of the doping level was carried out in Refs. 1 and 3. The results of these publications will be used here in our analysis. Reliable data for $YBa_2Cu_3O_{6+x}$ can be obtained only from polarization experiments involving crystals without twins. Among the few publications in this field, mention must be made of two communications[2,15] from well-known groups of scientists engaged in HTSC spectroscopy.

The optical conductivity spectrum of the dielectric phase of HTSC is isotropic and characterizes the excitation spectrum of interband current emerging as a result of charge transport from oxygen to copper ($O^{2-}Cu^{2+}\rightarrow O^{-}Cu^{+}$) in CuO_2 plane (planes). The excitation of current requires the threshold energy $\hbar\omega_g=E_g$ equal to the optical (dielectric) gap between the lower and upper bands. Interband absorption of a light quantum generates a hole in the valence band (photodoping effect). Starting from the threshold energy, the interband conductivity spectrum $\Sigma_{\text{meas}}(\omega)=\sigma^{CT}(\omega)$ (charge-transfer conductivity) extends to the high-frequency range, filling the visible region in oxygen–copper HTSC. The values of the optical gap vary from $E_g=1.35$ eV for

Pr_2CuO_4 to 1.8 eV for La_2CuO_4.[16] For the dielectrics $YBa_2Cu_3O_6$ and $La_{2-x}Sr_xCuO_4$ ($x<0.01$), E_g assumes intermediate values (1.5 and 1.65 eV, respectively).[16] The value 1.5 eV was confirmed by measurements of the spectral threshold for photocurrent in $YBa_2Cu_3O_{6.1}$.[17] Typical values of conductivity in the frequency range from E_g to $\simeq 3.5$ eV, in which oxygen–copper interband transitions are concentrated, are $\sigma^{CT}=500-1000\ \Omega^{-1}\ \mathrm{cm}^{-1}$.

The introduction of a doping impurity into a dielectric crystal and the emergence of metallization reduce the integral interband conductivity $\sigma^{CT}(\omega)$, while the intraband conductivity component increases in the spectral range $\hbar\omega<E_g$. Intraband conductivity characterizes the excitation of current due to electron transfer over the hole states formed near the top of the valence band. The intraband conductivity spectrum for a- and b-directions in a metallized crystal extends from the infrared (IR) region to $\omega=0$, where the Drude conductivity peak is formed as a result of doping, with the characteristic values $\Sigma_{ab}^{\mathrm{meas}}\gtrsim 3000\ \Omega^{-1}\ \mathrm{cm}^{-1}$ for optimally doped $YBa_2Cu_3O_{6+x}$ ($x\simeq 0.9$) and $La_{2-x}Sr_xCuO_4$ ($x\simeq 0.15$). Such a form of conductivity spectra indicates that the intraband component is determined by the emergence of mobile holes in the crystal. It should be noted in this connection that no metallization is observed in $La_{2-x}Sr_xNiO_4$ crystals doped to $x=0.5$,[3] no peak is observed at $\omega=0$, but a broad conductivity band having a peak near 1 eV is formed in the middle infrared region (MIR). Such a spectrum of the intraband component should be attributed to electron transitions to the mainly d-type local hole states formed upon doping, Consequently, the redistribution of the conductivity spectrum (from the high-frequency MIR region to the low-frequency Drude region for $\omega=0$) within the intraband component itself can serve an optical evidence of sample metallization. We shall denote the intraband component subjected to such a spectral evolution as the dynamic component in contrast to the static interband component at local levels.

High-temperature superconductors with mobile holes, in which metallization is accompanied with an increase in the dynamic intraband component and a simultaneous suppression of the interband component, exhibit an interesting spectral peculiarity. The conductivity spectra clearly manifest a narrow frequency range near a certain frequency ω_C (crossover point), in which the conductivity remains virtually unchanged during doping. Optical conductivity increases as a result of doping for $\omega<\omega_C$ and decreases for $\omega>\omega_C$. The frequency ω_C is also called the isobestic point by some authors.[1] The crossover point clearly demarcates two regions with opposite directions of evolution in conductivity spectra. The crossover point itself is displaced slightly on the frequency scale on the $\Sigma_a^{\mathrm{meas}}(\omega)$ and $\Sigma_b^{\mathrm{meas}}(\omega)$ curves, remaining near ω_g, but differing from the threshold frequency for interband transitions. We can state that virtually the entire weight of the intraband dynamic component is concentrated in the frequency range $0\leqslant\omega\leqslant\omega_C$, while the interband conductivity component lies higher on the frequency scale. The existence of the crossover point is confirmed by theoretical analysis of the evolution of optical conductivity of the planar structure with hole filling.[5] The crossover point is important for an analysis of integral characteristics of optical conductivity. For example, the integration of the measured spectrum between 0 and ω_C determines almost completely the integral intraband conductivity of a metallized crystal at a given doping level:

$$\int_0^{\omega_C}\Sigma^{\mathrm{meas}}(\omega)d\omega=S^{DM}, \tag{1}$$

while the integration from ω_C and higher gives the integral interband conductivity due to charge transfer between ions:

$$\int_{\omega_C}^{\omega_0}\Sigma^{\mathrm{meas}}(\omega)d\omega=S^{CT}, \tag{2}$$

where ω_0 is the upper limiting frequency of interband transitions. The interrelation between variations ΔS^{DM} and ΔS^{CT} of integral characteristics reflects most accurately the redistribution of optical conductivity spectra. The total contribution from interband and intraband transitions is determined by the well-known integral relation connecting optical conductivity with the plasma frequency ω_P of charge carriers:

$$\int_0^{\infty}\sigma(\omega)d\omega=\frac{\omega_P^2}{8}=\frac{\pi e^2 n}{2m^*}, \tag{3}$$

where e is the electron charge, m^* the effective mass, and n the volume concentration of charge carriers. In order to separate these contributions, we can use the spectral function $N(\omega)$ (the results of experiments are often presented in terms of this quantity):

$$N(\omega)=\frac{2m_0V_{\mathrm{cell}}}{\pi e^2F}\int_0^{\omega}\Sigma^{\mathrm{meas}}(\omega)d\omega. \tag{4}$$

Here m_0 is the mass of a free electron, V_{cell} the unit cell volume, F the number of structural units of the compound per unit cell, and $N(\omega)$ is equal to the number of electrons participating in optical transitions at frequencies $\leqslant\omega$. Let the hole band contain h holes per unit cell. As we approach the crossover frequency, the electrons creating the intraband current must ''actuate'' all the holes by virtue of (1), and hence $N(\omega)\to h$. Consequently, at the crossover frequency we have

$$N(\omega_C)=\frac{1}{Q^DF}\int_0^{\omega_C}\Sigma_{ab}^{\mathrm{meas}}(\omega)d\omega=h. \tag{5}$$

The quantity $\pi e^2/(2m_0V_{\mathrm{cell}})=Q^D$ (or $\hbar Q^D$) can be regarded as a measure of integral intraband conductivity of charge carriers. According to the results of experiments,[1–3] the position of the crossover point is $\hbar\omega_C=1.5$ eV for $La_{2-x}Sr_xCuO_4$ and $\hbar\omega_C=1.25$ eV for $YBa_2Cu_3O_{6+x}$. The values of the volume V_{cell} are 176 and 185 Å^3 for Y–Ba–Cu–O and La–Sr–Cu–O, respectively. The volumes of the primitive and unit cells for Y–Ba–Cu–O coincide, and hence $F=1$, while the volume of the primitive cell for La–Sr–Cu–O is half the volume of the unit cell, and hence $F=2$ for this compound.

In the general case, $h(x)$ for HTSC is determined by the number of doping impurity atoms x. The number of holes h for $YBa_2Cu_3O_{6+x}$ and $La_{2-x}Sr_xCuO_4$ is equal to x, which

determines the expected behavior of the spectral function $N_{ab}(\omega_C)=x$ in the ab plane. In actual practice, measurements made for the metallic phase of $La_{2-x}Sr_xCuO_4$ for $x\leqslant 0.1$ give $N_{ab}(\omega_C)=2x$,[1,3] while for the conductivity of the entire cell of $YBa_2Cu_3O_{6+x}$ ($x\leqslant 0.95$) the behavior $N_{ab}(\omega_C)=N_a(\omega_C)+N_b(\omega_C)=1.8x$ is observed.[1)2] Consequently, integral interband conductivity of ab planes of these materials increases at a rate 1.8–2 times higher than the expected rate. It can be expected that the relation $N_a(\omega_C)=(1/3)x$ is valid for the structure of CuO_2 in $YBa_2Cu_3O_{6+x}$ in the ortho–II phase ($x<0.65$) on account of the fact that a CuO_2 plane accommodates one third of the holes in a unit cell (the holes in the ortho–II phase are distributed almost uniformly among the three structures of the ab plane). In the ortho–I phase under moderate doping conditions with doubled number of chains ($0.65<x\leqslant 0.95$), a CuO_2 plane assimilates $(1/4)x$ holes, while the chain structure contains $(1/2)x$ holes.[18] Consequently, the expected behavior of the spectral function at the crossover frequency for this phase is $N_a(\omega_C)=(1/4)x$. However, the results of measurements of $\Sigma_a^{\text{meas}}=\sigma(CuO_2)$ demonstrate the dependence $N_a(\omega_C)=0.65x$ on the average for the two phases,[2] i.e., with the coefficient 2 and 2.5 times larger than the values expected for the ortho–II and ortho–I phases, respectively. Thus, we can say that HTSC cuprates under doping acquire excess holes determining the excess component of the spectral function for mobile charge carriers.

The emergence of an excess weight of the spectral function is regarded as the result of transport due to doping of free (predominantly copper) states from the upper to the lower band.[4] Following these ideas, we assume that the upper band of the dielectric phase contains a certain number h_{v0} of virtual holes (predominantly of the d-type) which ''store'' integral interband conductivity $h_{v0}Q^{CT}$, where Q^{CT} is the minimum value of integral interband conductivity. During doping, this stored integral conductivity is transferred due to a transition of virtual holes to the system for real holes.

A transition of a virtual hole occurs along the copper–oxygen link of length a_0, which is similar to a transition of an electron from oxygen to copper, resulting in the generation of a hole in the valence band. Hence such a transition corresponds to the minimum value of integral interband conductivity is e^2/ha_0, where h/e^2 is the resistance quantum. In this case, the minimum value of the integral interband conductivity is $\hbar Q^{CT}=(e^2/ha_0)\hbar\omega_g$, where $\hbar\omega_g$ is the gap excitations energy. The value of $\hbar Q^{CT}=3000\ \Omega^{-1}\ \text{cm}^{-1}\ \text{eV}$ is for $YBa_2Cu_3O_{6+x}$ ($a_0=1.9$ Å, $\hbar\omega_g=1.5$ eV), while $\hbar Q^{CT}=3330\ \Omega^{-1}\ \text{cm}^{-1}\ \text{eV}$ is for $La_{2-x}Sr_xCuO_4$ ($a_0=1.92$ Å, $\hbar\omega_g=1.65$ eV). A transition of virtual holes from the upper to the lower band can occur only under certain conditions. In a Hubbard system with pure d-bands, the emergence of holes in the lower band itself triggers the transfer of integral conductivity for any value of the parameter U/t, where U is the Hubbard repulsion energy and t the interband interaction integral. In particular, an excess weight of spectral function emerges even for $U/t=\infty$ and has doubled coefficient ($N=2x$).[4] The upper and lower bands in real HTSC systems are formed due to mixing of p-orbitals of oxygen with d-orbitals of copper. Real HTSC are rather systems with the $p-d$ charge transfer than Hubbard systems with $d-d$ splitting. In such a situation, the pumping of interband conductivity into intraband conductivity is determined by the degree of hybridization between p- and d-states and by the width of the optical gap with charge transfer. Let us consider two limiting cases that can be observed in such a system.

We first assume that all the holes in the metallic phase are pure p-holes forming a p-network of current, $t_{pp}\neq 0$, and hybridization does not take place ($t_{pd}=0$). In this case, the transport of interband conductivity is forbidden,[4] and hence the integral intraband conductivity and the spectral function are determined only by the value of Q^D:

$$\frac{1}{F}\int_0^{\omega_C}\Sigma^{\text{meas}}(\omega)d\omega=Q^Dx, \tag{6}$$

where $x=x_p$ ia the number of oxygen holes. The presence of hybridization ($t_{pd}>0$) allows the transport of interband conductivity.[4] This leads to the other limiting case in which the transferred integral conductivity $(h_{v0}-h_v)Q^{CT}$ determined completely the integral conductivity $Q^{CT}x$ of real holes, i.e., the relation $x+h_v=h_{v0}$ is observed under doping of the metal. In this case, the results of measurements must show that

$$\frac{1}{F}\int_0^{\omega_C}\Sigma^{\text{meas}}(\omega)d\omega=Q^{CT}x,$$

$$N(\omega_C)=\frac{Q^{CT}}{Q^D}\,x. \tag{7}$$

Here $x=x_{pd}$ defines the number of weakly hybridized holes which are predominantly of the d-type. In the general case, the system can be in the mixed state, in which each group of charge carriers has its own mobility, i.e.,

$$N(\omega_C)=x_p+\frac{Q^{CT}}{Q^D}\,x_d, \tag{8}$$

and the relation between x_p and x_d changes upon a variation of the total number x of hole carriers and the degree of hybridization. It should be noted in this connection that the metallization with the widest band corresponds to the maximum number of light oxygen p-holes since pure d-holes are completely localized. The factor Q^{CT}/Q^D in (7) and (8) determines the excess weight of the spectral function. Thus, the parameter Q^{CT}/Q^D introduced by us and equal to the ratio of two integral conductivity ''quanta'' is an important characteristic of spectral redistribution. The parameter $Q^{CT}/Q^D=1.75$ for $YBa_2Cu_3O_{6+x}$, while for $La_{2-x}Sr_xCuO_4$ it is equal to 2.1.

In order to find out which of the limiting cases (6) or (7) is closer to a given HTSC system, we must analyze the frequency dependences of the function $N(\omega)$. In the most general case, the following two scenarios of the behavior of $N(\omega)$ for an HTSC under doping, which are shown schematically in Fig. 1a and 1b, are possible. Let us first consider Fig. 1a demonstrating the behavior of $N(\omega)$ typical of $La_{2-x}Sr_xCuO_4$ ($x\leqslant 0.1$). Starting from the threshold frequency ω_g, curve *1* in this figure describes the $N(\omega)$

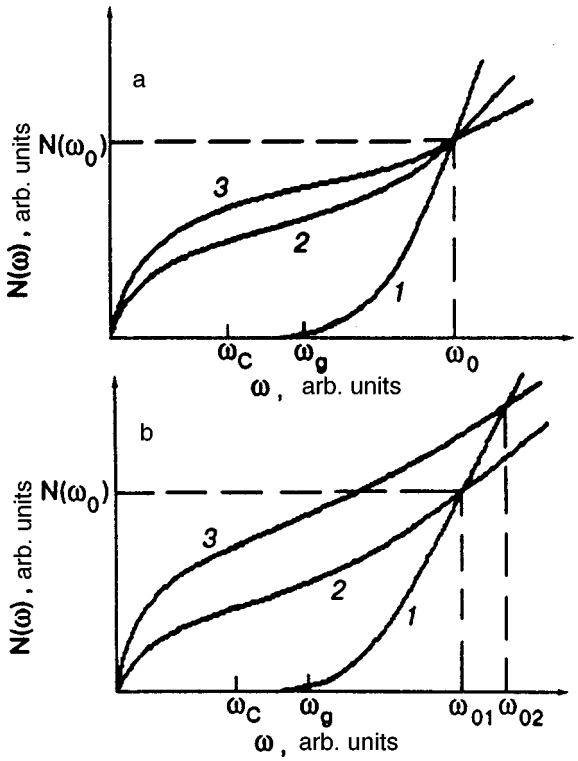

FIG. 1. Schematic diagram illustrating two typical types of behavior of the spectral function $N(\omega)$ measured in HTSC materials.

dependence for an insulator. The frequency ω_0 corresponds to the upper boundary of interband transitions, and hence the value of $N(\omega_0)$ gives the number of electrons participating in these transitions. Since one electron must go over to the upper band under the action of light, $N(\omega_0)=1$. In experiments with $La_{2-x}Sr_xCuO_4$, the value of $N(\omega_0 \simeq 3.2\ \text{eV}) = 0.5$, indicating that m_0 in expression (4) should be replaced by $2m_0$. In other words, an electron with the doubled free mass must participate in interband transitions. (in the insulator $YBa_2Cu_3O_{6+x}$, the value of $N(\omega_0 \simeq 3.2\ \text{eV}) = 1$.) In the case of sample metallization, the dependences $N(\omega)$ behave like curves *2* and *3*. The peculiarity in the behavior of the spectral function $N(\omega)$ upon an increase in x is that all the curves intersect at the same point $\omega=\omega_0$ irrespective of the doping level. Such a metallization indicates that the sum

$$\frac{1}{FQ^D}\int_0^{\omega_C}\Sigma^{\text{meas}}(\omega)d\omega+\frac{1}{FQ^D}\int_{\omega_C}^{\omega_0}\Sigma^{\text{meas}}(\omega)d\omega = N(\omega_0)=\text{const}, \tag{9}$$

is conserved for any doping level, and

$$S^{DM}+S^{CT}=\text{const}. \tag{10}$$

in accordance with (1) and (2). Consequently, the increase in the integral intraband conductivity of a metal upon an increase in the doping level in the case presented in Fig. 1a is determined by the decrease in the integral interband conductivity (component with charge transfer):

$$\Delta_x S^{DM} = -\Delta_x S^{CT}. \tag{11}$$

Consequently, the behavior of the spectral function must obey the limiting relation (7) in the case when the intraband dynamic component is determined by the *d*-component of the spectrum. The $N(\omega)$ curves measured in experiments with $La_{2-x}Sr_xCuO_4$ behave exactly as shown in Fig. 1a. The independence of $N(\omega_0)$ of x is preserved in the doping region from the beginning of metallization up to the indices $x=0.1$.[1,3] According to the results obtained by Tajima,[3] the interband and interband components increase simultaneously for $x>0.1$, i.e., condition (11) is violated in this case.

In experiments with doping, e.g., for $YBa_2Cu_3O_{6+x}$ with $x \geqslant 0.6$, another behavior of $N(\omega)$ illustrated in Fig. 1b can be observed. As x increases, the value of $N(\omega_0)$ does not remain unchanged, and each $N(\omega)$ curve has its own point of intersection with curve *1* of the dielectric phase. Such a pattern indicates that the intraband component is formed only partly at the expense of the interband component during doping. Consequently, the system rather corresponds to the mixed state (8).

The subsequent detailed analysis of experimental data on the frequency behavior of $N(\omega)$ will prove that the state of the system depends on the doping index, and $YBa_2Cu_3O_{6+x}$ as well as $La_{2-x}Sr_xCuO_4$ evolve upon an increase of x from the state (7) determined by the interband contribution to the state (6) with a complete loss of the effect of correlated redistribution of spectra.

Let us return to the limiting relation (7) and try to obtain an explicit form of the spectral function for this case on the basis of the model of existence of virtual holes. If the upper band contains one monoenergetic ''gap''-type hole, its conductivity along the Cu–O bond is $\sigma=Q^{CT}/\omega_g$. A virtual hole may has a spectral composition, but we shall assume that its spectral composition is of the Drude type, but is shifted by a certain frequency Ω since this hole determines the emergence of the intraband component in the metal:

$$\sigma_v(\omega)=\frac{Q^{CT}\Gamma}{\Gamma^2+(\Omega+\omega)^2}\,h_v \equiv \sigma_{v0}(\omega)h_v\,. \tag{12}$$

Here h_v is the number of virtual holes in the upper band and Γ their attenuation. Since holes are of the ''over-the-gap'' type, the values of Γ and Ω must be comparable with ω_g. We choose $\Gamma=\Omega=\omega_g/2$ since the chemical potential in the dielectric phase lies at the middle of the optical gap. Ultimately, the choice of the model spectrum in the form (12) and of the quantities Γ and Ω is justified by good agreement between the results obtained by using (12) and the experimental data for the integral spectrum and for the frequency dependence of intraband conductivity. It is sufficient to note here that the relation $\sigma(0)=Q^{CT}/\omega_g$ holds, as before, for a hole in the lowermost state. If a solitary hole has the spectral composition $\sigma_{v0}(\omega)$, the integral conductivity $\int\sigma_{v0}(\omega)d\omega$ is transferred to the valence band. We require that a hole carries the minimum value of integral conductivity Q^{CT} along the Cu–O bond in the frequency range from $\omega=0$ to $\omega=\omega_C$. For this purpose, we must make the substitution $\sigma'_{v0}=\sigma_{v0}/\beta$, where β is the normalization factor, so that

$$\int_0^{\omega_C}\sigma'_{v0}(\omega)d\omega=Q^{CT}.$$

The value of $\beta=0.45$ ($\hbar\omega_C=1.5$ eV, $\hbar\omega_g=1.65$ eV) for $La_{2-x}Sr_xCuO_4$ and $\beta=0.42$ ($\hbar\omega_c=1.25$ eV, $\hbar\omega_g=1.5$ eV) for $YBa_2Cu_3O_{6+x}$. If x holes go over to the valence band, the complete pumping of the interband conductivity indicates that

$$\frac{1}{F}\int_0^{\omega}\Sigma^{\text{meas}}(\omega)d\omega=\frac{x}{\beta}\int_0^{\omega}\sigma_{v0}(\omega)d\omega$$

$$=\frac{xQ^{CT}}{\beta}\arctan\frac{\omega}{\omega+\omega_g}$$

and

$$N(\omega)=x\frac{Q^{CT}}{\beta Q^{D}}\arctan\frac{\omega}{\omega+\omega_g}. \tag{13}$$

At the crossover frequency $\omega=\omega_C$, these relations are transformed into (7).

In the dielectric phase, a certain number of holes h_{v0} ''store'' the integral interband conductivity $h_{v0}Q^{CT}$, which must be equal to the integral conductivity with charge transfer measured for the insulator:

$$\frac{1}{F}\int_{\omega_g}^{\omega_0}\Sigma^{\text{meas}}(\omega)d\omega=Q^{D}N(\omega_0)=h_{v0}Q^{CT}.$$

For example, it was mentioned above that $N(\omega_0)=0.5$ for $La_{2-x}Sr_xCuO_4$ with $m^*=m_0$. Consequently, the dielectric phase in the model under investigation corresponds to the number $h_{v0}=0.25$ of virtual holes. In the case of doping, the relation $h_v+x=0.25$ holds in the CuO_2 plane of the system $La_{2-x}Sr_xCuO_4$ by virtue of relation (10).

COMPARISON WITH EXPERIMENTAL RESULTS

$La_{2-x}Sr_xCuO_4$ system

The spectral function $N_{ab}(\omega)$ measured for $La_{2-x}Sr_xCuO_4$ single crystals characterizes the CuO_2 plane. The data on integration of the optical conductivity spectrum $\Sigma_{ab}^{\text{meas}}=\sigma(CuO_2)$ fit quite well into the dependence $N_{ab}(\omega_C)=2x$ in the range from the beginning of metallization to values of $x=0.1-0.12$ at which the maximum superconducting transition temperature is virtually attained. The critical values of T_c for $La_{2-x}Sr_xCuO_4$ single crystals are slightly lower than for a polycrystal and amount to $\simeq 25$ K.[1] The experimental behavior of the function is in very good agreement with the limiting relation (7): $N(\omega_C)=Q^{CT}/Q^{D}=2.1x$. If was emphasized above and will be additionally confirmed below that the emergence of intraband component in $La_{2-x}Sr_xCuO_4$ is due to the transfer of interband component. In units of integral interband conductivity $\hbar Q^{CT}=3330\ \Omega^{-1}\text{cm}^{-1}$ eV, the system behaves as follows under doping:

$$\frac{1}{2Q^{CT}}\int_0^{\omega_C}\Sigma_{ab}^{\text{meas}}(\omega)d\omega=\frac{Q^{D}}{Q^{CT}}N_{ab}(\omega_C)=x.$$

For the doping level $x=0.1$, this means that about 300 Ω^{-1} cm^{-1} eV (approximately 10 Ω^{-1} cm^{-1} eV per degree of the superconducting transition temperature) are ''pumped'' to the hole band of CuO_2.

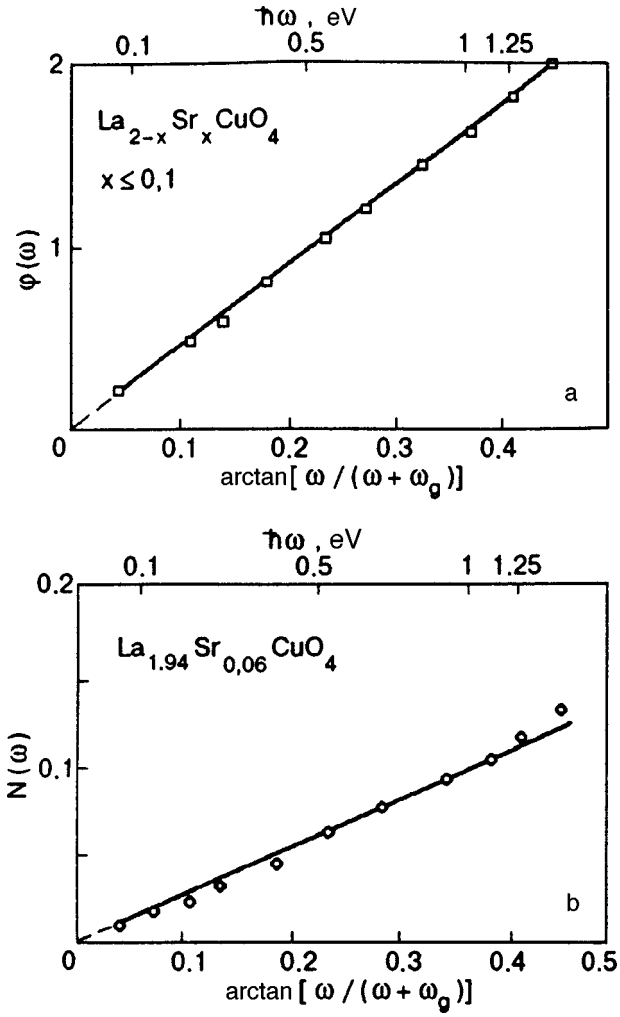

FIG. 2. Behavior of the function $\varphi(\omega)=(Q^{CT}/\beta Q^{D})\arctan[\omega/(\omega+\omega_a)]$ (a) and the spectral function $N(\omega)$ (13) (b) for La-based single crystal in the doping range $x\leqslant 0.1$. Symbols correspond to the experimental data obtained in Ref. 1 and the results of their processing.

A meticulous analysis of the experimental dependence of $N_{ab}(\omega_C)$ on x (see Fig. 3 in Ref. 3) shows that the behavior of $N_{ab}(\omega_C)$ changes significantly upon an increase in the doping level to the region $x>0.1$. In the interval $x\simeq 0.1-0.2$, where the superconducting transition temperature is virtually constant according to the phase diagram, the dependence is of the conventional noncorrelated nature: $N_{ab}(\omega_C)\simeq x$. Finally, for $x>0.2$, when the value of T_c decreases, $N_{ab}(\omega_C)$ is virtually independent of x.

A comparative analysis of the spectral relation (13) with experimental data on the frequency dependence $N_{ab}(\omega)$ is carried out as follows. Relation (13) can be written in the general form as $N(\omega)=x\varphi(\omega)$. For some frequencies ω' in the range 0.06–1.5 eV, the $N_{ab}(\omega')$ curves were plotted from the experimental data on $N_{ab}(\omega)$ as a function of x in the region $x\leqslant 0.1$ (see Fig. 3 from Ref. 1). The values of the function $\varphi(\omega')$ were determined from the slope of the obtained straight lines. Figure 2a shows the obtained values of φ as a function of $\arctan(\omega/(\omega+\omega_g)$. It can be seen that all the points characterizing the doping range to $x\leqslant 0.1$ fit into a single straight line whose slope is equal to 4.4. According to

(13), the slope of the straight line $\varphi(\omega)$ in this coordinates must be $Q^{CT}/\beta Q^{D}=4.65$. The agreement should be considered as good. Figure 2b shows directly the behavior of $N_{ab}(\omega)$ as a function of $\arctan(\omega/(\omega+\omega_g)$ for $x=0.06$. The straight line in the figure has a slope $\simeq 0.27$ which coincides with the value 0.28 obtained from (13) for this value of x. Figures 2a and 2b prove that the transfer of the integral interband conductivity completely determines the integral intraband conductivity of mobile charge carriers in the entire frequency range $\omega \leqslant \omega_C$. The asymptotic tendency of the straight lines in Figs. 2a and 2b to zero coordinate indicates the absence of an appreciable contribution to integral conductivity of a component other than the wide-band component determined by the transfer of ''over-the-gap'' excitations to the hole band of charge carriers in the doping range $x \leqslant 0.1$. It can be seen from Figs. 2a and 2b that this wide-band component occupies the spectral region from visible to $\omega=0$, where the absolute value of conductivity determines the static resistance of the ab plane. The system is in a state close to the limiting case (7), in which mobile holes are predominantly of the d-type. In a narrow band of d-type carriers, polaron effects can easily develop. An analysis of experimental results of thermoelectric and optical measurements leads to the conclusion[19,20] concerning the existence of polarons in $La_{2-x}Sr_xCuO_4$ for $x \leqslant 0.1$, the interaction between which is enhanced upon an increase in the number of charge carriers and becomes especially strong for $x>0.1$.[19]

A quite different situation is observed in the doping range $x \simeq 0.1-0.2$, in which the ''pumping'' of interband conductivity ceases, and a narrow conductivity peak with the center at zero frequency, which should be classified as a Drude peak, rises sharply in the measured spectra $\Sigma_{ab}^{\text{meas}}(\omega)$. Figure 3a demonstrates the behavior of $N(\omega)$ as a function of $\arctan(\omega/(\omega+\omega_g)$ for $x=0.2$, which is calculated by using the results obtained by Uchida *et al.*[1] A clearly manifested deviation from the functional dependence (13), which is especially strong in the low-frequency range, is observed. The conductivity for classical Drude charge carriers has the form

$$\sigma_D(\omega)=\frac{1}{4\pi}\frac{\omega_P^2\Gamma_0}{\omega^2+\Gamma_0^2}, \tag{14}$$

where the attenuation Γ_0 and the plasma frequency ω_P can be regarded as independent of frequency. We can easily find the spectral function of the classical Drude spectrum (14):

$$N(\omega)=\frac{2x}{\pi}\arctan\frac{\omega}{\Gamma_0}. \tag{15}$$

In Fig. 3b, the experimental data on $N_{ab}(\omega)$ obtained for $x=0.2$[1] are presented as a function of $\arctan(\omega/\Gamma_0)$ with $\hbar\Gamma_0=0.3$ eV, which is typical for strong doping region.[1–3,21] A good agreement with the frequency dependence (15) in the simple Drude model is observed up to the frequency $\hbar\omega=1$ eV. The slope of the straight line in the figure is 0.12, which virtually coincides with the value 0.127 following from (15). Thus, the ''pumping'' of interband conductivity into intraband ceases when the wide-band non-Drude spectrum of charge carriers is transformed to a considerable extent into the Drude spectrum, and the system becomes a non-

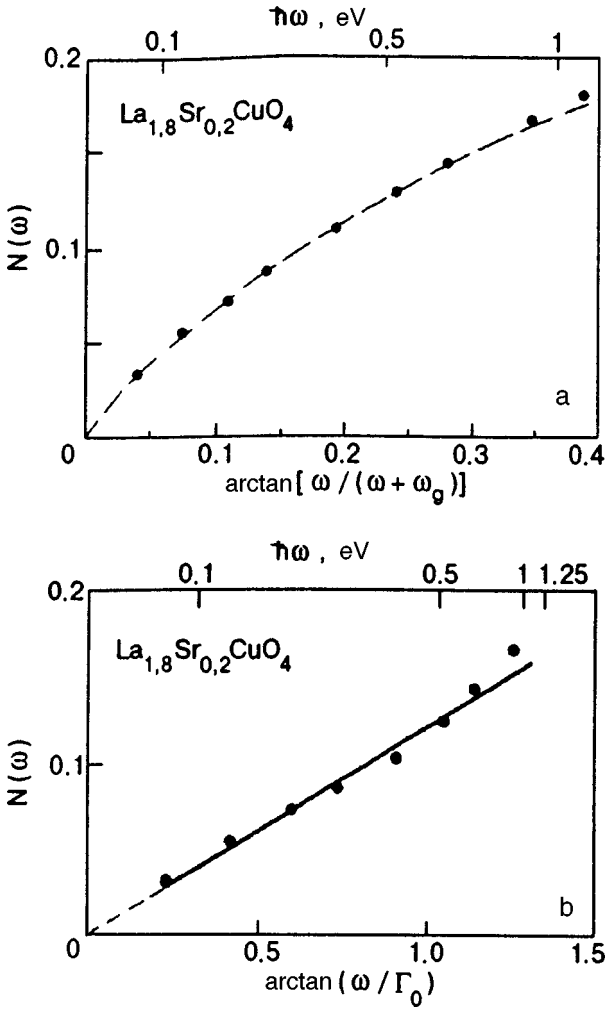

FIG. 3. Behavior of the spectral function $N(\omega)$ according to (13) (a) and in the classical Drude model (15) (b) for La-based single crystal in the overdoped region. Symbols correspond to the experimental data obtained in Ref. 1.

correlated metal. The CuO_2 plane under these conditions is close to the other limiting state (6), in which wide-band oxygen p-holes play the role of charge carriers. Subsequent metallization of the CuO_2 plane, which enhances the Drude contribution, leads only to complete loss of superconductivity for $x>0.2$.

It is interesting to compare the behavior of the spectral function under doping of $La_{2-x}Sr_xCuO_4$ and $La_{2-x}Sr_xNiO_4$. The addition of nickel to a La-based crystal lowers its metallization level, which is manifested, for example, in a decrease in the reflection coefficient in the MIR region below the plasma frequency $\hbar\omega_P \simeq 1$ eV.[22] The pure nickel system $La_{2-x}Sr_xNiO_4$ is an insulator, and the behavior of the spectral function under doping follows the law $N(\simeq 1\text{ eV})=x$,[3] indicating the absence of integral transfer of interband conductivity to the valence band. As a result, the charge carriers appearing in the valence band due to doping remain localized, and the intraband conductivity spectrum contains only a static MIR-band with a peak near 1 eV. The absence of a correlated redistribution of the spectrum in $La_{2-x}Sr_xNiO_4$ can be attributed to a very weak mixing of the $O^{2-}Cu^{2+}$

states of the valence band with the $O^{1-}Cu^{1+}$ states of the upper band. This is manifested in a high value of optical gap width in HTSC samples containing Ni, which attains the value of $E_g = 4$ eV in La_2NiO_4.[3] The suppression of the interband conductivity transfer upon an increase in E_g also follows from theoretical calculations.[4]

Metallization in $La_{2-x}Sr_xCuO_4$ is accompanied (caused) by the ''pumping'' of interband conductivity, and the intraband d-component becomes dynamic: an increase in the doping level in the MIR region broadens the conductivity band which is shifted from the initial position $\simeq 0.5$ eV for $x \simeq 0.02$ towards low frequencies. For $x > 0.1$, this wide-band d-component is transformed into a Drude peak predominantly for p-holes. The evolution of the spectrum considered above reflects the enhancement of hybridization of p- and d-holes in the ground state, but the reason behind such a scenario of metallization is the mixing of ''over-the-gap'' excitations of the upper band with the ground state.

$YBa_2Cu_sO_{6+x}$ system

The 1–2–3 system is a complicated object for an analysis of spectral redistribution due to the presence of a chain structure and the phase transition ortho–II→ortho–I near $x = 0.65$. The spectral function for the two phases has the dependence $N_{ab}(\omega) = 1.8x$ on the average over the entire unit cell, while $N_a(\omega) = 0.65x$ for the CuO_2 lane. In Ref. 15, polarization measurements of $\Sigma_a^{\text{meas}}(\omega)$ and $\Sigma_b^{\text{meas}}(\omega)$ were made for perfect single crystals with $x = 0$, 0.2, 0.39, 0.57, 0.71, and 0.91, but the data were not processed to obtain $N(\omega)$. Using Fig. 3 and the results obtained by Zibold *et al.*,[15] we carried out an independent analysis of the data which led to the following conclusions. For the ortho–II phase for $x \leqslant 0.57$, the spectral function follows the law $N_{ab}(\omega_{u.c.}) = (2-2.2)x$. A jump in the spectral function by $\Delta N_{ab} \simeq 0.2$ due to the doubling of the number of chains upon a transition to the ortho–I phase is clearly seen at $x = 0.65$ (a jump of the same magnitude is observed for the spectral function of the chain plane CuO_x). The results of experiments[2,15] on doping of the ortho–I phase fit into the dependence $N_{ab} \approx 1.5x$. Consequently, the value of $N_{ab}(\omega_C)$ for $x = 1$ is equal to 1.75–1.8, which is in accord with the above-mentioned value of 1.8 from Ref. 2. In the units of integral interband conductivity, $\hbar Q^{CT} = 3000\ \Omega^{-1}\ \text{cm}^{-1}$ eV, which means that for $x = 1$, when one hole appears in the unit cell, we have

$$\frac{1}{Q^{CT}} \int_0^{\omega_C} \Sigma_{ab}^{\text{meas}}(\omega)\, d\omega = \frac{Q^D}{Q^{CT}} N_{ab}(\omega_C) \simeq 1,$$

since the value of the parameter $Q^{CT}/Q^D = 1.75$ for $YBa_2Cu_3O_{6+x}$. Consequently approximately $30\ \Omega^{-1}\ \text{cm}^{-1}$ eV are ''pumped'' into the intraband conductivity of $YBa_2Cu_3O_7$ for the ab plane per degree of the superconducting transition temperature ($\sim 10\ \Omega^{-1}\text{cm}^{-1}$ eV/K for each of the three structures on the ab plane, which is equal to the corresponding value for the CuO_2 plane for $La_{2-x}Sr_xCuO_4$).

It was mentioned above that the transfer of interband conductivity in the $YBa_2Cu_3O_{6+x}$ system determines the intraband conductivity only partly. In order to separate the contribution of interband conductivity, show the $N(\omega)$ curves for the CuO_2 plane in Fig. 4a, plotted in accordance with relation (13), as functions of $\arctan[\omega/(\omega+\omega_g)]$ for $x = 0.6$ and $\simeq 0.95$. The curves are plotted by using the values of $N_a(\omega)$ measured for twinless crystals.[1] A good agreement with the functional dependence (13) is observed in a wide energy range from 0.07 to 1.25 eV. The slopes of the straight lines are 0.85 and 1.1 for $x = 0.6$ and 0.95, respectively. The values of the slopes are in satisfactory agreement with the values $(1/3-1/4)xQ^{CT}/\beta Q^D$ of expression (13), where the

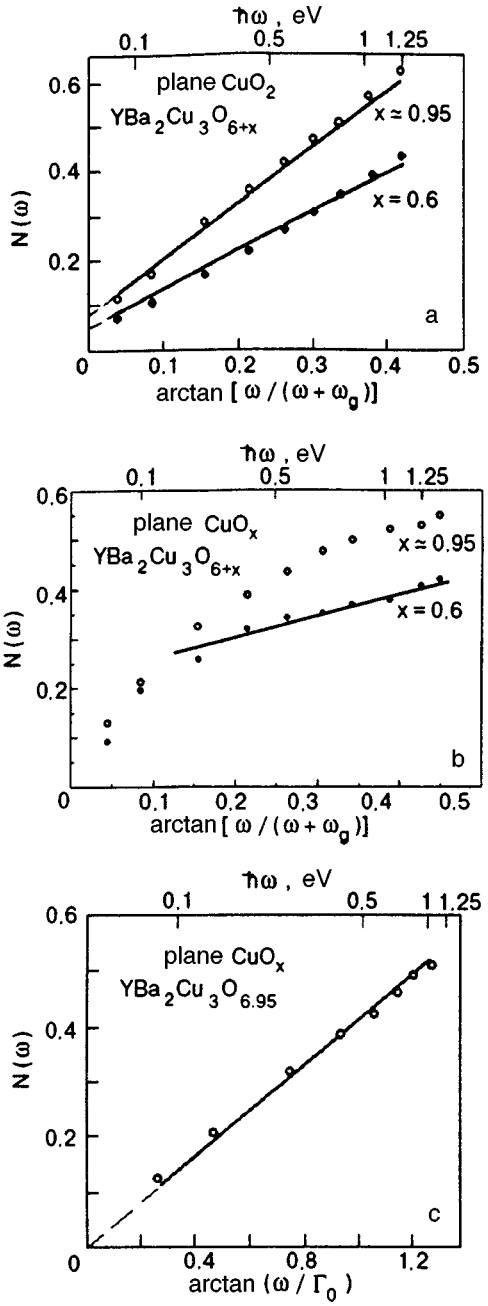

FIG. 4. Behavior of the spectral function $N(\omega)$ (13) of the CuO_2 plane (a), chain plane CuO_x (b), and in the classical Drude model (15) for the chain plane CuO_x (c) in Y-based single crystals with different doping indices. Symbols correspond to experimental results obtained in Ref. 2.

factor (1/3–1/4) takes into account partial population of a single CuO_2 plane by holes in the ortho–II and ortho–I phases. For example, the expected value of the slope is 0.83 for $x=0.6$ and ~ 1 for $x=0.95$. At the same time, the straight lines in Fig. 4a, in contrast to the situation with $La_{2-x}Sr_xCuO_4$, do not tend asymptotically to zero, thus demonstrating the existence of another integral contribution near zero frequency, which is not associated with the transfer of interband conductivity. Consequently, the CuO_2 plane in $YBa_2Cu_3O_{6+x}$ is in the mixed state (8) with two groups of coexisting charge carriers of the p- and d-type. However, the contribution of the low-frequency component to the total integral conductivity is small and is determined by a narrow Drude peak for p-holes.[2)] It follows from Fig. 4a that the ratio $N(0)/N(\omega_C)\simeq 1/6$ is small even in the region of strong doping ($x\simeq 0.95$) and decreases with the doping level. Thus, for the CuO_2 plane in $La_{2-x}Sr_xCuO_4$ ($x\leqslant 01$) and $YBa_2Cu_3O_{6+x}$ ($x\leqslant 0.95$) in the doping range in which the superconducting transition temperature increases, the integral intraband conductivity is mainly determined by the non-Drude component of the spectrum. In turn, this wide-band d-component owes its origin entirely to the intraband component of ''over-the-gap'' excitations.

The example with $La_{2-x}Sr_xCuO_4$ shows that the slowing down of increase in the superconducting transition temperature and the loss of superconductivity are associated with the formation of the Drude peak for p-carriers, in which the spectral weight of conductivity is concentrated. The entire transformation of the conductivity spectrum for $La_{2-x}Sr_xCuO_4$ takes place only in the CuO_2 plane. On the contrary, the integral spectrum of CuO_2 in $YBa_2Cu_3O_{6+x}$ is mainly determined by the d-component (see Fig. 4a) even for $x=0.95$ at the threshold of the overdoping mode with the loss of conductivity ($x>0.95$). The result that the chain structure CuO_x of $YBa_2Cu_3O_{6+x}$ rather than the CuO_2 plane is responsible for the formation of a high-intensity Drude peak and the loss of correlated redistribution of spectra appears as quite unexpected.

Figure 4b shows the results illustrating the behavior of the spectral function $N_{b-a}(\omega)$ of the chain structure as a function of $\arctan[\omega/(\omega+\omega_g)]$ for $x=0.6$ and $\simeq 0.95$ ($T_c=91$ K). The points in this figure were obtained from the values of $N_b(\omega)-N_a(\omega)$ from Ref. 2. It can be seen that the CuO_x structure is in the mixed state (8) for $x=0.6$. For $x=0.95$, a noticeable deviation from the frequency dependence (13) is observed in the entire frequency range. The values of $N_{b-a}(\omega)$ for $x=0.95$ are shown in Fig. 4c as a function of $\arctan(\omega/\Gamma_0)$ in the simple Drude model (15) with the attenuation $\hbar\Gamma_0=0.3$ eV. Up to 1 eV, the experimental points fit into the straight line whose slope is 0.4. In the ortho–I phase, 50% of holes are in the chain structure CuO_x, and hence the expected value of the slope of the straight line (15) for $x=0.95$ is 0.3. The qualitative and quantitative agreement speaks in favor of the statement that p-metallization of chains rules out the transport of interband conductivity and leads to superconductivity loss in the entire unit cell of $YBa_2Cu_3O_{6+x}$. It should be noted in this connection that IR studies of the optical conductivity of perfect $YBa_2Cu_3O_{6+x}$ single crystals with $x=0.95$ proved the existence of chains with a high metal-type conductivity $\simeq 2000\ \Omega^{-1}\ \mathrm{cm}^{-1}$, which are ordered properly to form a two-dimensional structure.[23] It was also shown[23] that the superconducting condensate exists not only in the CuO_2 plane, but also in the CuO_x structure, i.e., the superconductivity is not induced in chains. It can be seen from Fig. 4b that an increase in the doping level from $x=0.6$ to 0.95 in the chains indeed leads to the emergence of dynamic-type conductivity spectra, which is typical of metals with superconducting properties: the spectrum is transformed from the d-component to the p-type Drude component as indicated by a straight line.[3)] We can expect that the intraband conductivity of CuO_x in the ortho–II phase with lower doping indices $x<0.6$ is determined by the d-component to a still greater extent. For this reason, the CuO_2 and CuO_x planes at the initial stage of metallization of the Y-based system, like CuO_2 planes in a La-based system, are apparently in the state (7) with dominating influence of interband excitations on integral intraband conductivity.

CONCLUSIONS

1. At the present time, two approaches, based on one- and two-component models, are used in analysis of the evolution of optical conductivity spectra for the metallic phase of HTSC in the range of intraband transitions. In the one-component model, the entire optical conductivity is defined by the anomalous Drude spectrum of free charge carriers, in which the plasma frequency and attenuation are functions of frequency:

$$\sigma^*(\omega)=\frac{\omega_P^2(\omega)\Gamma(\omega)}{4\pi[(\omega^2+\Gamma^2(\omega)]}. \tag{16}$$

In HTSC systems, we must introduce a complex memory function for interaction processes in view of long relaxation times for charge or spin perturbations, which are comparable with the time of free motion of electrons. This leads to the frequency dependence of effective mass $[\omega_P(\omega)\sim 1/m^*(\omega)]$ and attenuation. For example, the attenuation for a ''marginal Fermi liquid'' [25] follows a linear frequency dependence $\Gamma\sim\alpha\omega$ with the coefficient $\alpha=0.6$–1.2 depending on the type of HTSC material, its doping level and temperature.[26] A strong frequency dependence of effective mass can be traced only up to $\simeq 0.5$ eV, and $m^*\to m_0$ in the region of crossover frequency.[2,26]

The two-component model defines the optical conductivity of HTSC on the basis of a resultant combination of the classical Drude (14) and anomalous Drude spectra (16),[21,27,28] or the resultant combination of the Drude spectrum (14) and the Lorentz spectrum due to transitions of bound electrons[24,28]:

$$\sigma_{\mathrm{MIR}}=\frac{\omega^2 S^2\Gamma_{\mathrm{MIR}}}{4\pi[(\omega_0^2-\omega^2)^2+\omega^2\Gamma_{\mathrm{MIR}}^2]}. \tag{17}$$

Here $\hbar\omega_0\simeq 0.2$–1 eV is the resonant frequency of the Lorentz circuit (17), $S\simeq 1$, eV the oscillator force of the transition, and $\Gamma_{\mathrm{MIR}}\simeq 0.5$–$1$ eV the attenuation with values typical of HTSC.[24] The introduction of expression (17) in the analysis makes it possible to take into account localization effects

inherent in charge carriers at frequencies in the MIR spectral range. Naturally, various combinations of the above approaches are possible. The conductivity spectrum for interband transitions with charge transfer is defined by the Lorentz circuit (17) with the parameters $\hbar\omega_0 \simeq 2$ eV and $S,\Gamma \simeq 1-2$ eV. In the general case, several parameters determining (14), (16), and (17) have to be reconstructed and correlated with one another in order to determine evolutionary changes of the spectrum with doping, temperature, etc. from the measured values of $\Sigma^{\text{meas}}(\omega)$. This often leads to ambiguous results which also depend on the chosen model.

In the present research, the genesis of optical conductivity spectra in the case of doped HTSC is analyzed by using integral characteristics $\int\Sigma^{\text{meas}}(\omega)d\omega$. The integral spectrum of optical conductivity for the metallic phase S^{DM} in the range of intraband transitions was verified in the form of two components ($S^{DM}=S_p+S_d$) pertaining to two groups of coexisting charge carriers of predominantly p- and d-type. In the electron structure of HTSC materials, these carriers can be referred to the wide and narrow bands whose existence is confirmed in ARPES experiments[29] and is considered in detail in Ref. 13. The integral spectrum S_p describes the behavior of classical Drude carriers, while the integral spectrum S_d characterizes more localized d-carriers and is completely determined by ''pumping'' of integral interband conductivity S^{CT} to the hole band as a result of doping ($\Delta S_d = -\Delta S^{CT}$). Consequently, we can state that optical excitations with charge transfer in the given model participate in the formation of metallic properties of HTSC: the integral spectrum of the d-component is determined by the two most important parameters of interband conductivity, viz., the optical (dielectric) gap $\hbar\omega_g$ and the characteristic length a_0 of the Cu–O bond in the ab plane of HTSC materials. In the description of the frequency dependences of integral conductivity, the introduction of the ''gap'' attenuation $\Gamma=\omega_g/2$ for interband excitations was of primary importance. It should be noted in this connection that, according to preliminary analysis, the two-component model [the Drude spectrum (14) plus the ''gap'' spectrum (12)] makes it possible to describe such experimental data on $\Sigma_a^{\text{meas}}(\omega)$ and $\Sigma_b^{\text{meas}}(\omega)$ with an error smaller than 5% in the entire frequency range $\omega \leqslant \omega_C$.

2. A comparison of theoretical relations for integral conductivity with experimental results obtained for $La_{2-x}Sr_xCuO_4$ and $YBa_2Cu_3O_{6+x}$ in a wide frequency range up to 1.5 eV and for doping levels from the beginning of metallization to the loss of superconductivity confirms the existence of two groups of charge carriers with different degrees of localization and coupling with interband transitions. The integral characteristics of optical conductivity of these group of charge carriers are in dynamic equilibrium. At the doping stage, when the superconducting transition temperature increases, the intraband conductivity is mainly determined by the d-component emerging due to correlated transfer of ''over-the-gap'' interband excitations to the narrow hole band. An increase in the integral contribution from free Drude p-carriers, which are not associated with ''over-the-gap'' excitations, slows down the increase in the superconducting transition temperature and ultimately leads to the emergence of an ordinary noncorrelated metal with a loss of superconductivity. The dynamic equilibrium in $La_{2-x}Sr_xCuO_4$ sets in the CuO_2 plane, while in $YBa_2Cu_3O_{6+x}$ the superconductivity loss is associated with Drude metallization of the chain structure CuO_x.

The strong interrelation between interband excitations and hole carriers of essentially local nature is confirmed by optical experiments with heterogeneous $YBa_2Cu_3O_{6+x}$ films carrying a direct current.[30] In the current mode, when charge carriers are hurled to regions of spatial localization, the intensity of interband absorption increases (optical absorption behaves similarly upon a decrease in the doping level). When the current is terminated, and charge carriers are delocalized, the interband absorption decreases, which corresponds to an increase in the doping index with enhancement of p-metallization.

3. Thus, correlated redistribution of the optical conductivity spectra is observed in the range of the normal metallic phase of CuO_2 and CuO_x provided that the system contains localized (narrow-band) d-carriers. The integral interband conductivity is pumped just to the system of heavy d-carriers, but the interband transition channel is actuated due to a finite degree of $p-d$ hybridization with wide-band oxygen p-carriers. The integral conductivity of d-carriers in this case is determined by interband electron excitations with energies not smaller than the optical (dielectric) gap width in the electron structure of HTSC. With increasing hybridization (and the number of d-carriers), the absolute value of integral interband conductivity ''pumped'' to the hole band increases (by approximately 10 Ω^{-1} cm^{-1} eV per degree of superconducting transition temperature). The superconducting transition temperature increases accordingly. At the same time, enhancement of hybridization decreases the extent of localization and increases the number of wide-band light p-carriers (the narrow d-band at the Fermi level is blurred and merges with the wide p-band, which is accompanied with the filling of the dielectric gap). Since p-carriers are not associated with interband excitations, hybridization at a certain stage becomes a factor hampering a further increase in the superconducting transition temperature. As soon as one of oxygen–copper planes CuO_2 or CuO_x in a unit cell of HTSC goes over to a predominantly p-metallic state with the standard Drude spectrum of charge carriers, a noncorrelated metal with lost superconductivity is formed.

The author is grateful to I. Ya. Fugol for fruitful discussions of the problems considered in the present research.

*)E-mail: samovarov@ilt.kharkov.ua

1)For $YBa_2Cu_3O_{6+x}$ crystals with twin boundaries, $N_{ab}(\omega_C)\approx 0.9x$.[2] Multiplying the left- and right-hand sides of (4) by two, we find that the effective electron mass for these crystals must be increased approximately by a factor of two: $m_0 \to 2m_0, N_{ab}(\omega_C)\to 1.8x$.

2)A comparison of experimental data on the frequency behavior of intraband conductivity and the results obtained in the two-component model (the Drude component (14) and the ''gap'' component (12)) shows that $\hbar\Gamma_0 \simeq 400$ cm^{-1} for $x=0.95$.

3)According to Calvani and Lupi,[24] the dynamic nature of intraband component is also observed for doped superconducting Tl-, Bi-, and Nd-based HTSC samples.

[1] S. Uchida, T. Ido, H. Takagi *et al.*, Phys. Rev. B **43**, 7942 (1991).
[2] S. L. Cooper, D. Reznik, A. Kotz *et al.*, Phys. Rev. B **47**, 8233 (1993).
[3] S. Tajima, Appl. Supercond. **1**, 313 (1993).
[4] H. Eskes, M. B. J. Meinders, and G. A. Sawatzky, Phys. Rev. Lett. **67**, 1035 (1991).
[5] E. Dagotto, Rev. Mod. Phys. **66**, 763 (1994).
[6] L. D. Rotter, Z. Schlezinger, R. T. Collins *et al.*, Phys. Rev. Lett. **67**, 2741 (1991).
[7] I. Fugol, G. Saemann-Ischenko, V. Samovarov *et al.*, Solid State Commun. **80**, 201 (1991); I. Ya. Fugol, V. N. Samovarov, Yu. I. Rybalko, and V. M. Zhuravlev, Sverkhprovodimost: Fiz., Khim., Tekh. **4**, 109 (1991).
[8] H. L. Dewing and E. K. H. Salje, Supercond. Sci. Technol. **5**, 50 (1992).
[9] V. I. Kudinov, A. I. Kirilyuk, N. M. Kreines *et al.*, Phys. Lett. A **151**, 358 (1990).
[10] G. Nieva, E. Osgniguil, J. Guimpel *et al.*, Appl. Phys. Lett. **60**, 2159 (1992).
[11] Th. Pruschke, M. Jarrell, and J. K. Freericks, Adv. Phys. **44**, 187 (1995).
[12] I. Ya. Fugol and V. N. Samovarov, Fiz. Nizk. Temp. **22**, 1241 (1996) [Low Temp. Phys. **22**, 945 (1996)].
[13] E. A. Pashitskii, Fiz. Nizk. Temp. **21**, 995 (1995) [Low Temp. Phys. **21**, 763 (1995)].
[14] V. M. Loktev, Fiz. Nizk. Temp. **22**, 3 (1996) [Low Temp. Phys. **22**, 1 (1996)].
[15] A. Zibold, L. Widder, H. P. Geserich *et al.*, Physica C **212**, 365 (1993).
[16] S. L. Cooper, G. A. Thomas, A. J. Millis *et al.*, Phys. Rev. B **42**, 10785 (1990).
[17] G. Yu, C. Lee, D. M. Mihailovic *et al.*, Phys. Rev. B **48**, 7545 (1993).
[18] P. F. Wood and M. A. Abdel-Raouf, Phys. Rev. B **51**, 11773 (1995).
[19] J. B. Goodenough and J.-S. Zhou, Phys. Rev. B **49**, 4251 (1994).
[20] J. Lorenzana and L. Yu, Phys. Rev. Lett. **70**, 861 (1993).
[21] S. Tanaka, Physica C **169**, 271 (1991).
[22] S. Etemad, D. E. Aspnes, P. Barboux *et al.*, in Materials Research Society Meeting, Boston, MA, USA (1988).
[23] D. N. Basov, R. Liang, D. A. Bonn *et al.*, Phys. Rev. Lett. **74**, 598 (1995).
[24] P. Calvani and S. Lupi, Solid State Commun. **85**, 665 (1993).
[25] C. M. Varma, P. B. Littlewood, S. Schmitt-Rink *et al.*, Phys. Rev. Lett. **63**, 1996 (1989).
[26] A. V. Puchkov, D. N. Basov, and T. Timusk, Preprint to J. Phys. Cond. Mat. (1996).
[27] Y. Yagil, F. Baudenbacher, M. Zhang *et al.*, Phys. Rev. B **52**, 15582 (1995).
[28] M. A. Quijada, D. B. Tanner, F. C. Chou *et al.*, Phys. Rev. B **52**, 15485 (1995).
[29] D. S. Dessau, Z.-X. Shen, D. M. King *et al.*, Phys. Rev. Lett. **71**, 2781 (1993).
[30] V. N. Samovarov, Fiz. Tverd. Tela (St. Petersburg) **39**, 1747 (1997) [Phys. Solid State **39**, 1556 (1997)].

Translated by R. S. Wadhwa

On the effect of dislocation arrays on the superconducting transition temperature in HTSC

A. V. Gurevich

Applied Superconductivity Center, University of Wisconsin, Wisconsin, MA 53076, USA

É. A. Pashitskiĭ

Institute of Physics, National Academy of Sciences of the Ukraine, 252650 Kiev, Ukraine[*]

(Submitted June 22, 1998)
Fiz. Nizk. Temp. **24**, 1058–1062 (November 1998)

It is shown that arrays of edge dislocations with parallel Burgers vectors in the slip plane can lead to significant local changes in the transition temperature T_c of the deformed crystals of high-temperature superconductors. These changes are due to the redistribution of free charge carriers in the elastic strain fields of the ionic crystal lattice and a strong nonmonotonic dependence of T_c on the concentration of charge carriers if the characteristic length of dislocation arrays is much larger than the coherence length and screening radius. © *1998 American Institute of Physics.* [S1063-777X(98)00311-9]

INTRODUCTION

The superconducting transition temperature T_c of high-temperature superconductors (HTSC) based on cuprate metaloxide compounds (MOC) assumes nonzero values only in a very narrow range of concentrations n of free charge carriers (holes and conduction electrons) and varies nonmonotonically with n (according to a nearly parabolic law):[1,2]

$$T_c(n)=T_{cm}-A(n-n_m)^2, \tag{1}$$

where n_m is the value of n for which the transition temperature attains its maximum value T_{cm}. In this communication, we shall show that if the elastic stress fields in the vicinity of the structural defects of the ionic crystal lattice of layered cuprates of MOC vary on macroscopic scales much larger than the coherence length ξ_0 and screening radius r_S, the electroneutrality condition leads to spatial redistribution of charge carrier concentration $n(r)$ as well as considerable local variations of $T_c(r)$ in accordance with Eq. (1).

DEPENDENCE OF T_C ON THE STRAIN TENSOR ε_{ik}

Assuming a linear dependence between $n(r)$ and $\varepsilon_{ik}(r)$ in the theory of elasticity, we can present T_c in an anisotropic deformed crystal in the form of the following quadratic function of the strain tensor ε_{ik}:[3]

$$T_c=T_{c0}-C_{ik}\varepsilon_{ik}-Q_{ijkl}\varepsilon_{ij}\varepsilon_{kl}. \tag{2}$$

Here T_{c0} is the value of T_c in an undeformed crystal, Q_{ijkl} a tensor of rank four which is symmetric to transpositions of indices $i\rightleftarrows j$ and $k\rightleftarrows l$ $(i,j,k,l=x,y,z)$, and the diagonal components $C_{xx}=C_a$, $C_{yy}=C_b$ and $C_{zz}=C_c$ of the rank-two tensor C_{ik} along the principal crystallographic axes determine the variation of T_c as a result of a weak uniaxial deformation of the crystal. The quantities C_a, C_b, and C_c are connected with the derivative of T_c with respect to pressure in the direction of the corresponding axis of the crystal. For example, experiments on uniaxial compression (extension) in optimally doped single crystals of $YBa_2Cu_3O_{7-\delta}$ lead to the following results:[4]

$$\frac{\partial T_c}{\partial P_a}\approx -1.9[\mathrm{K/GPa}];\quad \frac{\partial T_c}{\partial P_b}\approx 2.2[\mathrm{K/GPa}];$$

$$\frac{\partial T_c}{\partial P_c}\approx 0, \tag{3}$$

where P_a, P_b and P_c denote the uniaxial pressure along **a**, **b**, and **c** axes, respectively. According to Meingast *et al.*,[5] this corresponds to values $C_a\simeq -220$ K, $C_b\simeq 315$ K, and $C_c\simeq 0$.

Opposite signs of C_a and C_b in monodomain YBCO crystals are associated with a strong anisotropy of their elastic and electronic properties in the ab plane owing to the presence of ordered $1D$ CuO chains along the **b**-axis, which play the role of the ''reservoir'' during doping of $2D$ CuO_2 cuprate layers by holes.

In crystals of $Bi_2Sr_2CaCu_2O_x$, which are practically isotropic in the ab plane, uniaxial deformations lead to the values[6]

$$\frac{\partial T_c}{\partial P_a}\approx 1.6[\mathrm{K/GPa}];\quad \frac{\partial T_c}{\partial P_b}\approx 2.0[\mathrm{K/GPa}];$$

$$\frac{\partial T_c}{\partial P_c}\approx -2.8[\mathrm{K/GPa}], \tag{4}$$

which corresponds to close values of C_a and C_b. However, the dependence of T_c on (isotropic) hydrostatic pressure P is weak $(\Sigma_i \partial T_c/\partial P_i\approx 0)$ due to different signs of the derivatives $\partial T_c/\partial P_i$ along different axes in both cases (YBCO and BSCCO). On the other hand, the effect of hydrostatic pressure on T_c in crystals of $HgBa_2Ca_2Cu_3O_x$ is quite strong, $(\partial T_c/\partial P_i\simeq 1$ K/GPa and hence the value of T_c increases to 160 K and beyond for $P\geqslant 10$ GPa.[7,8]

Turning to the quadratic dependence (2) of T_c on ε_{ik}, we note that the tensor Q_{ijkl} has 9 independent components in crystals with orthorhombic symmetry.[9] Confining the analysis to planar deformations in the layer plane, we are left with just four independent components of the tensor Q_{ijkl}, and formula (2) assumes the form

$$T_c = T_{c0} - C_a\varepsilon_{xx} - C_b\varepsilon_{yy} - Q_a\varepsilon_{xx}^2 - Q_b\varepsilon_{yy}^2 - Q_1\varepsilon_{xx}\varepsilon_{yy} - Q_2\varepsilon_{xy}^2. \quad (5)$$

In an isotropic crystal (in the ab plane), when $C_a = C_b = C$, $Q_a = Q_b = (1/2)Q_1$ and $Q_2 = 0$, the dependence of T_c on the dilatation $\varepsilon = \varepsilon_{xx} + \varepsilon_{yy}$ can be represented in the form

$$T_c = T_{c0} - C\varepsilon - (C\varepsilon)^2/4\Delta T_m, \quad (6)$$

where $\Delta T_m = T_{cm} - T_{c0}$, and the coefficients are chosen in such a way that the maximum value T_{cm} is attained for $\varepsilon_m = -2\Delta T_m/C$.

ELASTIC DEFORMATION AND T_c AROUND EXTENDED DISLOCATION ARRAYS

The components of the deformation tensor $\varepsilon_{ik}(r)$ around a linear edge dislocation parallel to the axis $\mathbf{c}\|\mathbf{z}$ have the form[10]

$$\varepsilon_{xx}(x,y) = -\frac{By[(3-2\sigma)x^2 + (1-2\sigma)y^2]}{4\pi(1-\sigma)(x^2+y^2)^2}; \quad (7)$$

$$\varepsilon_{yy}(x,y) = -\frac{By[(1-2\sigma)y^2 - (1+2\sigma)x^2]}{4\pi(1-\sigma)(x^2+y^2)^2}; \quad (8)$$

$$\varepsilon_{xy}(x,y) = -\varepsilon_{yx}(x,y) = \frac{Bx(x^2\text{-}y^2)}{4\pi(1-\sigma)(x^2+y^2)^2}, \quad (9)$$

where B is the length of the Burgers vector $\mathbf{B}$, and σ is Poisson's coefficient. For an infinite periodic chain of dislocations (dislocation wall) along the axis $\mathbf{b}\|\mathbf{y}$ with the same separation d between adjacent dislocations and the Burgers vector $\mathbf{B}\perp\mathbf{y}$, replacement of the coordinate y by $(y-nd)$ in Eqs. (6)–(8) and summation over n from $-\infty$ to $+\infty$ gives (cf. stress tensor in Ref. 10)

$$\varepsilon_+^{\perp}(x,y) \equiv \varepsilon_{xx}^{\perp}(x,y) + \varepsilon_{yy}^{\perp}(x,y) = -\frac{\varepsilon_a \sin(q)}{\cosh(p) - \cos(q)}; \quad (10)$$

$$\varepsilon_-^{\perp}(x,y) \equiv \varepsilon_{xx}^{\perp}(x,y) - \varepsilon_{yy}^{\perp}(x,y) = -\frac{2\varepsilon_b p \sinh(p)\sin(q)}{[\cosh(p) - \cos(q)]^2}; \quad (11)$$

$$\varepsilon_{xy}^{\perp}(x,y) \equiv -\varepsilon_{yx}^{\perp}(x,y) = \frac{\varepsilon_b p[\cosh(p)\cos(q) - 1]}{[\cosh(p) - \cos(q)]^2}; \quad (12)$$

where

$$\varepsilon_a = \frac{B(1-2\sigma)}{2d(1-\sigma)}; \quad \varepsilon_b = \frac{B}{4d(1-\sigma)};$$

$$p = \frac{2\pi x}{d}; \quad q = \frac{2\pi y}{d}. \quad (13)$$

It can be seen that for $x \gg d/2\pi$, all components ε_{ik} are exponentially small [$\sim\exp(-2\pi x/d)$] owing to mutual compensation (''annihilation'') of periodic sign-alternating stresses in adjacent dislocations.

The situation changes radically for a domain wall for which the Burgers vectors lie in the slip plane ($\mathbf{B}\|\mathbf{y}$) and whose deformation tensor components are defined as (cf. Ref. 10)

$$\varepsilon_+^{\parallel}(x,y) \equiv \varepsilon_{xx}^{\parallel}(x,y) + \varepsilon_{yy}^{\parallel}(x,y) = -\frac{\varepsilon_a \sinh(p)}{\cosh(p) - \cos(q)}; \quad (14)$$

$$\varepsilon_-^{\parallel}(x,y) \equiv \varepsilon_{xx}^{\parallel}(x,y) - \varepsilon_{yy}^{\parallel}(x,y) = -\frac{2\varepsilon_b}{\cosh(p) - \cos(q)} \times \left\{\sinh(p) - \frac{p[\cosh(p)\cos(q) - 1]}{\cosh(p) - \cos(q)}\right\}; \quad (15)$$

$$\varepsilon_{xy}^{\parallel}(x,y) = \frac{\varepsilon_b \sin(q)}{\cosh(p) - \cos(q)}\left[1 - \frac{p \sinh(p)}{\cosh(p) - \cos(q)}\right]. \quad (16)$$

It can be seen that the components $\varepsilon_{\pm}^{\parallel}$ are finite and constant for $|x| \to \infty$:

$$\lim_{|x|\to\infty} \varepsilon_+^{\parallel} = -\frac{B(1-2\sigma)}{2d(1-\sigma)} \operatorname{sgn} x,$$

$$\lim_{|x|\to\infty} \varepsilon_-^{\parallel} = -\frac{B \operatorname{sgn} x}{2d(1-\sigma)}, \quad (17)$$

owing to the summation of deformations of the same sign caused by individual dislocations, but have opposite signs on both sides of the dislocation wall (for $x>0$ and $x<0$). At the same time, the nondiagonal component $\varepsilon_{xy}^{\parallel} \to 0$ for $|x| \to \infty$. However, such an infinite dislocation wall has infinitely large elastic energy per unit length (along the dislocations) and is therefore unstable (disadvantageous from the energy point of view). Hence real crystals can contain metastable dislocation walls (arrays) of finite length, fixed at both ends by some obstacle (grain boundaries, interfaces, etc.). The dislocations are pushed back at the obstacles (stoppers) and hence their density increases in the vicinity of the obstacles.

It was shown in Refs. 9, 11, 12 that, in the continual approximation, the distribution of the dislocation density $S(y)$ in a linear dislocation array of length $2L$ subjected to an external pressure P (along the x-axis) is described by the expression

$$S(y) = \frac{N + Gy}{\pi\sqrt{L^2 - y^2}}, \quad (18)$$

where $N = N_+ - N_-$ is the difference in the number of dislocations with positive ($\mathbf{B}>0$) and negative ($\mathbf{B}<0$) directions of the Burgers vector $\mathbf{B}\|\mathbf{y}$), and $G = 2\pi P(1-\sigma)/\mu B$, μ being the shear modulus.

The components of the nonuniform strain tensor in the vicinity of such a dislocation array can be calculated by using the relation

$$\tilde{\varepsilon}_{ij}(x,y)=\int_{-L}^{L} dy' S(y')\varepsilon_{ij}\,(x,y-y'), \tag{19}$$

where ε_{ij} are defined by formulas (7)–(9) from which it follows that the integral (19) can be reduced to integrals of the type

$$I_k(x,y)=\int_{-L}^{L} dy' \,\frac{(1+gy')[A(y-y')^2+Bx^2]}{\sqrt{L^2-y'^2}[x^2+(y-y')^2]^k}, \tag{20}$$

in which $g=G/N$, and $k=1,2$. Using the change of variables $y'=L\cos(t)$, we can easily show that the integrals I_1 and I_2 are presented in terms of the real and imaginary parts and their first derivatives of the complex function

$$F(z)=\int_0^{\pi}\frac{dt}{z+\cos(t)}=\frac{\pi\ \mathrm{sgn}\ z}{\sqrt{z^2-1}}, \tag{21}$$

where $z=\eta+i\zeta$, $\eta=x/L$ and $\zeta=y/L$. As a result of simple computations, we obtain

$$\tilde{\varepsilon}_{xx}+\tilde{\varepsilon}_{yy}=-\varepsilon_1(1-2\sigma)\mathrm{Im}\{F(z)(1-gz)\}; \tag{22}$$

$$\tilde{\varepsilon}_{xx}-\tilde{\varepsilon}_{yy}=-\varepsilon_1\ \mathrm{Im}\left\{\left(2-z\,\frac{\partial}{\partial z}\right)[F(z)(1-gz)]\right\}; \tag{23}$$

$$\tilde{\varepsilon}_{xy}=\frac{\varepsilon_1}{4}\,\mathrm{Re}\left\{\left(2-z\,\frac{\partial}{\partial z}\right)[F(z)(1-gz)]\right\}, \tag{24}$$

where $\varepsilon_1=NB/2\pi L(1-\sigma)$. In the simplest case of an isotropic crystal (in the ab plane), for which $\tilde{\varepsilon}_{xx}=\tilde{\varepsilon}_{yy}$ and $\tilde{\varepsilon}_{xy}=0$, we obtain the following expression for a nonuniform elastic dilatation:

$$\tilde{\varepsilon}(x,y)=\frac{NB(1-2\sigma)}{2\sqrt{2}\pi L(1-\sigma)}\,[I(\eta,\zeta)-gJ(\eta,\zeta)], \tag{25}$$

where

$$I(\eta,\zeta)=\frac{\eta}{|\eta|R(\eta,\zeta)}\,\sqrt{R(\eta,\zeta)+1+\eta^2-\zeta^2}; \tag{26}$$

$$J(\eta,\zeta)=\frac{\zeta}{|\zeta|}\,\frac{\eta}{R(\eta,\zeta)}\,\sqrt{R(\eta,\zeta)+\zeta^2-\eta^2-1}-\zeta I(\eta,\zeta); \tag{27}$$

$$R(\eta,\zeta)=\sqrt{(1+\eta^2-\zeta^2)^2+4\eta^2\zeta^2}. \tag{28}$$

Assuming that $L\gg r_S$, so that the concentration of carriers matches with the deformation of the ion lattice, and substituting Eq. (25) for ε into formula (6), we obtain an expression for the nonuniform distribution of the superconducting transition temperature in the vicinity of a dislocation array:

$$T_c(\eta,\zeta)=T_{c0}+T_0[I(\eta,\zeta)-gJ(\eta,\zeta)]-T_0^2[I(\eta,\zeta)-gJ(\eta,\zeta)]^2/4\Delta T_m, \tag{29}$$

where

$$T_0=\frac{CNB(1-2\sigma)}{2\sqrt{2}\pi L(1-\sigma)}. \tag{30}$$

For $L\gg\xi_0$, the distribution of the superconducting order parameter $\Delta(r)$ has the same kind of profile.

Figure 1 shows the spatial distribution of the difference (T_c-T_{c0}) in the vicinity of a dislocation array with $N\neq 0$ for $P=0$, while Fig. 2 shows the same distribution in the vicinity of a dislocation array with $N=0(N_+=N_-)$ for $P\neq 0$. The latter case corresponds to the creation of dislocation pairs with antiparallel Burgers vectors **B** under the application of a local pressure (Frank–Reid dislocation source). It can be seen that local variations of T_c have opposite signs and different magnitudes on opposite sides of the dislocation array. The suppression of T_c is a more pronounced effect (see Fig. 1). Such regions with lower values of $T_c(r)$ and $\Delta(r)$ may serve as good traps (pinning centers) for Abrikosov vortices if $L>\lambda_L$ (where λ_L is the London penetration depth for the magnetic field). Regions with higher values of $T_c(r)$ and $\Delta(r)$ may be more conducive to the passage of superconducting transport current since they are characterized by a higher value of the critical depairing current. These regions may be observed experimentally by using magneto-optical methods of trapped magnetic flux and are manifested in the diamagnetic response of HTSC above T_{c0}.

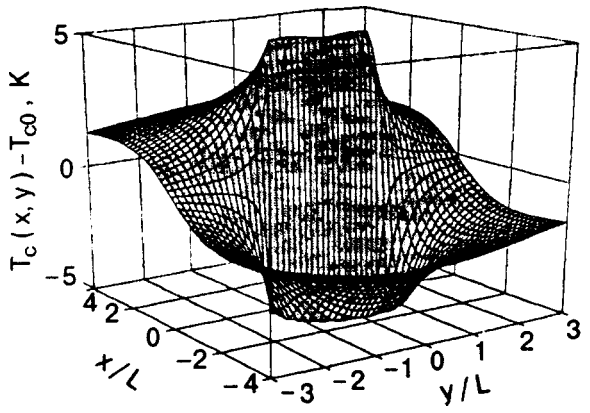

FIG. 1. Spatial distribution of the variation $\Delta T_c=T_c(x,y)-T_{c0}$ of the superconducting transition temperature in the CuO layer plane for a linear edge dislocation array along the x-axis with Burgers vectors localized in the slip plane $x=0$ between two stoppers at a distance $2L$ calculated by using formula (29) for $\Delta T_m=5$ K; $T_0=6$ K, and $g=0$.

This research is dedicated to the 70th birth anniversary

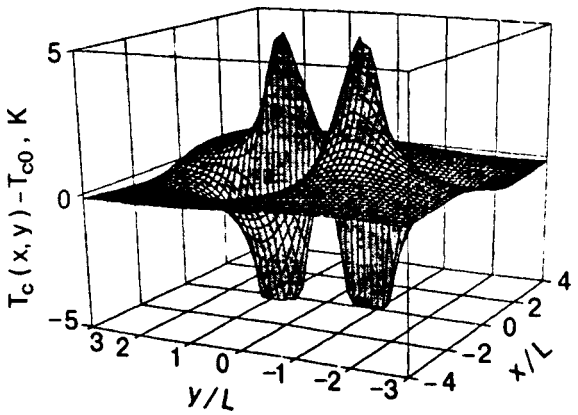

FIG. 2. Spatial distribution of the variation of the superconducting transition temperature in the CuO layer plane for a symmetric array with equal numbers of dislocations with opposite directions of the Burgers vector for $\Delta T_m=5$ K; $T_0=1$ K, and $gT_0=6$ K.

of Arnol'd Markovich Kosevich whose classical works on dislocation theory are well known.

*E-mail: pashitsk@iop.kiev.ua

[1] J. B. Torrance, A. Bezinge, A. I. Nazzal *et al.*, Phys. Rev. B **40**, 8872 (1989).
[2] S. D. Obertelli, I. R. Cooper, and J. L. Tallon, Phys. Rev. B **46**, 14928 (1992).
[3] A. Gurevich and E. A. Pashitskii, Phys. Rev. B **56**, 6213 (1997).
[4] U. Welp, M. Grimsditch, S. Fleshler *et al.*, J. Supercond. **7**, 159 (1994).
[5] C. Meingast, O. Kraut, T. Wolf *et al.*, Phys. Rev. Lett. **67**, 1634 (1991).
[6] C. Meingast, A. Junod, and E. Walker, Physica C **272**, 106 (1996).
[7] C. W. Chu, L. Gao, F. Chen *et al.*, Nature (London) **365**, 323 (1993).
[8] M. Nunez-Redueire, I. L. Tholence, E. V. Antipov *et al.*, Science **262**, 97 (1993).
[9] L. D. Landau and E. M. Lifshitz, *Theory of Elasticity* [in Russian], Nauka, Moscow (1976).
[10] J. P. Hirth and J. Loathe, *Theory of Dislocations*, Mcgraw-Hill, New York (1968).
[11] A. M. Kosevich, *Dislocations in the Theory of Elasticity* [in Russian], Naukova Dumka, Kiev (1978).
[12] A. M. Kosevich, *Theory of Real Crystals* [in Russian], Naukova Dumka, Kiev (1981).

Translated by R. S. Wadhwa

LOW-TEMPERATURE MAGNETISM

Temperature dependence of high-field magnetization of dilute spinels with cluster-type magnetic structures

N. N. Efimova

Kharkov State University, 310077 Kharkov, Ukraine[*)]

(Submitted June 17, 1998)
Fiz. Nizk. Temp. **24**, 1063–1069 (November 1998)

The isotherms $\sigma_T(H)$ and the high-field magnetization polytherms $\sigma_H(T)$ of polycrystals of the dilute spin-glass system $Li_{0.5}Fe_{2.5-x}Ga_xO_4$ are studied in the temperature range 4.2–380 K in fields up to 25 kOe. The nonmagnetic Ga^{3+} ions in the crystals have concentrations $x=1.4$ and 1.6 in the vicinity of the multicritical point $x_0=1.5$ on the x-T phase diagram, near which all types of magnetic states have cluster-type spatially inhomogeneous structures. It is found that the dependences $\sigma_H(T)$ obey Bloch's $T^{3/2}$ law in the paramagnet temperature range $T>T_f=18$ K, $x=1.6$ and $T>T_C=160$ K, $x=1.4$ for $H\geqslant 10$ kOe. This is attributed to spin wave excitations in individual noninteracting clusters. The $T^{3/2}$ law is violated at $T<T_f$ for $x=1.6$, but is obeyed at $T<T_C$ for $x=1.4$. The clearly manifested phase transition at the Curie point in the form of a kink on the linear dependence $\sigma_H(T^{3/2})$ suggests that the spin wave excitations are cooperative: their spectrum is formed at $T\leqslant T_C$ by the entire crystal, i.e., by the clusters and the matrix which is responsible for the long-range exchange coupling between clusters. At low temperatures, the $T^{3/2}$ law is violated at $T\sim 50$ K, where the sample with $x=1.4$ previously displayed a first-order phase-transition. © *1998 American Institute of Physics.* [S1063-777X(98)00411-3]

1. INTRODUCTION

Numerous experimental studies of spin-glass systems (magnets with competing exchange interactions)[1–5] have shown that their $x-T$ phase diagrams correspond to a certain general type shown schematically in Fig. 1 for dilute ferro- or ferrimagnets (we shall use the abbreviation FM for both). For concentrations $x\geqslant x_0$ of nonmagnetic ions (x_0 is the multicritical point on the $x-T$ phase diagram), the long-range FM order is not observed at any temperature $T\geqslant 0$ K, but a transition PM→SG from paramagnetic to spin-glass state is observed at temperature T_f [curve $T_f(x)$ on the phase diagram]. Disordered states, having the same phenomenological parameters at $T<T_f$ as the SG state, exist in a certain concentration range, and the reentrant region of the $x-T$ diagram is observed for $x<x_0$. In this region, the transition PM→FM is first observed at the Curie point T_C upon a decrease in temperature. This is followed by an FM→FSG transition at $T=T_f$. In the ferro- and ferrimagnetic spin glass (FSG) state, a long-range FM order with a nonzero spontaneous magnetization ($\sigma_S\neq 0$) coexists with typical spin-glass properties.[1–5] In a magnetic field H, a transition to the spin-glass states of either type occurs along the curve $T_f(H)$, the value of T_f decreasing in the same way upon an increase in H along the Almeida–Thouless and Gabay–Thoulouse critical curves.[3,5]

In general, the experimental phase diagrams (Fig. 1) are in accord with the theoretical curves calculated in the mean-field model with an infinite radius under the assumption that the magnetic states are homogeneous.[1–4] In real magnets (especially in dilute magnets with a short-range exchange), however, all types of magnetic states have spatially inhomogeneous cluster type structures at $x\sim x_0$, which are reflected in neutron diffraction studies and manifested in the form of peculiarities in their magnetic properties.[1,5,6] It is quite possible that spatial inhomogeneity of cluster type may also affect the spectrum of magnetic excitations.[7,8] The theoretical conclusion about the existence of spin waves with a linear dispersion relation[9] in spin glasses does not match with the dependence $C(T)\sim T^{1,10}$ observed experimentally for $T<T_f$. Moreover, the data obtained during attempts to observe spin waves directly in FSG and SG states by the inelastic neutron scattering technique are quite contradictory.[1,11–16]

For example, Hennion *et al.*[12] reported that spin waves exist in the Ni–Mn system at $T<T_f$, while Shapiro *et al.*[11] and Maletta *et al.*[13] failed to observe any spin waves in this system. For the canonical short-range spin-glass system (Eu–Sr)S, spin waves were observed both at $T<T_f$ (reentrant and SG regions of the phase diagram) and at $T>T_f$ in the PM state.[14] The inelastic scattering spectrum does not undergo any changes during the PM→SG transition. Wong *et al.*[14] carried out their investigations on samples with concentrations x close to the multicritical point on the $x-T$ phase diagram. In view of this, it is not possible to draw an unambiguous conclusion about the ''origin'' of the spin

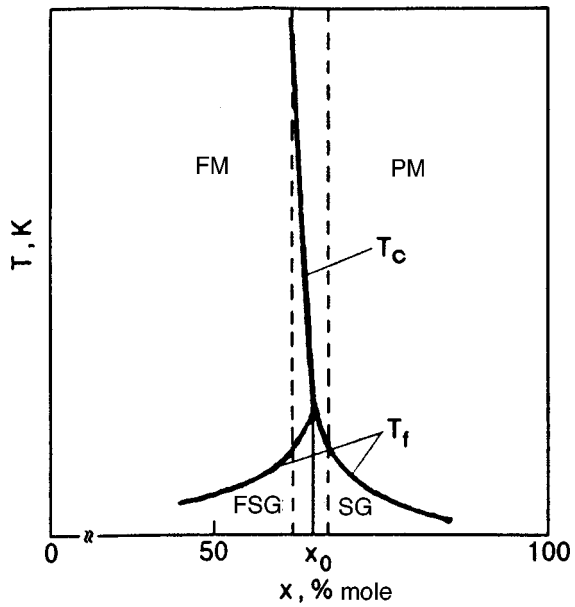

FIG. 1. Schematic $x-T$ phase diagram for dilute spin-glass systems (x is the dilution). See text for notation.

waves being recorded, i.e., about whether they are cooperative excitations in the traditional sense, or reflect local processes in ferromagnetically ordered clusters.

Thus, the problem of existence of collective excitations of the type of spin waves in disordered spin-glass states is associated with another problem, viz., the formation of the spectrum of excitations in spatially inhomogeneous states. In spin-glass systems, this problem is generally different from the one in the percolation theory, in which finite clusters do not interact with infinite clusters (percolation net) or with one another.[8] The formation of spatially inhomogeneous states in dilute magnets is a consequence of the compositional disorder (nonuniform distribution in the lattice of magnetic and nonmagnetic atoms), and their structure can be presented as the aggregate of two subsystems (clusters and matrices) with exchange coupling.[1,5,6,17,18] The enhanced concentration of nonmagnetic atoms weakens the exchange in the matrix, and the competition between exchange interactions facilitates the emergence of frustrated bonds. The matrix determines the nature of the magnetic states (FM, FSG, SG or PM) in a crystal as a whole, while FM order is preserved in the clusters.[5,6,17,18] Experimental studies of the formation of excitation spectrum in an exchange-coupled cluster–matrix system for various states of the latter (FM, FSG, and SG states in the crystal as a whole) are undoubtedly quite interesting. Unlike earlier publications on this subject,[11–16] we use the integral approach in the present work, i.e., the investigation of temperature dependences σ_H of high-field magnetization.

2. FORMULATION OF THE PROBLEM AND OBJECTS OF INVESTIGATION

In this communication, we present the results of investigation of temperature dependences $\sigma_H(T)$ of high-field magnetization in the temperature range 4.2–380 K and magnetic fields 5–25 kOe for polycrystalline samples of the spin-glass system $Li_{0.5}Fe_{2.5-x}Ga_xO_4$, i.e., dilute cubic spinels with collinear ferrimagnetic ordering for $x=0$.

The integral characteristics $\sigma_H(T)$ were studied in order to determine the existence of spin waves in systems of isolated and exchange-coupled ferrimagnetic (FM) clusters. For the model objects that can be used for studying the problem under consideration and which are optimal from the point of view of the experimental approach adopted by us, we chose samples with concentrations of nonmagnetic ions Ga^{3+} symmetric with respect to the multicritical point $x_0=1.5$:[5] $x=1.4$ ($x<x_0$) and $x=1.6$ ($x>x_0$). A ''reentrant'' sample with $x=1.4$ undergoes two transitions upon cooling, viz., a PM→FM transition at the Curie temperature $T_C=160$ K, and a FM→FSG transition at the freezing point $T_f=25$ K ($H=0$). The spin-glass sample with $x=1.6$ undergoes a single transition upon a decrease in temperature, viz., a PM→SG transition at the temperature $T_f=18$ K ($H=0$).[5] While choosing these concentration cross-sections (shown by dashed lines on the $x-T$ phase diagram in Fig. 1), we assumed that both these cases are characterized by a spatial inhomogeneity that is not only manifested sharply, but is also of the same kind (as regards the characteristics of the cluster subsystems). The latter circumstance makes it possible to analyze several situations simultaneously. For concentration $x=1.4$: an ensemble of noninteracting ferrimagnetic (FM) clusters at $T>T_C$; the emergence of long-range ferrimagnetic coupling between clusters at $T\leqslant T_C$, and the formation of frustrated bonds in the matrix at $T<T_f$ ($H=0$) and $T\to T_f$ (from the right). For concentration $x=1.6$: an ensemble of noninteracting ferromagnetic (FM) clusters existing right up to $T=T_f$ ($H=0$), which covers the ferrimagnetic state in a sample with $x=1.4$ on the temperature scale (see above), and the emergence of exchange coupling between clusters through a frustrated matrix at $T<T_f$. It should be observed that, although the term high-field magnetization of spin glass is used frequently in the literature,[1,2] the FSG and SG states are destroyed in high fields, which is reflected in the vanishing of characteristic phenomenological features of these states.[1–5]

It is well known[19–21] that ferrimagnets have a low-energy branch of spin waves with a quadratic dispersion relation. Hence the experimental approach was based on the assumption that such excitations may exist in large FM clusters (with the linear size r_0 of the order of several hundred angstroms),[18] in a wide temperature range, including the paramagnetism region. Since excitation of spin waves with a quadratic dispersion relation leads upon heating to a decrease in magnetization according to Bloch's $T^{3/2}$-law,[20,21] the ''test'' for the existence of spin waves is the possibility of describing the experimental dependences $\sigma_H(T)$ by the $T^{3/2}$ law. Premises for such an approach are also provided by the results of earlier experiments in which it was shown that a magnetic field suppresses excitations that exist together with spin waves in the spectrum of ferrimagnets with local violations of collinear order.[22]

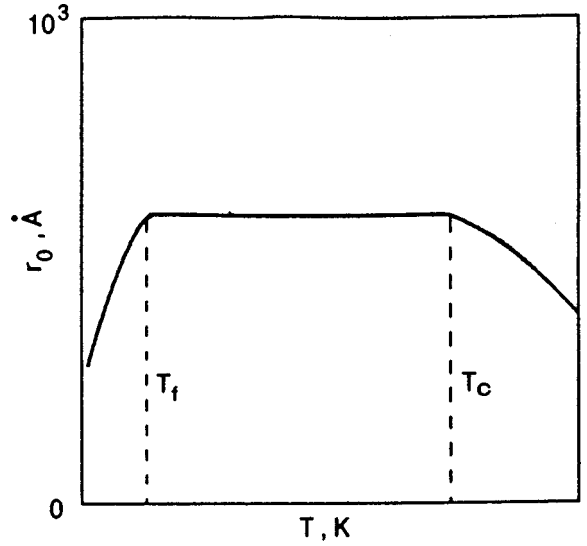

FIG. 2. Schematic diagram of the temperature dependence of the mean size of a ferrimagnetic cluster in Li–Ga spinels from the results of neutron diffraction studies.[18]

3. DISCUSSION OF EXPERIMENTAL RESULTS

The magnetization isotherms $\sigma_T(H)$ and polytherms $\sigma_H(T)$ were studied in the temperature interval 4.2–380 K in magnetic fields $H \leqslant 25$ kOe using ballistic magnetometers with a sensitivity 10^{-3} G·cm^3·g^{-1}. The polycrystalline samples and the types of experimental set-up used in these investigations were the same as the ones described in our earlier publications.[5,6]

3.1. Nature of spatial inhomogeneity of magnetic states in samples with $x=1.4$ and 1.6

It was mentioned in Sec. 2 that the possibility of solving the formulated problem with the help of the experimental approach used by us depends to a considerable extent on the choice of the objects of investigation, namely, the closeness of the spatial inhomogeneities of the magnetic states. The initial assumption concerning the strong spatial inhomogeneity of magnetic states in the samples under consideration was based on the data obtained from neutron diffraction analysis of a sample with $x=1.35$, which is close to the concentration in the above-mentioned samples.[18] The results presented by us in Ref. 18 are used in Fig. 2 to illustrate schematically the variation of average linear dimensions of an FM cluster for $x \to x_0$ (from the left). The results of magnetic studies, viz., the magnetization isotherms shown in Fig. 3 can also be used to draw certain qualitative and quantitative conclusions about the nature of spatial inhomogeneity. A comparison of the $\sigma_T(H)$ dependences in the paramagnetic region ($x=1.4$, curves *13–17* in Fig. 3a and $x=1.6$, curves *2–7* in Fig. 3b) reveals an almost complete qualitative and quantitative identity of these dependences. In contrast to the case of a homogeneous PM, high magnetization values are observed in both cases in comparatively weak fields for $T > T_C$ (160 K) or $T > T_f$ (18 K). Indeed, assuming that all spins are free, we can use the simple estimates based on the Langevin function approximation in the form

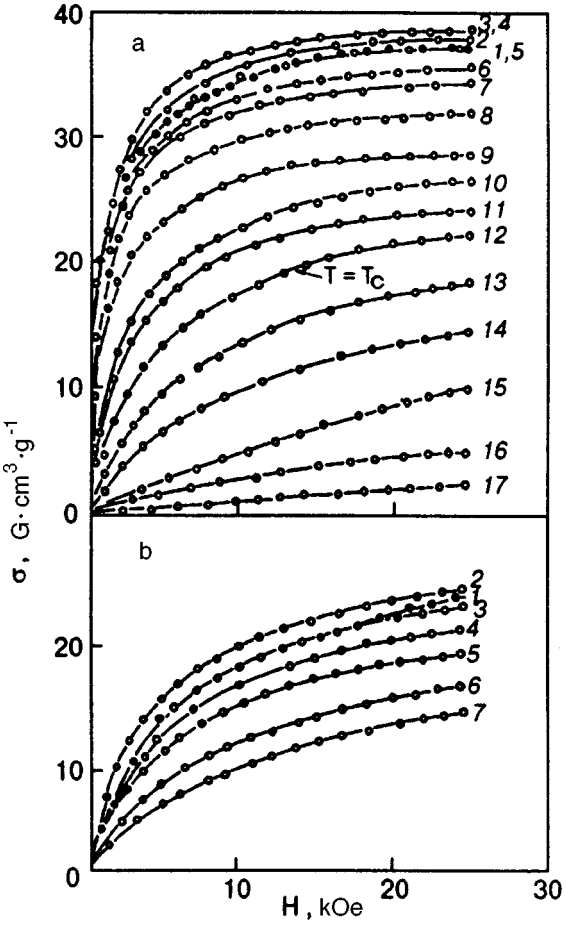

FIG. 3. Magnetization isotherms $\sigma_T(H)$ for $Li_{0.5}Fe_{2.5-x}Ga_xO_4$ samples with concentrations $x=1.4$ (a) and 1.6 (b) at temperatures T, K: (a) 4,2 (*1*), 20 (*2*), 30; 40 (*3,4*), 60 (*5*), 70 (*6*), 80 (*7*), 100 (*8*), 120 (*9*), 130 (*10*), 153 (*11*), 160 (*12*), 193 (*13*), 225 (*14*), 280 (*15*), 294 (*16*), 387 (*17*); (b) 4,2 (*1*), 20 (*2*), 60 (*3*), 80 (*4*), 100 (*5*) 130 (*6*), 150 (*7*).

$$I = \rho\sigma = N\mu^2 H/3kT, \quad \mu H \ll kT, \tag{1}$$

(where ρ is the sample density, N the number of particles per unit volume, μ the magnetic moment in Bohr magnetons μ_B, and k the Boltzmann constant) to show that the magnetization must be much smaller than the experimental values. For example, $\sigma \simeq 0.08$ G·cm^3·g^{-1} at $T=100$ K and $H=20$ kOe ($\mu H \sim 3$ K), if $\mu = 5\mu_B$, i.e., equal to the magnetic moment of Fe^{3+}. Such a disparity between the experimental and theoretical values of $\sigma_T(H)$ obviously indicates that spatially inhomogeneous superparamagnetic type states are realized in both cases.

The average magnetic moment and volume of superparamagnetic clusters can be estimated in the weak-field limit (1) as well as in strong fields, where

$$I = n\mu\left(1 - \frac{kT}{\mu H}\right) = \frac{\mu}{V} - \frac{kT}{VH}, \quad \mu H \gg kT. \tag{2}$$

Here V is the mean volume and n the concentration of clusters. Plotting the experimental dependences in the I, T/H coordinates [the dependences $\sigma_T(H)$ must be linear in this case], we can determine the values of (μ/V) and (k/V) from

the intercept on the I-axis and the slope of the straight line relative to the T/H-axis, respectively. Using such an approach, we obtained from Fig. 3 the mean value of $\mu \sim 10^3 \mu_B$ and the linear dimensions of the cluster $r_0 \sim 450$ Å. These results are in good agreement with the neutron diffraction analysis data.[18] It follows directly from here that ferrimagnetic order is preserved within the clusters and that the cluster size is quite large.

The spatial inhomogeneity of magnetic states obviously affects the shape of magnetization isotherms at $T<T_C$ or $T<T_f$ since their general form remains identical to that observed in the PM region. However, the formation of long-range FM order in a sample with $x=1.4$ at $T \leqslant T_C$ leads to a noticeable variation of the $\sigma_T(H)$ curves in fields $H<2$ kOe where the susceptibility increases sharply in comparison with the PM region. Such a behavior can naturally be associated with the emergence of domain structure and hence the processes of technical magnetization which terminate in magnetic fields $H \sim 2$ kOe. The values of σ_T attained during technical magnetization are about half the values obtained in strong fields ($H=25$ kOe). The shape of the isotherms at $H>2$ kOe is analogous to the ''paramagnetic'' curves $\sigma_T(H)$ at $T>T_C$, while the increment in magnetization is comparable with the magnetization of the cluster subsystem in the PM region. On the whole, it leads to the assumption that the cluster subsystem makes the main contribution to the magnetization in the FM region in fields $H>2$ kOe. Thus, so far as the magnetization processes are concerned, the cluster subsystem retains its identity to a certain extent in the FM state also.

Before concluding the discussion of results (see Fig. 3), it should be observed that for both samples the shape of magnetization isotherms does not change noticeably in the low-temperature region for $T \to 0$, but their arrangement becomes anomalous as compared to the conventional ferro- or ferrimagnets. It can be seen from Fig. 3 that the isotherms at $T=4.2$ K are lower than at higher temperatures. Their normal arrangement is restored only at $T \geqslant T_f$ for the spin-glass sample with $x=1.6$ and at much higher temperatures ($T \sim 50$ K for $x=1.4$. It should be remarked at the very outset that such a behavior is typical of the spin-glass systems and is responsible for the emergence of regularities associated with the existence of the disordered states of SG and FSG types for $H=0$.[1,2,5] At the same time, the ''former'' FSG ($x=1.4$) and SG ($x=1.6$) states have considerably different values of magnetization at low temperatures. Although the concentrations of nonmagnetic ions for $x=1.4$ and 1.6 differ just by 6.7%, the magnetization $\sigma_T(H)$ of the sample with $x=1.4$ at $T=4.2$ K is nearly double the value of $\sigma_T(H)$ of the sample with $x=1.6$ in a field $H=25$ kOe and more than double the value in fields $H<25$ kOe.

3.2. Temperature dependences of the high-field magnetization σ_H

The dependence $\sigma_H(T)$ for both the samples investigated by us is shown in Fig. 4 in σ, $T^{3/2}$ coordinates. The inset to this figure shows the magnetization polytherms directly in σ, T coordinates. It should be remarked by the way that, according to Fig. 4, the above-mentioned anomalous

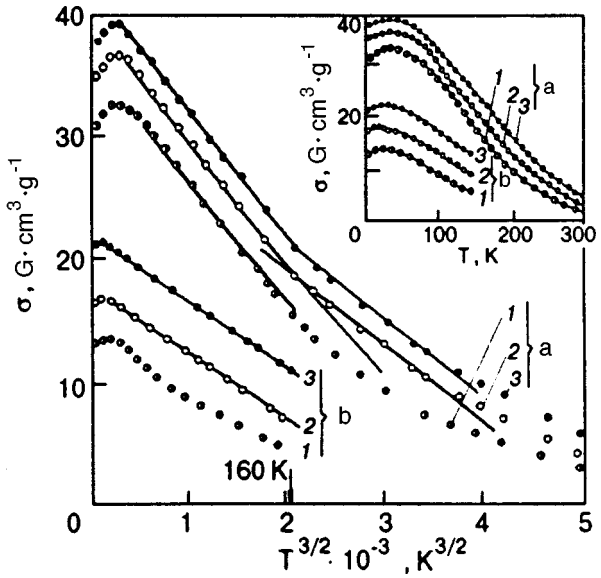

FIG. 4. Temperature dependence of high-field magnetization σ_H for samples with concentrations $x=1.4$ (a) and 1.6 (b) in magnetic fields H (in kOe): 5 (*1*), 10 (*2*), and 25 (*3*). The inset shows the same dependence in coordinates σ, T. The notation is the same as before.

arrangement of $\sigma_T(H)$ isotherms reflects the peculiarities of the temperature dependence of the magnetization $\sigma_H(T)$ in the form of a low-temperature peak which is characteristic of spin-glass systems.

The linear temperature dependence of the high-field magnetization in σ, $T^{3/2}$ coordinates (Fig. 4) shows that Bloch's $T^{3/2}$ law is observed over a wide range of temperatures. For the ''spin-glass'' sample with $x=1.6$, this range corresponds to the paramagnetic region $T>T_f$ ($H=0$), and $\sigma_H \sim T^{3/2}$ only in fields $H \geqslant 10$ kOe. For a sample with $x=1.4$, the $T^{3/2}$ law for spin waves is obeyed at $T \leqslant T_C$ ($H \geqslant 5$ kOe), as well as at $T>T_C$ ($H \geqslant 10$ kOe in the temperature interval $T_C \leqslant T \leqslant 1.8\ T_C$ (280 K). At low temperatures, the departure from the $T^{3/2}$ law for both samples is formally associated with the existence of a peak on the $\sigma_H(T)$ dependence followed by a decrease in magnetization for $T \to 0$ K. The decrease in magnetization is associated with a competition between exchange interactions which leads to the formation of not only SG-type disordered states ($H=0$), but also noncollinear ferromagnetic structures.[1,24] For example, a first-order phase transition to the noncollinear ordered ferrimagnetic state in zero field for a sample with $x=1.4$ occurs at $T \approx 45$ K.[24] Obviously, the FSG and SG states in a magnetic field are also replaced by noncollinear ferrimagnetic states whose ordering depends on the applied magnetic field. Obviously, the criterion used by us for ascertaining the presence of spin waves is no longer applicable in this case.

It can be seen clearly from the data presented in Fig. 4 that the phase transition occurring at T_C for a sample with $x=1.4$ is manifested as a kink on the dependence $\sigma_H(T^{3/2})$ whose position corresponds to $T=160$ K, i.e. the value of T_C determined in weak fields.[6] The slope of the straight lines

$\sigma_H(T^{3/2})$ relative to the $T^{3/2}$-axis increases upon a transition to the ferrimagnetic state. Before concluding the discussion of the results (Fig. 4), it must be mentioned in addition to what has been stated above that the dependences $\sigma_H(T^{3/2})$ are nearly parallel for all cases considered above ($x=1.6$ for $T>T_f$, $x=1.4$ for $T>T_C$ and $T<T_C$). This shows that the suppression of spin waves by a magnetic field described by an additional term $bTH^{1/2}$ in the Bloch's law[25] is quite small in the fields $0<H\leqslant 25$ kOe considered here.

To our knowledge, investigations similar to those undertaken by us have not been reported for the paramagnetic temperature range. However, the available experimental data together with the results of neutron diffraction studies[14] prove convincingly that spin-wave type excitations (even with a quadratic dispersion relation according to our results) exist in individual clusters that are not connected through exchange coupling. Indeed, it was mentioned above that for $T>T_f$ or $T>T_C$, the dependence $\sigma_H(T)$ is due to cluster subsystems. The field interval $H\geqslant 10$ kOe, in which the $T^{3/2}$ law is satisfied for both samples in the case of high-field magnetization, corresponds to saturation of a superparamagnet. In this case, the high-field magnetization is defined by formula (2) in which the magnetic moment of the cluster is $\mu\sim\sigma_{SC}(T)$ (here σ_{SC} is the spontaneous magnetization in the cluster). It follows hence that the experimentally measured magnetization $\sigma_H(T)\sim\sigma_{SC}(T)$. Consequently, $\sigma_{SC}(T)\propto T^{3/2}$ in each cluster, and spin waves with a quadratic dispersion relation are excited within the cluster. This is completely in accord with the fact that clusters have a size of several hundred angstroms (see above) and their Curie points have quite large values.

The manifestation of a PM→FM transition at the Curie point in the form of a kink on the high-field magnetization dependence $\sigma_H(T^{3/2})$ is also a new experimental result. Obviously, such an effect can be observed only in spatially inhomogeneous cluster-type ferro- or ferrimagnets in which spin waves exist in individual clusters at $T>T_C$, i.e., in the paramagnetic region. The change in the slope of the straight lines $\sigma_H(T^{3/2})$ (Fig. 4) corresponds to a decrease in the effective spin-wave rigidity constant in the ferrimagnetic region. This is quite logical in view of the fact that the long-range FM order is formed owing to the matrix in which the exchange coupling is weaker than in clusters. However, the relatively small magnitude of the effect indicates that both exchange-coupled subsystems, viz., clusters and the matrix, participate simultaneously in the formation of excitation spectrum. Thus, if long-range order prevails in the crystal, the cluster system completely loses its identity (which is manifested in the specific features of magnetization processes) during the formation of excitation spectrum: for $T<T_C$, spin waves exist as collective excitations of the entire crystal.

CONCLUSIONS

The results of investigation of temperature dependences $\sigma_H(T)$ of high-field magnetization in two samples from the system of dilute ferrimagnetic spinels $Li_{0.5}Fe_{2.5-x}Ga_xO_4$ with concentrations $x=1.4$ and 1.6 of nonmagnetic Ga^{3+} ions corresponding to reentrant and spin-glass regions on the $x-T$ phase diagram show that the dependence $\sigma_H(T)$ follows Bloch's $T^{3/2}$ law over a wide temperature interval including the paramagnetic region. At temperatures $T>T_f$ ($x=1.6$) or $T>T_C$ ($x=1.4$), this is due to the excitation of spin waves with a quadratic dispersion relation, localized in ferrimagnetic clusters whose size extends to several hundred angstroms according to the data of neutron diffraction and magnetic studies.

A clearly manifested phase transition at the Curie point, appearing in the form of a kink on the linear dependence $\sigma_H(T^{3/2})$ at $T=T_C=160$ K ($x=1.4$) indicates that spin waves become collective excitations of the entire crystal at $T\leqslant T_C$, due to the emergence of long-range exchange coupling between clusters.

The decrease in the value of the effective spin–wave rigidity constant at $T<T_C$ is in accord with the model of the spatially inhomogeneous magnetic states structure which can be presented as an aggregate of two exchange-coupled subsystems, viz., clusters and the matrix formed by spins with a weak exchange.

Although an analysis of the low-temperature region is beyond the scope of this research, it can be stated in conclusion that, if long-range FM order is preserved at $T<T_f$ (i.e., in the FSG state), the cluster subsystem cannot be independent just like at temperatures $T<T_C$. Hence we believe that the spin waves, which are detected in reentrant systems by neutron diffraction technique, are cooperative excitations of the system in the general sense.

*)E-mail: alexander.v.vankevich@univer.kharkov.ua

[1] K. Binder and A. P. Young, Rev. Mod. Phys. **58**, 801 (1986).
[2] I. Ya. Korenblit and E. F. Shender, Usp. Fiz. Nauk **157**, 267 (1989) [Sov. Phys. Usp. **32**, 139 (1989)].
[3] J. R. L. De Almeida and D. J. Thouless, J. Phys. A **11**, 983 (1978).
[4] M. Gabay and G. Thoulouse, Phys. Rev. Lett. **47**, 201 (1981).
[5] N. N. Efimova, Yu. A. Popkov, and N. V. Tkachenko, Zh. Éksp. Teor. Fiz. **90**, 1413 (1986) [Sov. Phys. JETP **63**, 827 (1986)]; Fiz. Nizk. Temp. **15**, 1055 (1989) [Sov. J. Low Temp. Phys. **15**, 584 (1989)]; Fiz. Nizk. Temp. **16**, 1565 (1990) [Sov. J. Low Temp. Phys. **16**, 881 (1990)].
[6] N. N. Efimova, Fiz. Nizk. Temp. **23**, 1067 (1997) [Low Temp. Phys. **23**, 802 (1997)].
[7] L. E. Wenger and P. H. Keesom, Phys. Rev. B **13**, 4053 (1975).
[8] I. Ya. Korenblit and E. F. Shender, Usp. Fiz. Nauk **126**, 233 (1978) [Sov. Phys. Usp. **21**, 832 (1978)].
[9] B. I. Halperin and W. M. Saslow, Phys. Rev. B **16**, 2I54 (1977).
[10] N. N. Efimova, V. A. Pervakov, V. I. Ovcharenko, and N. Yu. Tyutryumova, Fiz. Tverd. Tela (St. Petersburg) **35**, 2838 (1993) [Phys. Solid State **35**, 1405 (1993)].
[11] S. M. Shapiro, C. R. Fincher, A. C. Palumbo, and R. D. Parks, J. Appl. Phys. **52**, 1729 (1981).
[12] B. Hennion, M. Hennion, F. Hippert, and A. P. Murami, Phys. Rev. B **28**, 5365 (1983); J. Phys. F **14**, 489 (1984).
[13] H. Maletta, W. Zlnn. H. Scheuer, and S. M. Shapiro, J. Appl. Phys. **52**, 1735 (1981).
[14] Po-Zen Wong, H. Joshizawa, S. M. Shapiro *et al.*, Phys. Rev. Lett. **58**, 1276 (1987).
[15] I. Murebeau and M. Hennion, J. Magn. Magn. Mater. **140–144**, 1999 (1995).
[16] K. H. Fischer, Phys. Stat. Sol. **116**, 357 (1983).
[17] H. Maletta, J. Appl. Phys. **53**, 2185 (1982).
[18] N. N. Efimova, Yu. A. Popkov, G. A. Takzei *et al.*, Fiz. Tverd. Tela (St. Petersburg) **36**, 490 (1994) [Phys. Solid State **36**, 271 (1994)].
[19] T. A. Kaplan, Phys. Rev. **109**, 782 (1958).

[20] Yu. A. Izyumov and R. P. Ozerov, *Magnetic Neutron Diffraction* [in Russian], Plenum Press, NY, 1966.
[21] K. P. Belov, *Ferrites in Strong Magnetic Fields* [in Russian], Nauka, Moscow (1972).
[22] N. N. Efimova, Zh. Éksp. Teor. Fiz. **113**, 1339 (1998) [JETP **86**, 731 (1998)].
[23] S. V. Vonsovskii, *Magnetism* [in Russian], Nauka, Moscow (1971).
[24] N. N. Efimova, Pis'ma Zh. Éksp. Teor. Fiz. **67**, 329 (1998) [JETP Lett. **67**, 346 (1998)].
[25] T. Holstein and H. Primakoff, Phys. Rev. **58**, 1098 (1940).

Translated by R. S. Wadhwa

Polaron conductivity of $La_{0.7}\square_{0.3}MnO_{3-\delta}$ thin films in the magnetic phase transition range

V. N. Krivoruchko and S. I. Khartsev

A. Galkin Physicotechnical Institute, National Academy of Sciences of the Ukraine, 340114 Donetsk, Ukraine[*)]

(Submitted April 9, 1998; revised June 11, 1998)
Fiz. Nizk. Temp. **24**, 1070–1076 (November 1998)

The magnetoresistive $\rho(T,H)$ and thermoelectric (the Seebeck coefficient) $S(T,H)$ properties of $La_{0.7}\square_{0.3}MnO_{3-\delta}$ thin films ($\square$ is a cation vacancy) grown by the magnetron deposition technique are investigated. The magnetic polaron origin of the conductivity of such systems is established in the temperature range 77 K$\leqslant T\leqslant$350 K in magnetic fields $0\leqslant H\leqslant$10 kOe. The experimental dependences $\rho(T,H)$ and $S(T,H=0)$ are approximated by a universal phenomenological expression. Thermopower measurements indicate a considerable change of the mobility as well as the density of states of charge carriers in the region of magnetic phase transition. © *1998 American Institute of Physics.* [S1063-777X(98)00511-8]

INTRODUCTION

Recent intense studies of perovskite-type lanthanum manganites revealed a number of key factors determining the magnetoresistive properties of these compounds. Above all, these factors include the mean ionic radius of cations in the *A*-position as well as the concentration and mobility of charge carriers, which are determined by the ratio Mn^{3+}:Mn^{4+} of ions in the lattice (see, for example, Refs. 1–4). At the same time, it was found that two types of manganites for which the magnetoresistive effect (MRE) can assume completely different forms should be distinguished.[4,5] Manganites of type I exhibit a transition from the ferromagnetic metallic (FMM) to the paramagnetic semiconducting (PMS) state upon heating. The MRE peak is observed in the vicinity of the Curie point T_C, although its position may not coincide with this temperature. Type II manganites exhibit a transition from the antiferromagnetic insulator (AFMI) to the FMM state at a quite low temperature. An increase in temperature leads to a transition to the PMS state. A salient feature of type II manganites is the charge-ordered state in the AFMI phase. Typical representatives of such manganites are $Nd_{1-x}Sr_xMnO_3$ and $Pr_{1-x}Sr_xMnO_3$ with values of x close to 0.5.[5–7]

The mechanism of magnetoresistive properties of type II manganites in the AFMI–FMM transition region has apparently been determined. This is a first-order transition from a charge-ordered state to a charge-disordered state (a transition of the type of Wigner crystal melting). The physical factor responsible for the emergence of the charge-ordered phase is the Coulomb attraction of charge carriers.[5–7] As regards the change in the transport properties in the FMM–PMS transition region, the situation is unclear as in the case of type I manganites.

Although the sharp change in the resistance of manganites near the FMM–PMS transition is usually regarded as a phase transition, no arguments have been formulated supporting this point of view unambiguously. As before, the electrical conductivity mechanism ensuring giant values of MRE remain unclear. It has not been established whether the change of the metal-type conductivity to hopping conductivity near the Curie point is a true metal–semiconductor phase transition and, finally, whether the transition is caused by a change in the mobility of charge carriers or/and a change in their number density. The attempts to explain the large magnitude of the MRE by using the double exchange model encounter considerable difficulties (see, for example, Ref. 8). At the same time, the same double exchange model supplemented with effects of disordering and localization of electron states leads to reasonable qualitative results.[9–11] It is well known that a magnetic semiconductor under certain conditions can go over to a spatially inhomogeneous state in which samples contain nonferromagnetic regions with the activation conductivity along with ferromagnetic regions with a metal-type conductivity. The colossal magnetoresistance of manganites in this model can be regarded as a percolation-type metal–semiconductor phase transition.[12–14] However, the model of inhomogeneous state in the present form has a number of drawbacks and cannot be applied to manganites directly.

Various versions of the polaron scenario of conductivity, which are being developed most intensely at the present time, take into account the strong interaction of charge carriers with the subsystem of localized spins and with the lattice (in some models).[15–22] It should be noted that the participation of the lattice in magnetic phase transitions follows from the ''isotopic effect'' discovered recently: a displacement of the Curie point (by $\sim$10 K) upon a change of the isotope ^{16}O by the isotope ^{18}O in $(La_{1-x}Ca_x)_{1-y}Mn_{1-y}O_3$.[19] At the same time, the FMM–PMS transition can occur as a true phase transition or as a transition of the type of conductivity crossover for the polaron type of conductivity also. The possibility of the second version has become an object of serious discussion only recently.[16,18,20–22] The most simple and physically clear model was proposed by Zhang.[16]

According to Zhang,[16] magnetic polarons are charge carriers above and below the temperature T_m corresponding to the resistance peak. The formation of resistance above and below T_m is governed by two independent mechanisms: elastic and inelastic processes of interaction between polarons and the magnetic subsystem. The conductivity determined by elastic mechanisms can be described by the band model, while in the case of inelastic processes, ''dressed'' electrons move by hopping with the emission and absorption of magnons. These two mechanisms exhibit completely different temperature dependences: in the band description, the resistance increases with temperature, while in the case of inelastic processes the resistance decreases upon heating. It was found that if the properties of a system satisfy certain requirements (the existence of such properties for lanthanum manganites naturally requires a verification), the crossover from one conductivity mechanism to the other is not only abrupt, but also sensitive to the external magnetic field. Obviously, the experimental data confirming the crossover from the metal-type to hopping conductivity upon a change in temperature in a magnetic field and without it would be of fundamental importance for the choice of mode; and the construction of the theory of magnetotransport properties of manganites.

To our knowledge, the only attempt of processing the experimental data by using the phenomenological approach[16] was made by Rubinstein *et al.*[20] The authors obtained a satisfactory description of magnetoresistive and thermoelectric properties of thin manganite films doped with Co and Ni for reasonable values of phenomenological parameters of the system. Earlier experimental results[21,22] are also worth mentioning. O'Donnell *et al.*[21] studied high-quality $La_{0.7}Ca_{0.3}MnO_3$ films grown by the atomic layer-by-layer molecular-beam epitaxy technique. The authors emphasized that they observed a crossover rather than a change in the physical mechanisms of conductivity in the vicinity of T_C and described the behavior of resistivity $\rho(T,H)$ above and below T_C by a universal expression $\rho(T,H) \simeq \rho(0)\exp[-C(M/M_{\text{sat}})]$, where M_{sat} is the saturation magnetization. Hundley *et al.*[22] analyzed thin $La_{0.7}A_{0.3}MnO_{3+\delta}$ films with A=Ba, Ca and Sr grown by pulsed laser deposition. It was found that the film resistance is successfully described by the same phenomenological expression $\rho(T,H) \sim \exp[-C(M/M_{\text{sat}})]$ not only in the vicinity of the magnetic phase transition, but also in the entire explored temperature range 10 K$\leqslant T \leqslant$272 K.

In this paper, we report on the results of experimental studies of magnetoresistive and thermoelectric properties of thin $La_{0.7}\square_{0.3}MnO_{3-\delta}$ films ($\square$ is a cation vacancy) grown by reactive magnetron deposition technique. The model developed by Zhang[16] is used for analyzing the phenomenological expressions describing the experimental dependences $\rho(T,H)$ and $S(T,H)$ in the entire explored range of temperatures and magnetic fields. The obtained results indicate that the behavior of $\rho(T,H)$ can be described correctly in the model of conductivity crossover from the metal-type to thermally activated hopping conductivity in the region of magnetic phase transition. On the other hand, the measurements of thermoelectric properties indicate a change not only in the type of film conductivity, but also in the density of states of charge carriers near the Fermi surface in this region. It was found that the sign in the coefficient of the field dependence of thermopower in the magnetically ordered phase is reversed. The physical meaning of phenomenological parameters of the system is discussed.

MEASURING TECHNIQUE AND MATERIALS

The material for targets was obtained from the oxides La_2O_3 and MnO_2 taken in the appropriate proportions. (The details of sample preparation technique are described in Ref. 23.) X-ray diffraction studies revealed that the synthesized powder contains only one phase and exhibits rhombohedral distortions of the perovskite structure. The films of $La_{0.7}\square_{0.3}MnO_{3-\delta}$ having a thickness $\sim$3500 Å were grown by reactive magnetron deposition on the VUP-5M device. The targets for deposition were obtained in the form of 40×1 mm disks by hydrostatic compacting of the synthesized powder into pellets and additional fritting for six hours at 1050 °C. The films were deposited on (001)-oriented $SrLaAlO_4$ substrates whose temperature was maintained at 600 °C. The pressure of the gas medium having a composition $Ar:O_2=4:1$ was 10 mtorr, and the residual pressure in the chamber was $5\cdot 10^{-7}$ torr. The results of x-ray diffraction analysis proved the one-phase composition of film samples and their perovskite structure. The epitaxial structure of the films in the (001) plane was established.

It is well known (see, for example, Ref. 24) that the films obtained by magnetron deposition are deficient in oxygen. In order to optimize the ratio Mn^{3+}:Mn^{4+}, the films were annealed additionally in oxygen flow for 30 min; the annealing temperature was 700 °C.

The resistance and magnetoresistance of the films were measured as a function of temperature and magnetic field by using the four-probe method. The magnetic field was applied parallel to the film surface, the magnetoresistance being independent of the mutual orientation of the field and current. The thermopower was measured in vacuum as the potential difference between two contacts at the film surface with a controlled temperature gradient.

RESULTS OF MEASUREMENTS AND DISCUSSION

Magnetoresistance

It is well known (see, for example, Refs. 25 and 26) that the structures with lanthanum deficiency of the type $La_{1-x}\square_xMnO_{3-\delta}$ synthesized at comparatively low temperatures (1000–1100 °C) are self-doped systems. The presence of vacancies leads to the emergence of Mn^{4+} ions and to a colossal magnetoresistance.

Light circles in Fig. 1 show the results of measurements of temperature dependences $\rho(T,H)$ of the resistivity of $La_{0.7}\square_{0.3}MnO_{3-\delta}$ films in magnetic fields up to 10 kOe. The $\rho(T,H)$ curves have a broad peak at a certain temperature T_m. The value of T_m increases with magnetic field and lies in the region 210–230 K in the field range under investigation. The measurements of magnetization of the films (made at the Institute of Physics, Polish Academy of Sciences, War-

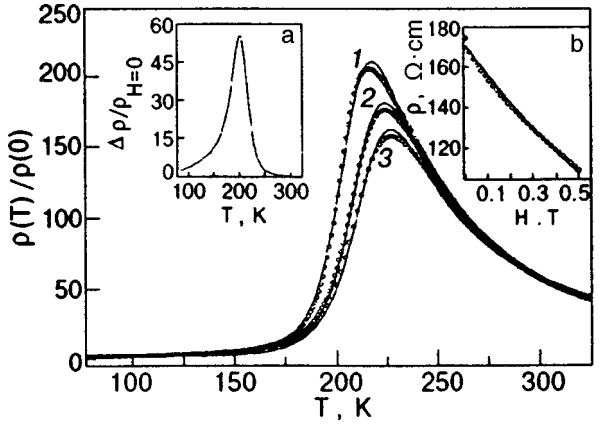

FIG. 1. Temperature dependences of resistivity $\rho(T,H)$ for various values of magnetic field H, T: 0 (curve *1*), 0.65 (curve *2*), and 1 (curve *3*). Circles correspond to experimental results and solid curves are the results of processing by formula (1). Inset (a) shows the temperature dependence of magnetoresistive effect $[\rho(0)-\rho(H)]/\rho(0)$ in the field $H=1$ T. Inset (b) illustrates the behavior of $\rho(T,H)$ at $T=202$ K; the solid curve shows the results of processing by formula (1).

saw) proved that the temperature T_m is close to the temperature of transition from the ferromagnetic to the paramagnetic state. The inset a to Fig. 1 shows the temperature dependence of MRE $[\rho(0)-\rho(H)]/\rho(0)$, whose magnitude was 56% in the field $H=1$ T. The inset b in Fig. 1 illustrates the field dependence of $\rho(T,H)$ at a fixed temperature.

The experimental data on $\rho(T,H)$ were processed by using the following empirical relation:[16]

$$\rho(77\ \text{K},0)/\rho(T,H)=\exp[-\alpha N(\omega_0+g\mu_B S_C H)] + \frac{b^2}{E_\rho kT}\exp\left(\frac{E_\rho}{kT}\right). \quad (1)$$

Here $N(\varepsilon)=[\exp(\varepsilon/kT)-1]^{-1}$ is the distribution function for magnons with energy ε, E_ρ the activation energy of a magnetic polaron, k the Boltzmann constant, $g=2$; μ_B the Bohr magneton, and α the structural factor. The first term in (1) describes the band conductivity mechanism for an electron ''dressed'' by magnons, while the second term takes into account the conductivity due to thermally activated hops by polarons. The coefficient T^{-1} in this case corresponds to adiabatic hopping mode. The nonadiabatic mode (with the coefficient $T^{-3/2}$) was also tested, but the difference between the adiabatic and nonadiabatic models was insignificant in the paramagnetic temperature range in which the second term determines the behavior of $\rho(T)$. We chose the adiabatic model of hopping conductivity which was preferred by other authors also (see, for example, Refs. 9, 20, and 27).

The quantities E_ρ, ω_0, S_C, α, and b are functions of microscopic parameters of the system whose explicit form is not known so far. We shall use these quantities as fitting parameters. The values of E_ρ, ω_0, α, and b were determined from the dependence $\rho(T,H=0)$, and the quantity S_C was then reconstructed from the field dependences $\rho(T,H)$ for fixed values of these parameters. The results of approximation of experimental data by formula (1) in the entire explored range of temperatures and magnetic fields are depicted by solid curves in Fig. 1.

The reconstructed values of the parameters are $E_\rho=(119\pm 0{,}6)$ meV, $\omega_0=(953\pm 10)$ K, $S_C=30-40$, $\alpha=530\pm 30$ and $b=(750\pm 13)$ K. The obtained values of $E_\rho\sim 100-200$ meV are typical of perovskite manganites (see, for example, Refs. 17, 20, 21, and 27). The most significant difference from the results obtained in Ref. 20 was observed for the parameter ω_0; in Ref. 20, this parameter is close to the energy of indirect exchange interaction in manganites $\sim 150-220$ K, while our value of ω_0 rather corresponds to the Hund energy. In our opinion, the latter fact indicates that the corresponding quasiparticles should be rather interpreted as optical ferromagnetic magnons.[28] A noticeable difference is also observed for the parameter S_C which is larger than in Ref. 20 by a factor of several units. According to Zhang,[16] S_C should be regarded as cluster spin of nanoscale. It should be noted that magnetic inhomogeneity of nanoscale was noted in a number of recent publications[27,29,30] as an intrinsic properties of perovskite-type lanthanum manganites exhibiting a colossal MRE.

It can be seen from Fig. 1 that electric transport properties of $La_{0.7}\square_{0.3}MnO_{3-\delta}$ films can be described satisfactorily in the model of conductivity crossover in the regions of magnetic phase transition. However, the coincidence of the results of theory and experiments can be false since a number of the parameters of the system are not defined at the modern stage of evolution of the theory (see above), and can be treated as fitting parameters. It should also be noted that the model[16] reduces the change in the transport properties only to a change in the mobility of charge carriers. At the same time, we can expect that not only the mobility of charge carriers, by their number density also changes in the vicinity of T_C. Taking into account this circumstance, we made thermoelectric measurements for the films. It is well known that the temperature behavior of thermopower (Seebeck coefficient) is very sensitive to the electron structure of conductors near the Fermi surface and is an effective indicator of various types of phase transitions.[31] The study of thermoelectric properties[1,15,20,27,32–34] demonstrates that this method is quite informative for manganite compounds also.

Thermopower

The Seebeck coefficient $S(T,H)$ is defined as the ratio of the potential difference between two points of the sample, appearing as a result of temperature difference between these points. The circles in Fig. 2 show the results of measurements of the $S(T,H)$ dependences for $La_{0.7}\square_{0.3}MnO_{3-\delta}$ films in fields up to 0.07 T. In the low-temperature range ($T<190$ K), the Seebeck coefficient has a value of several μV/K typical of metals. At $T>190$ K, a sharp increase is observed, and the value of $S(T,H)$ becomes an order of magnitude higher. The peak is attained at a temperature slightly higher than T_m. In the paramagnetic region ($T\sim 300$ K), the thermopower changes its sign. The insets to Fig. 2 show the values of $S(T,H)$ as a function of magnetic field at a fixed temperature: inset (a) for $T<T_m$ and inset (b) for $T\geqslant T_m$.

The experimental data for $S(T,H)$ were processed by using the following empirical relation:

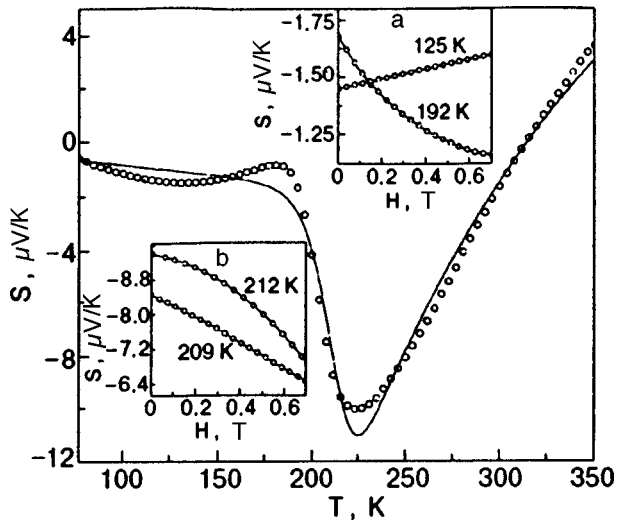

FIG. 2. The results of measurements of temperature dependences of the Seebeck coefficient $S(T,H)$; circles correspond to the results of experiments, and the solid curve is the result of processing by formula (2). The inset shows the magnetic field dependence $S(T,H)$ at a fixed temperature at $T<T_m$ (a) and $T\geqslant T_m$ (b).

$$-\frac{|e|}{k}\,\sigma_{\text{tot}}(T,H)S(T,H)=AT\,\exp[-\alpha N(\omega_0+g\mu_B S_C H)]+\left(\frac{E_S}{kT}-B\right)\times\frac{b^2}{E_\rho kT}\exp\left(-\frac{E_\rho}{kT}\right),\qquad(2)$$

where e is the electron charge, $\sigma_{\text{tot}}(T,H)$ the right-hand side of formula (1), and the values of the parameters E_ρ, ω_0, S_C, α, and b have already been determined from the dependence $\rho(T,H)$. Here we use the fact that the resultant value of thermopower is determined by the sum of partial contributions and that the expression for the Seebeck coefficient has different functional dependences for different mechanisms of motion of charge carriers. The results of approximation of experimental data by formula (2) in the explored temperature range at $H=0$ are depicted by the solid curve in Fig. 2.

The reconstructed values of the parameters are $E_S=(827\pm16)$ meV, $A=(8\pm0.6)\times10^{-3}$ μV/K^2, $B=(30.6\pm0.7)$ μV/K. The parameter B determines the asymptotic form of the Seebeck coefficient at $T\gg T_m$; it has the physical meaning of the entropy per charge carrier. The value of $S_\infty\sim10$ μV/K is typical of perovskite-type lanthanum manganites.[15,20,27,32,33] If one type of charge carriers makes a dominating contribution to the transport properties of the system, and the temperature range is such that thermally activated hops of polarons take place, we have $E_\rho=E_S+W_H$, where the energy W_H is equal to half the polarization energy of the lattice.[31] The value of E_S determined by us is several times larger than E_ρ, which is probably due to a noticeable contribution of hole states to the conductivity of $La_{0.7}\square_{0.3}MnO_{3-\delta}$ films. It is well known (see, for example, Refs. 27, 33, and 34) that two types of charge carriers (electrons and holes) with high and low mobilities can be expected in perovskite-type lanthanum manganites. The presence of holes also follows from the sign reversal of thermopower near 300 K. (It should be noted, however, that sometimes the sign reversal of thermopower can be due not to the competition between the electron and hole conductivities, but to random factors.[32])

The form of the field dependence of $S(T,H)$ at fixed temperatures is illustrated in the insets to Fig. 2. It should be noted that the coefficient in the field dependence of thermopower in this case changes sign from positive to negative near 150 K (see the inset (a) to Fig. 2). (Such a behavior of $S(H)$ in the magnetically ordered phase of manganites has not been described in the literature to our knowledge.) As the temperature increases, the value of $|S|$ decreases monotonically with increasing field. The behavior of $S(H)$ for $La_{0.7}\square_{0.3}MnO_{3-\delta}$ films is now similar to that established by Asamitsu *et al.*[33] for $La_{0.75}Sr_{0.25}MnO_3$ single crystals. (We can also mention the analysis of field dependences of the Seebeck coefficient for $La_{0.67}Ca_{0.33}MnO_3$ carried out by Chen *et al.*,[34] who noted a linear correlation between $S(H)$ and $\ln\rho(H)$.) The field dependences of thermopower in the vicinity of magnetic phase transition can be interpreted by taking into account the fact that an increase in the field corresponds to an increase in spin polarization, i.e., the $S(H)$ dependence must be similar to the $S(T)$ dependence for cooling in the region below (but close to) T_m. It can be seen from Fig. 2 that the absolute value of the Seebeck coefficient decreases in this region. The reasons behind the change in the form of the field dependence of thermopower in a magnetically ordered phase are not clear and require further investigations.

We failed to obtain a satisfactory description of the field dependence of the thermopower of the system by using formula (2), although the same mechanism is undoubtedly responsible for magnetoresistance and field dependences of thermopower. The most realistic physical reason behind the observed behavior of $S(T,H)$ can be formulated as follows. According to the prevailing ideas, perovskite-type lanthanum manganites are distinguished by a relatively narrow conduction band ($\sim$1.5 eV) and a high Hund energy ($\sim$2.5 eV). At low temperatures, the conduction band is completely spin-polarized and is separated by a large gap from the band with the opposite spin orientation.[35,36] Spin-polarized charge carriers determine the electric-transport and thermoelectric properties of the system in this temperature range. As we approach the Curie point, band splitting decreases, and the contribution of states with opposite spin orientations increases. We can expect that the contribution of such states in the region of T_m and higher is significant. At the same time, Zhang's model[16] disregards the effects of the change in the density of states with temperature in the vicinity of the Fermi surface and should be developed in this direction. As regards the change in the form of the field dependence of thermopower in the magnetically ordered phase, further investigations are also required in this field (see above).

Thus, the results of analysis of the Seebeck coefficient for $La_{0.7}\square_{0.3}MnO_{3-\delta}$ films indicate a considerable rearrangement of the band structure of the system in the vicinity of the magnetic phase transition. In this respect, self-doped systems

of the type of $La_{1-x}\square_x MnO_{3-\delta}$ are similar to other compounds of lanthanum manganites.

CONCLUSION

The magnetoresistive and thermoelectric properties of thin $La_{0.7}\square_{0.3}MnO_{3-\delta}$ films grown by reactive magnetron deposition have been investigated. The polaron nature of the conductivity of such films above and below the point of magnetic phase transition is established. The experimental dependences $\rho(T,H)$ and $S(T,H)$ are analyzed under the assumption on the crossover of the conductivity of the films from the metal type to hopping conductivity upon a change in temperature and the absence of a sharp FMM–PMS phase transition. The values and meaning of the phenomenological parameters of the system are discussed. The obtained experimental results indicate that not only the nature of the mobility of charge carriers changes in the region of magnetic phase transition, but the band structure also undergoes a considerable rearrangement in the vicinity of the Fermi surface.

The authors are grateful to V. P. Pashchenko for the preparation and synthesis of the ceramic materials for film deposition and to V. I. Kamenev for carrying out x-ray diffraction experiments.

*)E-mail: krivoruc@host.dipt.donetsk.ua

[1] E. P. Perekalina and L. P. Shlyachkina, Vestn. Mosk. Univ. Fiz. Astron. **34**, 9 (1993).
[2] S. Jin, M. McCormack, T. H. Tiefel, and R. Ramesh, J. Appl. Phys. **76**, 6929 (1994).
[3] R. Mahesh, R. Mahendran, A. K. Raychaudhuri, and C. N. R. Rao, J. Solid State Chem. **120**, 204 (1995).
[4] B. Raveau, A. Maignan, V. Caignaert, and Ch. Simon, J. Phys. (Paris) **7**, C1-621 (1997).
[5] Y. Tokura, Y. Tomioka, H. Kuwahara *et al.*, J. Appl. Phys. **79**, 5288 (1996).
[6] Y. Tomioka, A. Asamitsu, Y. Moritomo *et al.*, Phys. Rev. Lett. **74**, 5108 (1995).
[7] H. Kuwahara, Y. Tomioka, A. Asamitsu *et al.*, Science **270**, 961 (1995).
[8] A. J. Millis, P. S. Littlewood, and B. I. Shraiman, Phys. Rev. Lett. **74**, 5144 (1995).
[9] C. V. Varma, Phys. Rev. B **54**, 7328 (1996).
[10] R. Allub and B. Alascio, Phys. Rev. B **55**, 14 113 (1997).
[11] L. Sheng, D. Y. Xing, D. N. Sheng, and C. S. Ting, Phys. Rev. Lett. **79**, 1710 (1997).
[12] E. L. Nagaev, Usp. Fiz. Nauk **166**, 833 (1996) [sic].
[13] M. K. Gubkin and T. M. Perekalina, Pis'ma Zh. Éskp. Teor. Fiz. **60**, 727 (1994) [JETP Lett. **60**, 747 (1994)].
[14] V. N. Kriviruchko, Fiz. Nizk. Temp. **22**, 1047 (1996) [Low Temp. Phys. **22**, 798 (1996)].
[15] J. C. Miller, R. R. Heikes, and R. Mazelsky, J. Appl. Phys. **32**, 2202 (1961).
[16] S. Zhang, J. Appl. Phys. **79**, 4542 (1996).
[17] R. M. Kusters, J. Singleton, D. A. Keen *et al.*, Physica B **155**, 362 (1989).
[18] J. D. Lee and B. I. Min, Phys. Rev. B **55**, 12 454 (1997).
[19] G. Zhao, M. B. Hunt, and H. Keller, Phys. Rev. Lett. **78**, 955 (1997).
[20] M. Rubinstein, D. J. Gillespie, J. E. Snyder, and T. M. Tritt, Phys. Rev. B **56**, 5412 (1997).
[21] J. O'Donnel, M. Onellion, M. S. Rzchowski *et al.*, Phys. Rev. B **54**, R6841 (1996).
[22] M. F. Hundley, J. J. Neumeier, R. H. Heffner *et al.*, J. Appl. Phys. **79**, 4535 (1996).
[23] V. P. Pashchenko, S. I. Khartsev, O. P. Cherenkov *et al.*, Neorg. Mater. **34**, (1998).
[24] S. I. Khartsev, V. N. Krivoruchko, and V. P. Pashchenko, Fiz. Nizk. Temp. **23**, 840 (1997) [Low Temp. Phys. **23**, 631 (1997)].
[25] T. R. McGuire, A. Gupta, P. R. Duncombe *et al.*, J. Appl. Phys. **79**, 4549 (1996).
[26] A. Maignan, C. Michel, M. Hervieu, and B. Raveau, Solid State Commun. **101**, 277 (1997).
[27] M. F. Hundley and J. J. Neumeier, Phys. Rev. B **55**, 11 511 (1997).
[28] V. N. Krivoruchko and A. M. Yakovenko, Fiz. Nizk. Temp. **24**, 330 (1998) [Low Temp. Phys. **24**, 250 (1998)].
[29] M. Dominguez, S. E. Lofland, S. M. Bhagat *et al.*, Solid State Commun. **97**, 193 (1996).
[30] G. Allodi, R. De Renzi, G. Guidi *et al.*, Phys. Rev. B **56**, 6036 (1997).
[31] N. F. Mott and E. A. Devis, *Electronic Processes in Non-Crystalline Materials*, Oxford (1971).
[32] T. T. M. Palstra, A. P. Ramirez, S.-W. Cheong *et al.*, Phys. Rev. B **56**, 5104 (1997).
[33] A. Asamitsu, Y. Moritomo, and Y. Tokura, Phys. Rev. B **53**, R2952 (1996).
[34] B. Chen, C. Uher, D. T. Morelli *et al.*, Phys. Rev. B **53**, 5094 (1996).
[35] T. Amira, Y. Tokura, and J. B. Torrance, Phys. Rev. B **48**, 17 006 (1993).
[36] Y. Okimoto, T. Tatsufuji, T. Ishikawa *et al.*, Phys. Rev. Lett. **75**, 109 (1995).

Translated by R. S. Wadhwa

Nonlinear localized excitations in magnets with a weak exchange interaction as a soliton problem

M. V. Gvozdikova

Kharkov State University, 310077 Kharkov, Ukraine

A. S. Kovalev

B. Verkin Institute for Low Temperature Physics and Engineering, National Academy of Sciences of the Ukraine, 310164 Kharkov, Ukraine)*

(Submitted June 26, 1998)
Fiz. Nizk. Temp. **24**, 1077–1085 (November 1998)

Spin dynamics of soliton-like localized excitations in a discrete ferromagnetic chain with an easy-axis anisotropy and weak exchange interaction is studied. The relation of these excitations and dynamic magnetic solitons in the long-wave approximation is determined, and the dependence of frequency of localized excitations on the exchange interaction parameter for a fixed value of the total number of spin deviations is constructed. It is shown that this dependence is modified significantly for values of exchange interaction of the order of the one-ion anisotropy value.
 [S1063-777X(98)00611-2]

INTRODUCTION

Specific nonlinear localized excitations in magnetically ordered media (magnetic solitons) have been studied thoroughly and comprehensively in recent years.[1,2] However, these studies were mainly carried out in the long-wave approximation presuming that one-ion anisotropy is smaller than exchange interaction, which is justified for traditional magnets. In a series of subsequent theoretical publications,[3–6] it was shown that the structure and dynamics of localized excitations is modified qualitatively in magnets with a weak exchange interaction (for which the exchange integral J becomes of the order of or smaller than the one-ion anisotropy constant β), and the results obtained in the long-wave description become inapplicable.

Additional interest to this problem was stimulated in connection with recent synthesis of quasi-one-dimensional and quasi-two-dimensional magnets with $J\sim\beta$ and even with $J\ll\beta$. Examples of such materials are quasi-one-dimensional magnets $[(CH_3)_3NH]NiCl_3\cdot 2H_2O$, $(C_9H_7NH)NiCl_3\cdot 1.5H_2O$,[7] layered antiferromagnets such as $(CH_2)_n(NH_3)_2MnCl_4$, $(C_nH_{2n+1}NH_3)_2MnCl_4$ with the J/β ratio of the order of 10^{-2},[8–12] and most of high-temperature superconductors and their isostructural analogs. It is important that measurements in layered antiferromagnets were made for a series of samples with different indices n of organic molecules intercalating magnetic layers, and hence with different intensities of exchange interaction of magnetic layers. This permits an experimental study of variation of the structure and dynamic properties of localized excitations as a function of the exchange integral J.

The characteristic size of the magnetization field nonuniformity (e.g., domain wall width) in the long-wave approximation is of the order of the ''magnetic length'' $l_0=\sqrt{J/\beta}$ which decreases with exchange interaction. However, it was proved in Ref. 3 that for comparable values of the constants J and β, the domain wall ''collapses'' to atomic distances to form a collinear structure with parallel and antiparallel spin orientation. Later, Goncharuk *et al.*[4] considered a more complex compact collinear structure with an ''inverted'' spin, which is formed in the case of weak exchange interaction. (It should be noted that compactization of nonlinear localized excitations and the emergence of specific exotic solitons (compactons) has been discussed intensely in recent years.[13] The existence of compactons is associated with anomalously low spatial dispersion of elementary excitations in a system. In the case of magnetically ordered media, low dispersion of magnons is due to strong anisotropy of exchange interaction. Thus, the above two problems, i.e., the formation of collinear structures in systems with weak exchange interaction and the formation of compactons in systems with a strong anisotropy of this interaction, are interrelated.)

Stepanov and Yablonskii[14] presented the results of experiments on resonant properties of layered antiferromagnets and proved the presence of an additional absorption band in the gap of the magnon spectrum. These authors attributed the presence of such a band to the emergence of an intrinsic mode at domain walls or to the existence of specific structures with local spin flip in a magnetic layer. The transformation of the intrinsic mode of domain walls near the point of transition of a wall from collinear to canted structure was considered by us earlier.[6]

Since the collinear structure with an inverted spin proposed in Ref. 4 resembles a magnetic dynamic soliton, we shall study here the dynamics of localized nonlinear spin excitations of various types and the transformation of the collinear spin configuration analyzed in Ref. 4 into long-wave magnetic solitons by using the soliton theory.

FORMULATION OF MODEL AND LONG-WAVE DESCRIPTION OF MAGNETIC SOLITONS

Basic equations

Since the interaction of spin in the layers of layered magnets considered above is considerably stronger than the interaction between layers, we shall simulate each magnetic layer by an effective spin, thus reducing the problem to an analysis of a one-dimensional magnetic chain. The magnetization dynamics for such a chain is studied on the basis of the classical Heisenberg discrete model for an easy-axis ferromagnet. The expression for the total energy of a spin chain has the form

$$E=\sum_n \left\{ -J\mathbf{S}_n\mathbf{S}_{n+1}-\frac{\beta}{2}(\mathbf{S}_n\mathbf{e}_z)^2 \right\}, \tag{1}$$

where $\mathbf{S}_n$ is the lattice site spin ($|\mathbf{S}_n|^2=1$), J the exchange interaction constant ($J>0$ for a ferromagnet), and β the one-ion anisotropy constant ($\beta>0$ for an easy-axis ferromagnet with an easy axis directed along the axis $\mathbf{e}_z$); the lattice constant is assumed to be equal to unity. If we measure time in the units of $1/\omega_0$, where $\omega_0=2\beta\mu_0/\hbar$ is the frequency of uniform ferromagnetic resonance, and introduce the parameter $\lambda=J/\beta=l_0^2$, the dynamic equations corresponding to energy (1) (discrete Landau–Lifshitz equations without damping) can be written in the form[2]

$$d\frac{\mathbf{S}_n}{dt}+\lambda[\mathbf{S}_n(\mathbf{S}_{n+1}+\mathbf{S}_{n-1})]+[\mathbf{S}_n\mathbf{e}_z](\mathbf{S}_n\mathbf{e}_z)=0. \tag{2}$$

The parameter λ characterizes the chain discreetness: the long-wave limit corresponds to large values of the parameter ($\lambda\gg1$), while in the essentially discrete limit $\lambda\sim1$. Besides the obvious integral of motion (total energy (1)), the system of equations (2) for an easy-axis ferromagnet has an additional integral of motion, i.e., the total number N of spin deviations. We choose it in the form

$$N=\frac{1}{2}\sum_n (1-S_n^z). \tag{3}$$

With such a choice of normalization, the total number of spin deviations in a configuration with several completely inverted spins is equal to the number of such inverted spins.

It is convenient to go over to the complex-valued quantity $\Psi_n=S_n^x+iS_n^y$ (classical analog of the creation operator for magnons) and to the spin projection on the z-axis: $S_n^z=m_n$ ($m_n=\sqrt{1-|\Psi_n|^2}$). Henceforth, we shall consider only stationary dynamic states in which the entire dependence on time is reduced to uniform precession of sins about the easy axis $\Psi_n=\psi_n\exp(i\Omega t)$, where ψ_n are real-valued quantities. In this case, Eq. (2) can be written in the form

$$-\Omega\psi_n+\lambda[\psi_n(m_{n+1}+m_{n-1})-m_n(\psi_{n+1}+\psi_{n-1})]+\psi_n m_n=0. \tag{4}$$

In some cases, we shall use a slightly different form for this system of equations in terms of the variables $\vartheta_n=\arccos m_n$:

$$-\Omega\sin\vartheta_n+\lambda[\sin(\vartheta_n-\vartheta_{n+1})+\sin(\vartheta_n-\vartheta_{n-1})]+\sin\vartheta_n\cos\vartheta_n=0. \tag{5}$$

Long-wave description of magnetic solitons

The long-wave description of magnetization dynamics on the basis of differential equations is valid in the limit $\lambda\gg1$. In this case, we can go over from the discrete number n to the continuous coordinate x and write the system of difference equations (5) in the form

$$\lambda\vartheta_{xx}=\sin\vartheta\cos\vartheta-\Omega\sin\vartheta. \tag{6}$$

Soliton solutions of this equation are well known.[2] For the sake of simplicity, we shall confine our analysis to the particular case of symmetric (''positive-frequency'') magnetic solitons for which $\psi_n=\psi_{-n}$. The magnetization field distribution in such solitons has the form

$$\vartheta(x)=2\arctan\left[\frac{\sqrt{1-\Omega}}{\sqrt{\Omega}}\operatorname{sech}\left(\frac{\sqrt{1-\Omega}}{\sqrt{\lambda}}x\right)\right]. \tag{7}$$

In an analysis of soliton solutions, all parameters of a substance (the parameter λ in our case) are usually assumed as given, and the transformation of the soliton structure upon a change in its dynamic parameters (in particular, frequency Ω in our case) is studied. It can be seen from (7) that this solution in the limit $1-\Omega\ll\Omega$ is transformed into the solution for a small-amplitude soliton. In the opposite limiting case $\Omega\ll1$, a magnetic soliton is a bound state of two domain walls of width $l_0=\sqrt{\lambda}$ and with the separation $L\propto\ln\Omega$ between the walls. A change in the frequency of precession changes the number of spin deviations bound in the soliton. In the long-wave limit, this integral of motion is defined by the formula

$$N=\frac{1}{2}\int_{-\infty}^{\infty}dx(1-\cos\vartheta(x)). \tag{8}$$

Substituting solution (7) into formula (8), we find the dependence $N(\Omega)$ for $\lambda=$const:

$$N=2\sqrt{\lambda}\ \operatorname{Arth}\sqrt{1-\Omega}. \tag{9}$$

However, it was mentioned in Introduction that the dynamics of magnets can be studied at present on a batch of similar samples differing in the value of exchange interaction (i.e., the value of the parameter λ). In this case, formula (9) can be presented as a dependence of the precession frequency in a soliton from the discreetness parameter λ and the number N of spin deviations. In order to compare the characteristics of similar excitations, we fix the integral of motion N and analyze the dependence $\Omega(\lambda)$ for $N=$const:

$$\Omega=\operatorname{sech}^2\frac{N}{2\sqrt{\lambda}}. \tag{10}$$

Since we want to compare long-wave magnetic solitons and the collinear configuration with an inverted spin corresponding to the value $N=1$, which is considered in Ref. 4, we fix this value in formula (10):

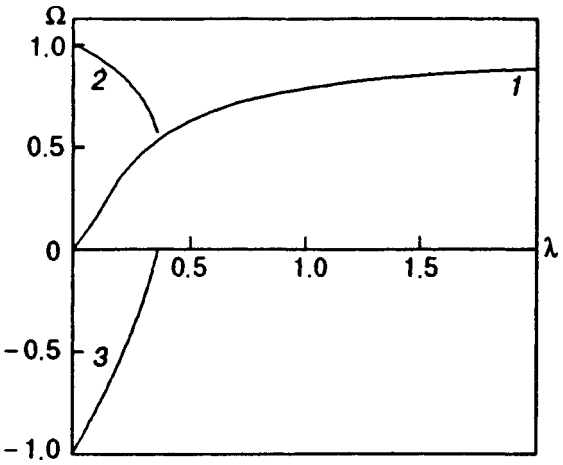

FIG. 1. Frequency Ω as a function of the discreteness parameter $\lambda = J/\beta$ for a magnetic soliton with the total number of spin deviations $N=1$ in the long-wave approximation (curve *1*) and for a collinear localized structure with an inverted spin from Ref. 4 (curves *2* and *3*).

$$\Omega = \operatorname{sech}^2 \frac{1}{2\sqrt{\lambda}}. \tag{11}$$

This dependence is plotted in Fig. 1 in the form of curve *1*. The asymptotic form of the dependence in the long-wave limit has the form $\Omega \simeq 1-1/(4\lambda)$. Although the long-wave approximation used by us is valid only for $\lambda \gg 1$, we depicted in Fig. 1 this dependence for all values of λ. (It will be proved below that the formulas of the long-wave limit hold well for $\lambda \sim 1$ as well.) If we formally consider the limit $\lambda \ll 1$ in which $\Omega \to 0 (\Omega \simeq \exp(-1/\sqrt{\lambda}))$, the solution differs significantly from the soliton solution in the limit $\Omega \to 0$ for a fixed value of λ: the localization domain tends to zero for $N=1$, and the soliton is transformed to a collinear configuration with a single inverted spin. However, the long-wave analysis becomes meaningless in this limit, and the problem must be solved by using discrete equations.

COLLINEAR STRUCTURE OF MAGNETIC SOLITONS

Let us consider again the system of discrete equations (4) describing stationary dynamic states with the precession frequency Ω. We confine our analysis to solutions with a symmetry of positive-frequency solitons (7), i.e., assume that $\psi_{-n} = \psi_n$, $m_{-n} = m_n$ (we assume that the center of a localized excitation corresponds to the spin with number $n=0$). Collinear states of this type were considered in Ref. 4 for values of the discreetness parameter $\lambda < \lambda_0$, where $\lambda_0 = (7 - \sqrt{17})/8$.

A collinear structure with a single inverted spin corresponds to the values $m_0 = -1$ and $m_n = 1$ for $n \neq 0$. We can linearize the discrete equations (4) in spin deviations ψ_n and obtain the following system of linear algebraic equations:

$$\begin{aligned}
&(2\lambda - 1 - \Omega)\psi_0 + 2\lambda\psi_1 = 0, \quad n = 0,\\
&(1-\Omega)\psi_1 - \lambda(\psi_0 + \psi_2) = 0, \quad n = 1,\\
&(2\lambda + 1 - \Omega)\psi_n - \lambda(\psi_{n+1} + \psi_{n-1}) = 0, \quad n \geqslant 2.
\end{aligned} \tag{12}$$

The solution of this system of equations decreasing at infinity has the form[4]

$$\psi_0 = B, \quad \psi_n = A \exp[-G(|n|-1)], \quad n \geqslant 1, \tag{13}$$

where

$$G = \operatorname{Arcch}\left[\frac{1-\Omega}{2\lambda} + 1\right]; \tag{14}$$

$$\frac{A}{B} = \left(\frac{1+\Omega}{2\lambda} - 1\right], \tag{15}$$

and the relation between the discreetness parameter λ and frequency Ω has the form

$$\lambda = \frac{(7 + 2\Omega - 5\Omega^2) - \sqrt{(7+2\Omega-5\Omega^2)^2 - 32(1-\Omega^2)^2}}{8(1-\Omega)}. \tag{16}$$

It follows from formula (16) that the given value of the parameter λ for $\lambda < \lambda_0$ corresponds to two solutions with different signs of frequency Ω. These solutions are depicted in Fig. 1 in the form of curves *2* and *3*. For the critical value of λ_0, the frequency corresponding to the lower branch vanishes. This fact was used by Goncharuk *et al.*[4] to draw the erroneous conclusion that the collinear structure with a single inverted spin under investigation is unstable in the region $\lambda > \lambda_0$.

In actual practice, this statement is valid when dissipation of the medium with zero integral of motion N is taken into account. In this case, the parallel ordering of spins in the region $\lambda > \lambda_0$ becomes unstable, and the localized inhomogeneous state is transformed from the collinear structure to a static canted phase with $m_0 = -1$ and $\psi_n = -\psi_{-n} \neq 0$, in which $N \neq 1$. In the absence of dissipation and with preserved value of the integral N, dynamic collinear structure are possible for $\lambda > \lambda_0$ also. Their stability is ensured by the conservation of the integral of motion N.

It can be seen that dynamic positive-frequency magnetic solitons and collinear spin configurations considered above possess the same symmetry and structure (the same total number of spin deviations and the same decrease in fields at infinity). Consequently, it is natural to assume that a decrease in the discreetness parameter λ leads to transformation of magnetic solitons into a collinear structure with inverted spin.

TRANSFORMATION OF MAGNETIC SOLITONS INTO COLLINEAR SPIN STRUCTURES

Let us consider first of all the solution of (13)–(16) for a collinear spin configuration in the entire region of its existence. The complete correspondence between the parameters Ω and λ for a state with an inverted spin following from formula (16) is depicted in Fig. 2 in the form of curve *1*. It can be seen that the critical value of the discreetness parameter is equal not to λ_0, but to λ_* at which the derivative $d\Omega/d\lambda$ is equal to infinity. It can easily be verified that the value of frequency at the critical point satisfies the equation

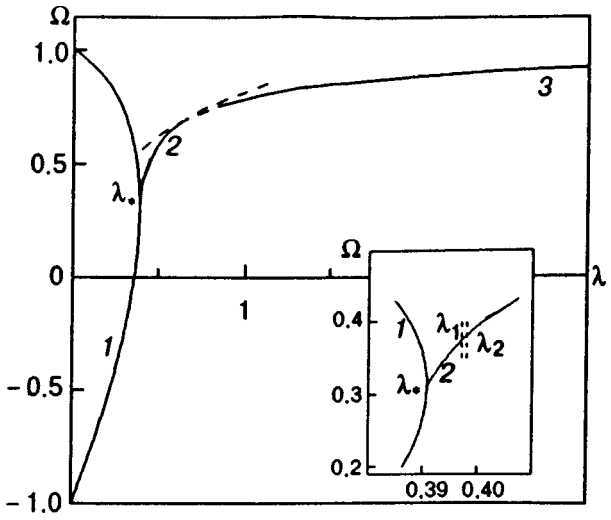

FIG. 2. Total dependence $\Omega(\lambda)$ for a dynamic collinear structure with an inverted spin (curve *1*) and the corresponding dependence for a canted phase of a dynamic magnetic soliton with $N=1$ in a discrete magnetic chain (curve *2*). (The dependence $\Omega(\lambda)$ obtained in the long-wave description of a magnetic soliton (curve *3*) is shown for comparison.) The inset shows the neighborhood of the bifurcation point on a magnified scale.

$$7\Omega^4-8\Omega^3-18\Omega^2+48\Omega-13=0. \tag{17}$$

The approximate solution of this equation gives the following values of parameters at the critical point: $\lambda_* \simeq 0.3907$ and $\Omega_* \simeq 0.3107$. As we move along the $\Omega(\lambda)$ curve from the point ($\Omega=1$, $\lambda=0$) to the point ($\Omega=-1$, $\lambda=0$), the solution is transformed as follows. Near the point $\Omega=1$, $\lambda=0$, the $\Omega(\lambda)$ dependence has the asymptotic form $\Omega\simeq 1-\lambda/2$. In this case, the value of $A/B\to\infty$, i.e., the central spin does not precess, and the decrease in spin deviations is described by the formula $\psi_{n+1}/\psi_n \simeq 0.5$. At the critical point (Ω_*,λ_*), the ratio of spin deviations at the center of a nonhomogeneous state and the rate of decrease in these deviations with number n are defined by the formulas $A/B \simeq 0.677$ and $\psi_{n+1}/\psi_n \simeq 0.2876$. Thus, practically the central inverted spin and its nearest neighbors only precess near this point. Finally, in the limit $\Omega\to -1$, $\lambda\to 0$, for $\Omega\approx -1+2\lambda$, we have $A/B\to 0$ and $\psi_{n+1}/\psi_n \approx (\lambda/2)\to 0$, i.e., only the inverted spin precesses.

It is natural to assume that long-wave magnetic solitons with the fixed value of $N=1$ are transformed into a collinear structure with a single inverted spin for $\lambda\sim\lambda_*$. In order to verify this assumption, we shall find first of all possible bifurcation points on the $\Omega(\lambda)$ curve, at which noncollinear solutions with $\psi_n\neq 0$ and $N=1$ can split from the solution with a collinear configuration. The point of bifurcation can be determined from the condition of fixation of the total number of spin deviations. Since $m_n \simeq \mathrm{sgn}(m_n)(1-\psi_n^2/2)$, for small deviations of spins from the ground state, formula (3) and the form of solution in the linear approximation (13)–(15) lead to the relation

$$N=1-\frac{B^2}{4}+\frac{A^2}{2(1-\exp(-2G))}. \tag{18}$$

The condition of conservation of the total number of spin deviations $N=1$ can be used to find the additional relation for the amplitudes of spin deviations in the linear approximation: $A/B=\sqrt{1-\exp(-2G)/2}$. Combining this relation with (14) and (15), we find the dependence $\Omega(\lambda)$ which must be satisfied at the point of bifurcation:

$$3\Omega^3+(1-14\lambda)\Omega^2+(1-4\lambda+20\lambda^2)\Omega+(3-6\lambda-4\lambda^2 -8\lambda^3)=0. \tag{19}$$

It can easily be verified that simultaneous fulfillment of formulas (16) and (19) gives the point of bifurcation coinciding with the point on the vertical tangential $\Omega=\Omega_*$, $\lambda=\lambda_*$. Thus, a dynamic symmetrical solution with nonzero deviations of rotating spins bifurcates in the form of a dynamic soliton with $N=1$ at this critical point from the collinear structure with one inverted spin. In spite of the smallness of spin deviations from the ground state near the bifurcation point, the solution for a magnetic soliton with noncollinear structure can be found only if we take into account the nonlinearity of discrete equations of spin dynamics, which complicates the problem significantly.

In order to simplify calculations, we can take advantage of the fact that spin deviations at the bifurcation point decrease rapidly with increasing distance from the center of a localized excitation (spin with the number $n=0$), and only precession amplitudes for spins with numbers $n=0,\pm 1$ actually differ from zero. Moreover, it will be proved below that this property of the solution is preserved up to large values of λ for which the long-wave approximation becomes applicable.

We shall use the system of difference equations for stationary states in the form (5). We shall take exact equations for spins with numbers $n=0,\pm 1$, in the equations for spins with numbers $n=\pm 2$, we take into account completely the nonlinearity of dynamic terms as well as the energies of anisotropy and the energies of exchange interaction with spins with the numbers $n=\pm 1$, respectively, but the energy of exchange interaction with neighbors having the numbers $n=\pm 3$ will be taken into account in the linear approximation. Finally, all the remaining equations for particles with numbers $|n|\geqslant 3$ are linearized in spin deviations ϑ_n. Taking into account the symmetry of the solution ($\vartheta_n=\vartheta_{-n}$), we can write the system of equations (5) in the form

$$\begin{aligned}
&-\Omega\sin\vartheta_0+\sin\vartheta_0\cos\vartheta_0+2\lambda\sin(\vartheta_0-\vartheta_1)=0,\\
&-\Omega\sin\vartheta_1+\sin\vartheta_1\cos\vartheta_1+\lambda\sin(\vartheta_1-\vartheta_0)\\
&\quad+\lambda\sin(\vartheta_1-\vartheta_2)=0,\\
&-\Omega\sin\vartheta_2+\sin\vartheta_2\cos\vartheta_2+\lambda\sin(\vartheta_2-\vartheta_1)\\
&\quad+\lambda(\vartheta_2-\vartheta_3)=0,
\end{aligned} \tag{20}$$

$$\cdots\cdots\cdots\cdots\cdots\cdots\cdots\cdots\cdots\cdots$$

$$-\Omega\vartheta_n+\vartheta_n+\lambda(2\vartheta_n-\vartheta_{n-1}-\vartheta_{n+1})=0,\quad |n|\geqslant 3.$$

The linearization of equations with large spin numbers allows us to select easily the solution decreasing at infinity:

$$\vartheta_n=\vartheta_2\exp[-G(|n|-2)],\quad |n|\geqslant 2, \tag{21}$$

where the dependence $G(\Omega,\lambda)$ is defined by formula (14) as before.

Thus, the equation for ϑ_2 in system (20) can be written in the form

$$-\Omega \sin \vartheta_2 + \sin \vartheta_2 \cos \vartheta_2 + \lambda \sin(\vartheta_2 - \vartheta_1) + \lambda \vartheta_2 [1 - \exp(-G)] = 0 \quad (22)$$

and forms with the first two equations from (20) a closed system of three nonlinear algebraic equations for the amplitudes $\vartheta_0, \vartheta_1, \vartheta_2$.

The first equation in (20) can be used to express the dependence $\vartheta_1(\vartheta_0, \Omega, \lambda)$ in a cumbersome, but explicit form, while the second equation leads to the explicit dependence $\vartheta_2(\vartheta_0, \Omega, \lambda)$. After this, Eq. (22) can be reduced to a cumbersome nonlinear algebraic equation for the amplitude ϑ_0 of a magnetic soliton, containing the parameters Ω and λ. This equation, which is not written here in view of its cumbersome form, was solved numerically. For a given value of the discreetness parameter λ, the solution for ϑ_0, and hence for all ϑ_n, was determined for various values of precession frequency Ω, and the obtained distribution of magnetization was substituted into formula (3) for the total number of spin deviations in a soliton, which has the following form to within the accuracy of our calculations:

$$N = \frac{1}{2}(1 - \cos \vartheta_0) + 2 - \cos \vartheta_1 - \cos \vartheta_2 + \frac{\vartheta_2^2}{2[\exp(2G) - 1]}. \quad (23)$$

From all the roots of the equation, we chose the one for which the value of N was close to unity and determined the value of frequency for which $(N-1)$ changed its sign. Thus, we determined the sign of the derivative $d\Omega/dN$ apart from the dependence $\Omega(\lambda, N=1)$.

The results of numerical analysis of the problem can be formulated as follows.

Above all, we have verified that the solution for a canted (noncollinear) phase of a magnetic soliton indeed bifurcates from the solution for a collinear phase with inverted spin at the critical point $\Omega = \Omega_*$, $\lambda = \lambda_*$, and the curves $\Omega(\lambda)$ for the collinear and canted structures at the critical point are not perpendicular to each other as in the conventional theory of bifurcations.

The structure of a magnetic soliton changes radically in a narrow region near the critical point, the spin deviations for five central particles from their equilibrium positions in the collinear phase amounting to ~ 0.5 even when the discreteness parameter λ exceeds its critical value by 0.06. However, spin deviations at the remaining sites of the chain in this case remain small ($\vartheta_n < 0.1$), which justifies the approximations made by us in the search of solutions in the approximation. The obtained dependence is presented by curve *2* in Fig. 2, while curve *3* corresponds to the dependence $\Omega(\lambda)$ obtained earlier in the long-wave description of magnetic solitons with the number of spin deviations $N=1$. The segments *2* and *3* on the solid curves in Fig. 2 correspond respectively to the values of the parameter λ for which the discrete model in our approximation and the long-wave approach are applicable. Although the magnitude of spin deviations at sites with numbers $n \geqslant 3$ increases with the parameter λ, the dependence $\Omega(\lambda)$ following from discrete equations is in good agreement with the results of long-wave analysis. It can be seen that the results of the long-wave description correctly approximate the structure of a dynamic magnetic soliton in a discrete spin chain in a wide range of values of the discreetness parameter. However, the results of long-wave and discrete descriptions differ significantly in a narrow range of λ near the critical value.

When the discreteness parameter of the system attains its critical value, a magnetic soliton ''collapses'' into a collinear structure with parallel and antiparallel spin orientations. In this case, the frequency dependence is modified significantly.

Unfortunately, the discrete description of the structure and dynamics of a magnetic soliton in the noncollinear phase in the case of an infinite spin chain requires numerical calculations, and the analysis becomes complicated. However, only three central spins actually participate in spin dynamics in the region of strong transformation of the soliton solution from the collinear to the canted form near the bifurcation point. Consequently, we can assume that an analysis of finite-length spin chains can give additional information concerning the transformation of solitons into a compact structure (especially, in the case when the study can be carried out analytically). This was verified in an analysis of intrinsic modes of domain walls in discrete ferromagnetic chains (see Ref. 6). In Appendix, we shall consider a chain of three spins in a configuration with the inverted central spin, and demonstrate analytically that a transition of a soliton from a canted to a collinear form has qualitatively the same form as in an infinite chain, although it has some distinguishing features.

In conclusion, we consider the sign of the derivative $d\Omega/dN$ for the obtained magnetic solitons in discrete spin chains. This question is of primary importance in the theory of solitons since the stability of soliton solutions is connected with the sign of this derivative. In the long-wave description, relation (10) implies that $d\Omega/dN < 0$. The numerical analysis carried out by us proved that this result is also valid for small values of the discreetness parameter λ including a narrow neighborhood of the critical point. However, the derivative $d\Omega/dN$ changes its sign in this neighborhood. To within the accuracy of our calculations, $d\Omega/dN$ vanishes for $\lambda = \lambda_2 = 0.398$, remains equal to zero in the interval $\lambda_1 < \lambda < \lambda_2$, and becomes positive for $\lambda_* < \lambda < \lambda_1 = 0.397$. The existence of the finite interval of zero values of this derivative is probably associated with insufficient accuracy of numerical calculations; as the accuracy is improved, this interval contracts into a point at which $d\Omega/dN$ changes its sign. It is interesting to note that the inequality $d\Omega/dN < 0$ holds in the entire frequency range for solitons in the collinear phase.

The negative sign of the derivative $d\Omega/dN$ for dynamic solitons in the theory of solitons in media with distributed parameters usually indicates their stability, while the positive sign points towards their modulation instability. However, such a simple relation between stability and the sign of $d\Omega/dN$ may not be observed for systems without translational invariance (see Ref. 15). In the case of a discrete spin chain, the system does not possess translational invariance,

and the problem of stability of discrete solitons requires additional analysis.

The authors are grateful to M. M. Bogdan for fruitful discussions and valuable remarks.

This research was supported by the Foundation of Fundamental Studies of the Ukrainian State Committee on Science and Technology (project ''Soliton 3'').

APPENDIX

Let us consider a chain of three spins with free ends in the symmetry configuration considered in this work. The system of equations (4) can be reduced to the following system of two equations:

$$-\Omega\psi_0+2\lambda(\psi_0 m_1-\psi_1 m_0)+\psi_0 m_0=0,$$
$$-\Omega\psi_1+\lambda(\psi_1 m_0-\psi_0 m_1)+\psi_1 m_1=0. \quad \text{(A1)}$$

This system should be supplemented with the condition of equality of the total number of spin deviations to unity: $m_0+2m_1=1$. Using the relation between m_i and ψ_i ($m_i^2+\psi_i^2=1$), we can express all quantities only in terms of $m_1=m$:

$$(1-m)[3m^3+(6\Omega-5)m^2+m-\Omega^2]=0,$$
$$(1-3m)[(3-8\lambda)m^3+(2-6\lambda)m^2+(2\lambda-1)m+\lambda^2]\sqrt{1-m}=0. \quad \text{(A2)}$$

The obtained equations have three different solutions. The simplest solution with $m=1$ ($m_1=m_{-1}=1$, $m_0=-1$) corresponds to a collinear structure with an inverted spin. Linearization of (A1) in the vicinity of this state with $\psi_i \ll 1$ leads to the following form of the dependence $\Omega(\lambda)$:

$$\Omega=\frac{1}{2}(\lambda\pm\sqrt{\lambda^2-12\lambda+4}), \quad \text{(A3)}$$

which is close qualitatively to the dependence (16) for an infinite spin chain. The critical value of the parameter λ is now equal to $\lambda_*=2(3-2\sqrt{2})\simeq 0.343$, and $\Omega_*=3-2\sqrt{2}\simeq 0.1716$. This dependence is represented by curve *1* in Fig. 3.

The second solution of Eqs. (A2) corresponds to a homogeneous state with $N=1$, in which $m_i=1/3$ and $\Omega=1/3$ (curve *3* in Fig. 3). In the theory of nonlinear excitations in finite-dimensional systems, such homogeneous states play a special role. Localized states of the soliton type exist in unbounded systems for infinitely small levels of excitation, while spatially nonhomogeneous localized solutions in finite-size systems split from the homogeneous state with a finite excitation level of the system.[16] In the case under investigation, solutions for magnetic solitons with a fixed value of N split from nonlinear spatially homogeneous solutions for a finite value of the discreetness parameter λ. This critical value decreases with the length of the system and amounts to $\lambda_{**}=8/27\simeq 0.296<\lambda_*$ for a chain of three spins.

Finally, the most interesting solution for a ''noncollinear'' soliton and the corresponding dependence $\Omega(\lambda)$ are defined implicitly by the following system of equations:

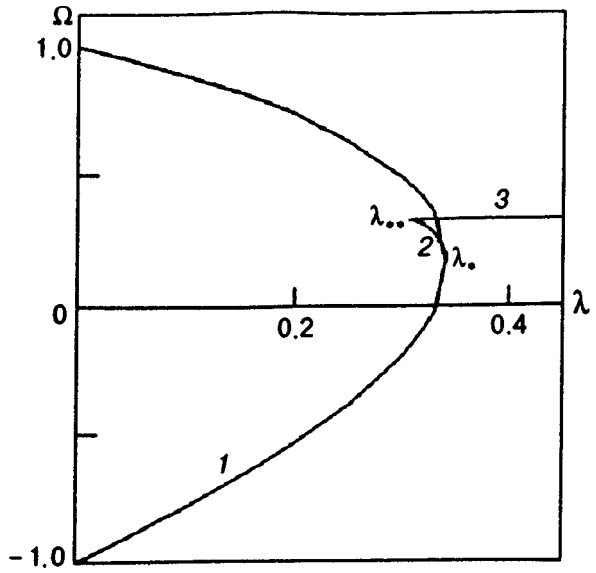

FIG. 3. Dependence $\Omega(\lambda)$ for a chain of three interacting spins. Curve *1* corresponds to a collinear configuration with an inverted central spin, curve *2* to a localized excitation of the soliton type in the canted phase; and straight line *3* to a uniform precession of magnetization.

$$\Omega=3m^2-(3m-1)\sqrt{m^2+m},$$
$$\lambda=m(1+m)(4m-1)-\sqrt{m(1+m)(4m^2+m-1)^2}. \quad \text{(A4)}$$

The dependence $\Omega(\lambda)$ for this solution is plotted in Fig. 3 in the form of curve *2*. It can be seen that it splits from the line corresponding to a collinear configuration at the point with the vertical derivative and is directed at an angle to it. Thus, the analytic result for a finite-length spin chain coincides qualitatively with the result of numerical analysis of the transformation of a magnetic soliton into a local collinear structure in an infinite discrete spin chain.

*)E-mail: kovalev@ilt.kharkov.ua

[1] A. Hubert, *Theorie der Domanenwande in geordneten Medien*, Springer, Heidelberg (1974).
[2] A. M. Kosevich, B. A. Ivanov, and A. S. Kovalev, *Nonlinear Magnetization Waves. Dynamic and Topological Solitons* [in Russian], Naukova Dumka, Kiev (1988).
[3] J. J. Van den Broek and H. Zijlstra, IEEE Trans. Magn. **7**, 226 (1971); M. M. Bogdan, A. M. Kosevich, and V. P. Voronov, in *Solitons and Applications* (Ed. by V. G. Makhankov, V. K. Fedyanin, and O. K. Pashaev), World Scientific, Singapore (1990).
[4] A. N. Goncharuk, A. A. Stepanov, and D. A. Yablonskii, Fiz. Tverd. Tela (Leningrad) **31**, 132 (1989) [Sov. Phys. Solid State **31**, 2099 (1989)].
[5] I. G. Gochev, Zh. Éksp. Teor. Fiz. **85**, 199 (1983) [Sov. Phys. JETP **58**, 115 (1983)]; I. V. Barashenkov, M. M. Bogdan, and V. I. Korobov, Europhys. Lett. **15**, 113 (1991).
[6] M. V. Gvozdikova, A. S. Kovalev, and Yu. S. Kivshar', Fiz. Nizk. Temp. **24**, 641 (1998) [Low Temp. Phys. **24**, 486 (1998)].
[7] A. S. Kovalev and M. V. Gvozdikova, Fiz. Nizk. Temp. **24**, 635 (1998) [Low Temp. Phys. **24**, 479 (1998)].
[8] A. G. Anders, V. G. Borisenko, and S. V. Volotskii, Fiz. Nizk. Temp. **15**, 39 (1989) [Sov. J. Low Temp. Phys. **15**, 21 (1989)].
[9] M. I. Kobets, A. A. Stepanov, and A. I. Zvyagin, Fiz. Nizk. Temp. **7**, 1473 (1981) [Sov. J. Low Temp. Phys. **7**, 714 (1981)].
[10] A. I. Zvyagin, M. I. Kobets, V. N. Krivoruchko *et al.*, Zh. Éksp. Teor. Fiz.

89, 2298 (1985) [Sov. Phys. JETP **62**, 1328 (1985)].
[11] A. I. Zvyagin, V. N. Krivoruchko, V. A. Pashchenko *et al.*, Zh. Éksp. Teor. Fiz. **92**, 311 (1987) [Sov. Phys. JETP **65**, 177 (1987)].
[12] A. A. Stepanov, V. A. Pashchenko, and N. M. Kobets, Fiz. Nizk. Temp. **14**, 550 (1988) [Sov. J. Low Temp. Phys. **14**, 304 (1988)].
[13] A. A. Stepanov, V. A. Pashchenko, and N. M. Kobets, Fiz. Nizk. Temp. **14**, 1114 (1988) [Sov. J. Low Temp. Phys. **14**, 611 (1988)].
[14] A. A. Stepanov and D. A. Yablonskii, Fiz. Nizk. Temp. **15**, 215 (1989) [Sov. J. Low Temp. Phys. **15**, 122 (1989)].
[15] M. M. Bogdan, I. V. Gerasimchuk, and A. S. Kovalev, Fiz. Nizk. Temp. **23**, 197 (1997) [Low Temp. Phys. **23**, 145 (1997)].
[16] A. M. Kosevich and A. S. Kovalev, *Introduction to Nonlinear Physical Mechanics* [in Russian], Naukova Dumka, Kiev (1990).

Translated by R. S. Wadhwa

ELECTRONIC PROPERTIES OF METALS AND ALLOYS

Non-linear effects in hopping conduction of single-crystal $La_2CuO_{4+\delta}$

B. I. Belevtsev, N. V. Dalakova, and A. S. Panfilov

B. I. Verkin Institute for Low Temperature Physics and Engineering, National Academy of Sciences of Ukraine, 47 Lenin ave. Kharkov, 310164, Ukraine[*]

(Submitted June 30, 1998)
Fiz. Nizk. Temp. **24**, 1086–1094 (November 1998)

The unusual non-linear effects in hopping conduction of single-crystal $La_2CuO_{4+\delta}$ with excess oxygen has been observed. The resistance is measured as a function of the applied voltage U (voltage controlled regime) in the temperature range $5\ \mathrm{K} \leqslant T \leqslant 300\ \mathrm{K}$ and voltage range $10^{-3}-25$ V. At relatively high voltage (approximately at $U>0.1$ V) the conduction of sample investigated corresponds well to variable-range hopping (VRH). That is, in the range $0.1\ \mathrm{V}<U\leqslant 1$ V the conductivity does not depend on U (Ohmic behavior) and the temperature dependence of resistance $R(T)$ follows closely Mott's law of VRH $[R\propto\exp(T_0/T)^{1/4}]$. In the range of highest applied voltage the conduction has been non-Ohmic: the resistance decreases with increasing U. This non-linear effect is quite expected in the frame of VRH mechanism, since the applied electric field increases the hopping probability. A completely different and unusual conduction behavior is found, however, in the low voltage range (approximately below 0.1 V), where the influence of electric field and (or) electron heating effect on VRH ought to be neglected. Here we have observed strong increase in resistance at increasing U at $T \leqslant 20$ K, whereas at $T>20$ K the resistance decreases with increasing U. The magnetoresistance of the sample below 20 K has been positive at low voltage and negative at high voltage. The observed unusual non-Ohmic behavior at low voltage range is attributable to inhomogeneity of the sample, namely, to the enrichment of sample surface with oxygen during the course of the heat treatment of the sample in helium and air atmosphere before measurements. At low enough temperature (below $\approx$20 K) the surface layer with increased oxygen concentration is presumed to consist of disconnected superconducting regions in a poorly conducting (dielectric) matrix. This allows us to explain the observed unusual non-linear effects in the conduction of sample studied. The results obtained demonstrate that in some cases the measured transport properties of cuprate oxides cannot be attributed to the intrinsic bulk properties. [S1063-777X(98)00711-7]

1. INTRODUCTION

High-temperature (high-T_c) superconductivity of cuprate oxides with perovskite-related structure is still a fascinating problem in solid state physics. Aside from superconductivity the investigations of these materials also give the possibility of studying other fundamental phenomena, for example, magnetism, electron localization and hopping, metal-insulator transition. It is well known that electronic and magnetic properties of cuprate oxides depend essentially on charge carriers density which in its turn depends strongly on chemical composition. Introducing the donor or acceptor impurities into oxides, or changing the oxygen concentration in them it is possible to vary their conductivity over wide limits and to cause the transition from insulating to metallic state in some cases. To judge whether a system is in the metallic, superconducting or insulating state the measurements of transport properties are used in most cases. From these measurements the magnitude, temperature and magnetic-field dependences of resistivity and other conduction characteristics can be obtained. These data are often used for the characterization of prepared samples and evaluation of their ''quality''. But it is not uncommon that the measured transport characteristics do not correspond to the intrinsic crystal, stoichiometric and, therefore, electronic and magnetic properties of the sample. In the majority of the cases the main reason for it is a sample inhomogeneity due to peculiarities of sample preparation procedure, heat treatment and other related factors. Two main possible sources for cuprate inhomogeneity can be distinguished: intrinsic and extrinsic. Intrinsic source is connected with phase separation of cuprate oxides on two phase with different concentration of charge carriers.[1] The extrinsic one is due to various technological factors of sample preparation. This may lead, among other things, to significant difference in charge carriers density between the surface and inner parts of the sample.[2]

In our opinion the investigations of influence of surface or volume inhomogeneity of cuprate oxides on their transport properties are of considerable importance in two following aspects. First, such kind of studies can help to answer the

question in what degree the observed transport properties can be attributed to intrinsic properties of the bulk crystal.[2] Second, under gaining enough experimental data on this matter (combined with necessary theoretical considerations and treatments) it is possible to apply the transport measurements not only for revealing of structural inhomogeneity, but also for identification of specific types of surface and volume inhomogeneities. Therefore, study of influence of inhomogeneity on transport properties of cuprate oxides is of both fundamental and applied importance.

In this communication we shall describe some new results of investigation of hopping conduction of single-crystal $La_2CuO_{4+\delta}$ with some amount of excess oxygen ($\delta \neq 0$). In the studies of high-T_c superconductivity these compounds have attracted considerable attention. The stoichiometric La_2CuO_4($\delta = 0$) is an antiferromagnetic insulator with Neel temperature T_N in the range 300–325 K.[1,3,4] However, the introducing of excess oxygen (as well as doping with bivalent metals such as Sr) leads to the violation of long-range antiferromagnetic order and to a transition to metallic and superconducting states. Excess oxygen doping introduces additional charge carriers (holes) in Cu-O planes.[5] For high doping level ($\delta \simeq 0.13$) the superconducting transition temperature T_c may be as high as $\simeq$50 K.[6] For the range of doping $\delta \simeq 0.01$–0.055 the $La_2CuO_{4+\delta}$ compounds undergo a phase separation below room temperature into the two phases with different oxygen content: the oxygen-poor phase is nearly stoichiometric and non-superconducting, while the oxygen-rich phase is superconducting.[1,5,7–10] Depending on the δ value, the different (sometimes coexisting) superconducting phases can emerge with T_c values from $\simeq$20 to $\simeq$45 K.[1,5,7–11]

It is known that low-temperature conduction of nearly stoichiometric $La_2CuO_{4+\delta}$ occurs by variable-range hopping (VRH) of localized holes[12–15] and can be fitted well to Mott's formula [with temperature dependence of resistance $R \propto \exp(T_0/T)^{1/4}$]. In Refs. 14 and 15 it was found that the transition from VRH to simple activation conduction $R \propto \exp(\Delta/kT)$ occurs at temperatures below 20 K (the similar effect was described also before in Ref. 13). In Refs. 14 and 15 this effect was explained by the influence of sample inhomogeneity, namely, by the presence of superconducting inclusions in the insulating sample due to phase separation of $La_2CuO_{4+\delta}$. As was mentioned in Ref. 2, in each case when some exotic transport behavior of cuprate oxides is found, the reason for it should be sought primarily in the possible influence of inhomogeneity. Our new experimental results support (as we believe) this point of view. We have observed the unusual non-linear behavior of hopping conduction of single-crystal $La_2CuO_{4+\delta}$: at low applied voltages (in conditions where the influence of electric field and (or) electron heating effect on VRH can be neglected) the resistance strongly increases with increasing of applied voltage at $T \lesssim 20$ K, but decreases with voltage increasing at temperatures above 20 K. This unusual non-Ohmic behavior is attributed to inhomogeneity of sample, namely, to the enrichment of sample surface with oxygen during the course of the heat treatment of the sample in helium and air atmosphere before measurements. At low enough temperature (below $\approx$20 K) the surface layer with increased oxygen concentration is presumed to consist of disconnected superconducting regions in a poorly conducting (dielectric) matrix.

2. SAMPLE AND EXPERIMENT

We have studied the hopping conduction of the same single-crystal sample of $La_2CuO_{4+\delta}$ as in Refs. 14 and 15, but with reduced and inhomogeneous oxygen content in it as a result of the heat treatment in helium gas and air outlined below. The original sample or, as it is better to say, the original state of this sample, is characterized by $T_N \simeq 230$ K and $\delta \approx 0.005$.[14,15] For reducing the oxygen content the sample was annealed in a furnace in an atmosphere of helium at $T \simeq 330$ °C for two hours. It was rather slowly cooled thereafter (about 4 h) in the same inert atmosphere. It is known that annealing in inert gas atmosphere is a very effective way to reduce the oxygen content in cuprate oxides.[12] The resistance of the sample after this procedure (measured by a standard four-probe technique) has appeared however to be too high (about 1.7 kΩ) for intended study of the hopping conduction at low temperatures (down to about 5 K). Therefore it was additionally annealed in air at $T \simeq 330$ °C for 2.5 h and (for lowering the contact resistance) at $T \simeq 80$ °C for 2 h. As a result of such heat and gas treatment, the oxygen content in single-crystal sample was reduced significantly. This is evidenced by an increase of Néel temperature T_N from 230 to 290 K and very large rise (of more than three order of magnitude at liquid helium temperatures) in resistance (see Figs. 1 and 2, in which the temperature dependences of magnetic susceptibility and resistance are shown for the original state of the sample and for the state after above-described gas and heat treatment). The rather high crystal quality of sample investigated is characterized by the high anisotropy of magnetic susceptibility (Fig. 1).

The sample studied has dimensions approximately 3×3×2 mm. For resistance measurement the thin gold contact wires were connected to the sample by a silver epoxy paste which was hardened at $T \simeq 80$ °C for 2 h. The measuring direct current I was parallel to the Cu-O planes. Two techniques were used in resistance measurements: (i) A standard four-probe technique when sample resistance was less than $\approx 4 \cdot 10^6$ Ω; (ii) Two-probe technique for higher sample resistances. For both techniques, actually, the $I-V$ characteristics were measured with applied voltage varying U (voltage controlled regime). From these data we shall present below the obtained dependences $R(T,U)$ and $I(U)$.

In measurements of high-resistive semiconducting samples with non-Ohmic effects it is important to take into account the possible influence of contact resistances. Concerning our sample, we can say the following on this point. First, both of the (four-probe and two-probe) techniques give the same behavior of $I-V$ curves and very similar values of the resistance $R = U/I$ (as a rule, the difference is not more than about 2%) in the resistance range $2 \times 10^5 - 4 \cdot 10^6$ Ω. This range corresponds approximately to the temperature range 15–25 K. Second, the special estimation of influence of contact resistances (using different contact places or short-circuiting wires) at $R \geqslant 10^9$ Ω (this corresponds to

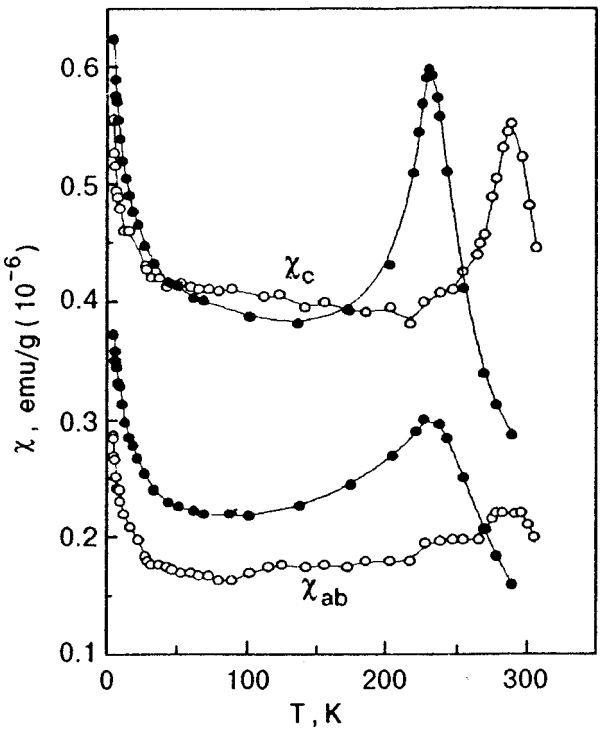

FIG. 1. Temperature dependences of the magnetic susceptibility χ in the magnetic field $H=0.83$ T of the single-crystal sample of the $La_2CuO_{4+\delta}$ in the initial state (●) and after the outlined heat treatment in helium and air (○). The quantity χ_c corresponds to the measurements in a magnetic field parallel to the crystallographic axis *c* (the unit cell corresponds to the crystallographic *Bmab* structure in which $a<b<c$, *c* being the tetragonal axis). The dependences $\chi_c(T)$ are represented by two upper curves. The quantity χ_{ab} is the susceptibility in a magnetic field parallel to Cu-O planes (two bottom curves). The positions of maximums of $\chi(T)$ dependences correspond to Néel temperature T_N.

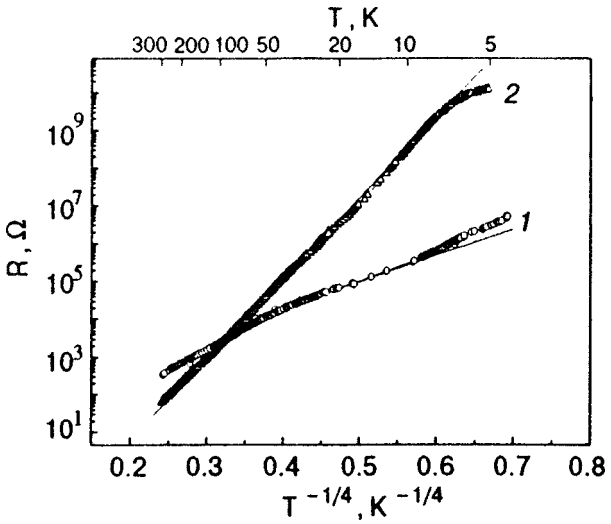

FIG. 2. The dependences of the resistance *R* (on logarithmic scale) on $T^{-1/4}$ of the sample in initial state (curve *1*) and after the outlined heat treatment in helium and air (curve *2*). The dependences were registered at applied voltage $U=25$ V.

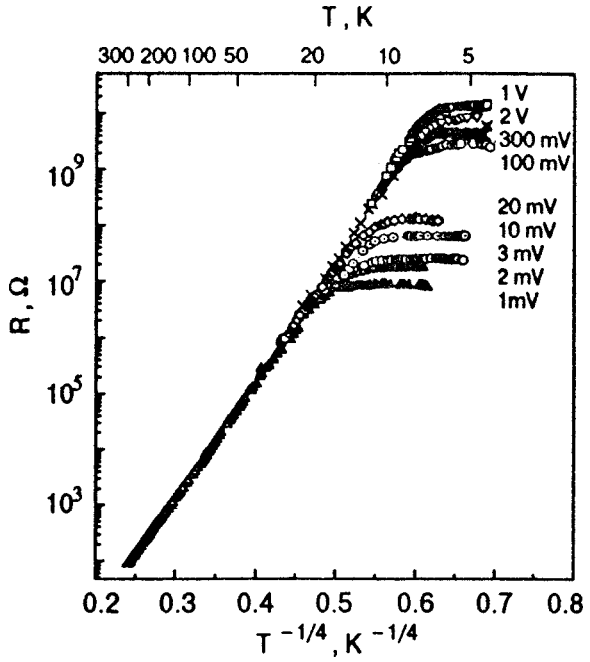

FIG. 3. The dependences of the resistance *R* (on logarithmic scale) on $T^{-1/4}$ of the sample studied at different magnitudes of applied voltage.

temperature below 10 K) has shown that the ratio of contact resistance to measured sample resistance is less than 10%. All this implies (as we believe) that the contact resistance has not much influence on reliability of the obtained results.

The $I-V$ curves and resistance were also recorded in a magnetic field H (with magnitude up to 5 T) in the temperature range 5–40 K. The magnetic field was directed along the Cu-O planes at the right angle to the measuring current.

3. RESULTS AND DISCUSSION

We found that hopping conduction of sample investigated follows the Mott's law of VRH closely:

$$R \propto \exp\left(\frac{T_0}{T}\right)^{1/4}, \tag{1}$$

where $T_0 \simeq 6.4 \cdot 10^6$ K. It can be seen in Figs. 2 and 3 that this law holds for broad temperature range (10–300 K) in which the resistance is varied up over 7 orders of magnitude. The same exponential $R(T)$ dependence in nearly stoichiometric $La_2CuO_{4+\delta}$ was found previously in Refs. 12–15 but in not as wide temperature and resistance ranges as in present study. In the theory of VRH the fractional exponent in Eq. (1) is written in general form as $\alpha=1/(D+1)$ where *D* is the system dimensionality.[16] Therefore, the case $\alpha=1/4$, observed in our and previous studies, corresponds to the behavior of a three-dimensional system. This seems to be contrary to the commonly accepted belief that the cuprate oxides with layered perovskite structure, in which the Cu-O planes are the main conducting units, should behave as electronic quasi two-dimensional systems.[17–19] If this is the case, the VRH behavior should be two-dimensional with $\alpha=1/3$, and this was indeed observed in some cuprate oxides.[17,18] However, as shown in Ref. 5, in $La_2CuO_{4+\delta}$ owing to special character of the excess oxygen as interstitial atom with weak oxygen-

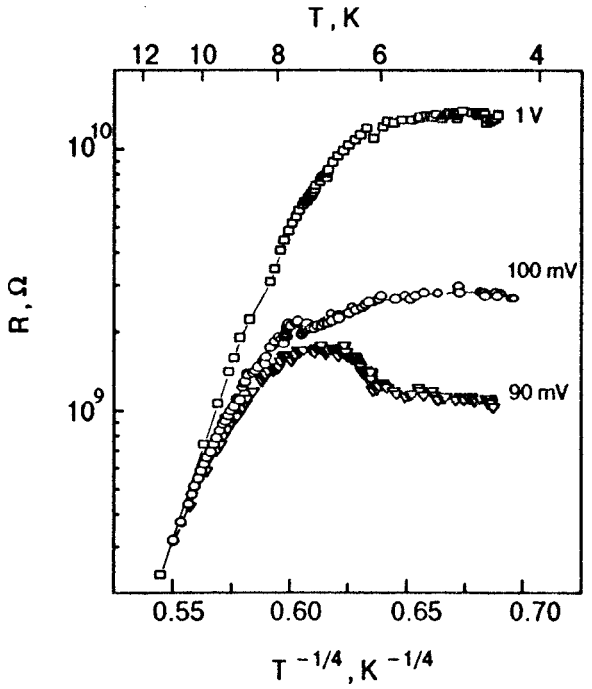

FIG. 4. A selection of dependences of resistance R (on logarithmic scale) on $T^{-1/4}$ presented on an enlarged scale as compared with Fig. 3. They demonstrate the peculiarities of $R(T)$ behavior at low temperature range at different magnitudes of applied voltage. It can be seen that at high voltage the resistance saturates with decreasing temperature, but at low enough voltage it decreases with decreasing temperature.

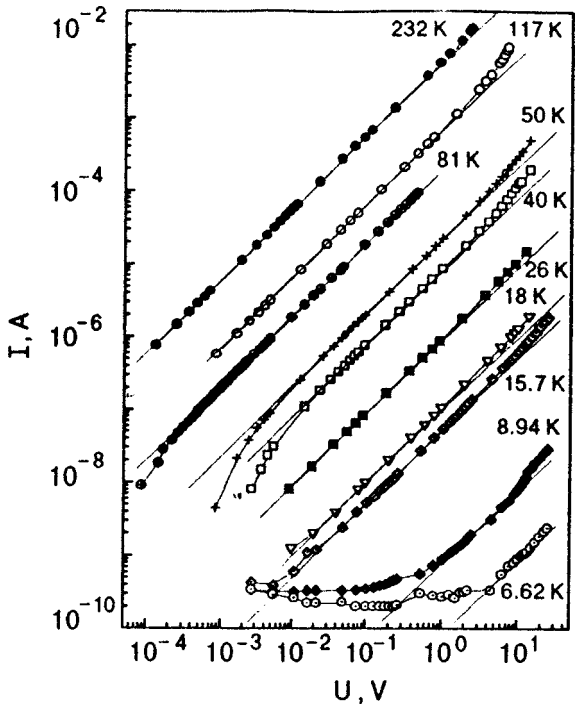

FIG. 5. A set of $I-V$ curves (in logarithmic coordinates) for different temperatures.

oxygen bonding a hole transfer between Cu-O planes is likely. Therefore, the VRH of this compound behaves as that of a three-dimensional system: In passing it should be mentioned that this is not true for Sr or Ba doped $La_2CuO_{4+\delta}$ systems which remain quasi two-dimensional.[5]

At $T \lesssim 20$ K, we observed very large deviations of $R(T)$ dependence from Mott's law (Fig. 3) which are determined by non-Ohmic effects in the sample conduction. In this temperature range the resistance rise with decreasing temperature is much less than the prediction of Eq. (1) and at low enough temperatures the resistance does not increase at all [approaches some constant value or even decreases with decreasing temperature at fairly low voltage (Fig. 4)]. The deviation temperature below which the appreciable deviations of this type take place decreases as the voltage U increases. A quite unusual and unexpected behavior for semiconductor in VRH regime of conduction is connected with this: at low enough temperature ($T \lesssim 20$ K) the resistance increases with U increasing (Fig. 3). Indeed, it is well known[16] that conductivity in this regime can only increase with the applied electric field E which (when it is large enough) enhances the electron hopping probability. For not very large E values ($eEL_c < kT$, where L_c is the localization length), the effect of electric field on resistance can be described by the following expression:[16]

$$R(T,E) = R_0(T)\exp\left(-\frac{eEr_h\gamma}{kT}\right), \tag{2}$$

where $R_0(T)$ is the resistance for $E \to 0$ [described by Eq. (1)]; r_h is the mean hopping distance; γ is a factor of the order of unity. It follows from Eq. (2) that at low enough field ($E \ll kT/eL_c$) the resistance does not depend on E; that is, Ohm's law holds. With increasing E and decreasing T the influence of the electric field must be enhanced and lead to decreasing in R with increasing E; that is quite contrary to what we have observed (Fig. 3).

The unusual behavior of $R(U)$ that has been described is one of the major non-Ohmic effects that we have observed. Before trying to explain it we should, however, present more a general picture of non-Ohmic effects found in $I-V$ characteristics and the corresponding $R(U)$ dependences of sample investigated (Figs. 5–7). At low enough voltage the resistance behavior was found to be non-Ohmic in the entire temperature range investigated (from 5 K to room temperature), but at $T \lesssim 20$ K the resistance increases with increasing U (as was shown above) whereas at $T \gtrsim 20$ K it decreases with increasing U (Figs. 6 and 7).[1)] These unusual $R(U)$ dependences at low voltage and the radical difference between them below and above $T \approx 20$ K are keys to understanding the conducting state of sample investigated and will be considered more thoroughly below. At higher voltage the $I(U)$ and $R(U)$ behaviors are basically the same for all temperature range investigated. That is, in some intermediate range of voltage the Ohm law is true and at maximal applied voltage (about 10 V or more) the resistance decreases with increasing U (Figs. 5–7). As was mentioned above, this type of transition from Ohmic to non-Ohmic regime of conduction at increasing of applied voltage is quite common for semiconductors with VRH and is attributed to the influence of the applied electric field.[16] We believe that this is also true for the sample studied and we can substantiate it with some numerical estimates using the Eq. (2). Indeed, it is

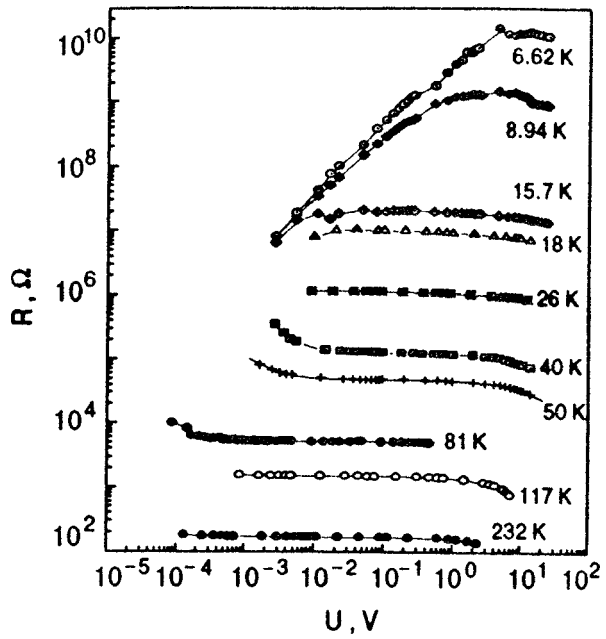

FIG. 6. A set of voltage dependences of resistance R (in logarithmic coordinates) for the same temperatures as in Fig. 5.

known[12,28] that electron localization length L_c in nearly stoichiometric $La_2CuO_{4+\delta}$ is about 0.8–1.0 nm. Taking into account that the mean hopping distance r_h in VRH regime of conduction is greater than L_c (say by a factor of 2 or 3), and using the above-indicated sample dimensions, it is easy to see that the electric field effect on hopping conduction is negligible ($eEr_h\gamma/kT \ll 1$) not only in low-voltage range where the above-mentioned non-linear $I(U)$ behavior and unusual $R(U)$ dependences were observed, but also in higher-voltage range, where Ohmic behavior takes place.

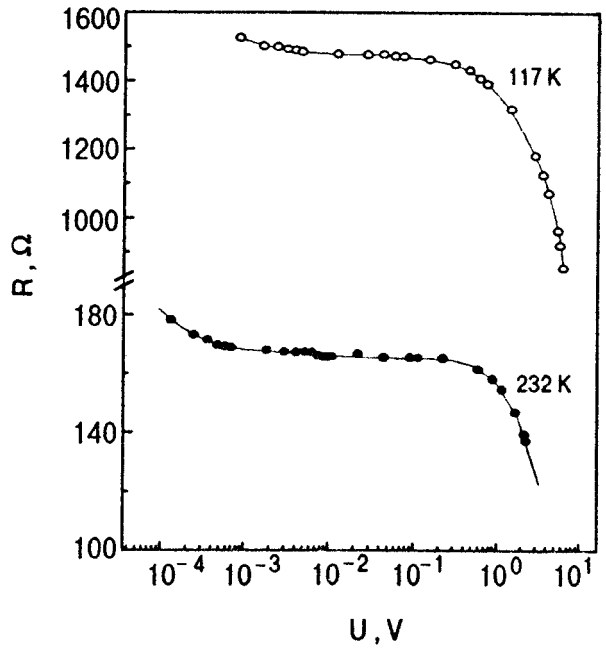

FIG. 7. The semilogarithmic plots of voltage dependences of resistance R for two temperatures above 100 K.

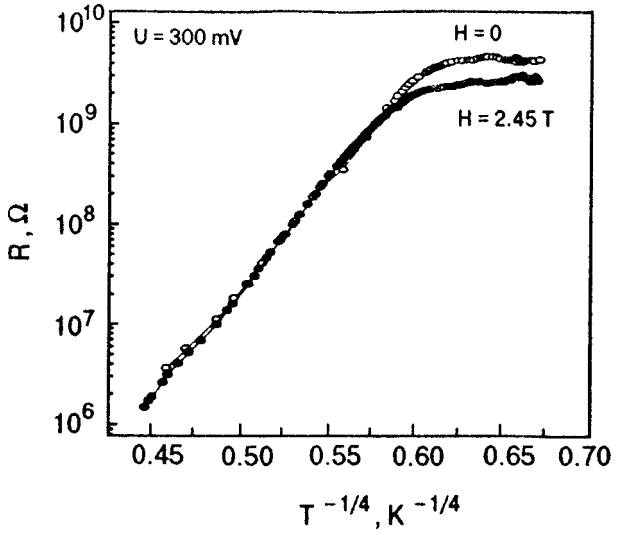

FIG. 8. The dependences of resistance R (on logarithmic scale) on $T^{-1/4}$ at $U=300$ mV registered in a magnetic fields $H=0$ and 2.45 T.

Only for the highest applied voltage (10 V and more) may the quantity $eEr_h\gamma/kT$ be about 0.1 and, hence, the influence of electric field E can be appreciable in accordance with Eq. (2). This can explain the resistance decrease with U increase at highest applied voltage (Figs. 5–7). In addition, at fairly high field the heating effect is possible at low temperatures. This can also lead to the resistance decrease with increasing U.

The magnetoresistance (MR) of sample studied was found to have appreciable and rather high magnitude only below $T \simeq 10$ K. It was negative at high voltage range, but at low voltage ($U \lesssim 0.1$ V) the MR becomes positive at low enough temperatures (Figs. 8 and 9). The negative MR is quite common for insulating $La_2CuO_{4+\delta}$ samples and may be determined by different mechanisms,[13–15,21] which we will not discuss here in detail. As far as we know, the positive MR in insulating $La_2CuO_{4+\delta}$ was not observed. Theoretically this phenomenon is considered, however, as quite possible in the VRH regime of conduction and is associated with the shrinking of the impurity wave function in a magnetic field.[22] In this connection we have calculated the possible value of MR using the appropriate equation in Ref. 22 for the case of ''weak'' magnetic field ($L_H \gg L_c$, where $L_H=(\hbar eH)^{1/2}$ is the magnetic length):

$$\ln\frac{R(H)}{R(0)} = t_1\left(\frac{L_c}{L_H}\right)^4\left(\frac{T_0}{T}\right)^{3/4}, \tag{3}$$

where $t_1=5/2016$. We have obtained the results that $\ln[R(H)/R(0)]$ is about 0.003 for $H=4$ T. This is much less than the experimental value of $\ln[R(H)/R(0)] \simeq 0.2$ (Fig. 9). We believe, therefore, that the observed positive MR is not determined by the mechanism proposed in Ref. 22.

From the above discussion it appears that the conduction behavior of sample studied at high voltage range, in particular, the transition from Ohmic to non-Ohmic regime of conduction with U increasing, is quite consistent with known properties of semiconductors. This is not the case, however, for the observed non-linear effects in low-voltage range. This

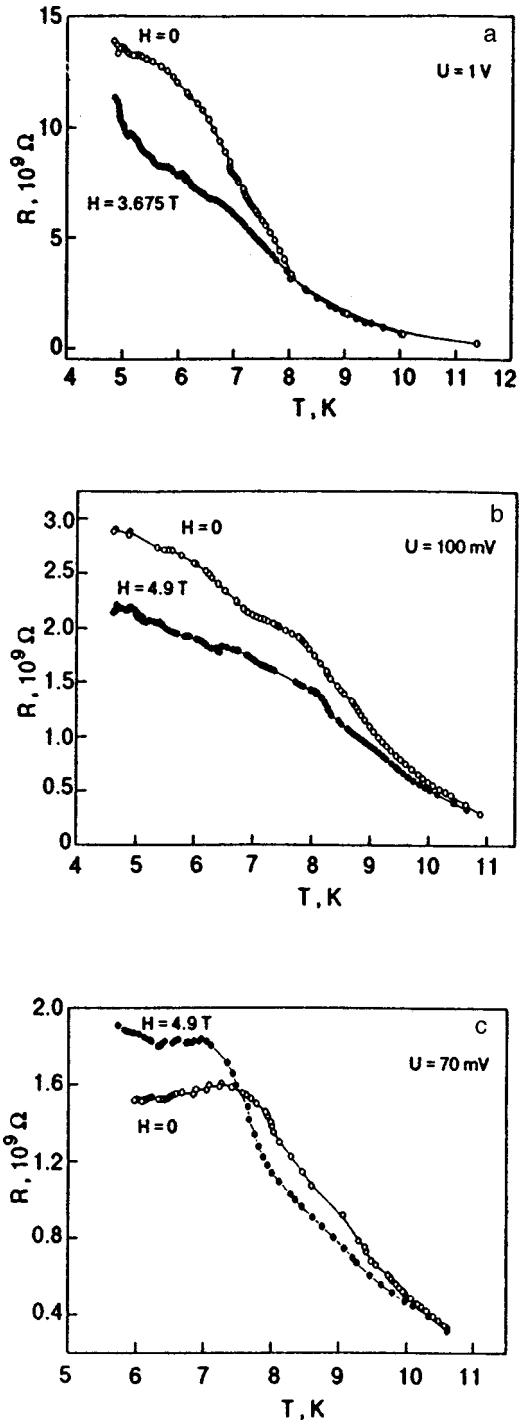

FIG. 9. The temperature dependences of resistance $R(T)$ at $H=0$ and at some constant magnitudes of H. These dependences were registered at different applied voltages U: 1 V (a); 100 mV (b); 70 mV (c).

raises the two main questions: (i) why do non-Ohmic effects take place at all at so low voltage [in conditions where the influence of electric field and (or) Joule heating on VRH can be neglected]? (ii) what is the cause of the radical difference between non-Ohmic effects below and above $T\approx 20$ K in this voltage range? What is more, the observed transition from negative to positive MR at decreasing U should also be considered. After examination of obtained results and taking into account the known properties of cuprate oxides we arrive at the conclusion that the sample inhomogeneity, namely, surface enrichment with oxygen may be responsible for the observed non-linear conduction effects. For the rest of the paper we shall present the points substantiating this conclusion.

First of all we would like to point out that as the result of the above-described heat treatment of the sample in helium and air (see Sec. 2) the oxygen concentration at the surface of sample may be considerably higher than in central (inner) region of it. Indeed, the first step of the treatment was an annealing in helium gas. This should cause[12] an effective reduction in oxygen content in the sample. However, the second step was an annealing in air (partly for the purpose of reducing contact resistance) and this could definitely cause the oxygen enrichment of sample's surface region. This is quite possible if after the helium treatment the oxygen concentration in the sample was low enough. Consider in this connection once again the temperature dependence of the magnetic susceptibility $\chi(T)$ of sample studied (see Fig. 1). It can be seen that after the described heat and gas treatment the Néel temperature has increased from ≈230 K to ≈290 K. The later value of T_N corresponds to nearly stoichiometric $La_2CuO_{4+\delta}$ (very low oxygen content). Therefore, the heat treatment in helium was fairly effective in reducing the of oxygen concentration. At the same time, if a considerable volume part of the sample (in our estimate 1/10 or more) has gained some additional oxygen after the heat treatment in air, this should be reflected in the form of the $\chi(T)$ curves as well. However, any marked evidence of sample inhomogeneity in this curves, can not be seen. There is only one distinct peak in $\chi(T)$ dependence. But it should be taken into account that in the case, when only fairly thin surface layer has increased oxygen concentration, the influence of it on $\chi(T)$ dependence may be quite negligible. It should be also noted that the marked difference between the surface and inner oxygen content is rather common for the $La_2CuO_{4+\delta}$ and other cuprate oxides.[2,6] For example, in Ref. 6 in $La_2CuO_{4+\delta}$ films, which were oxidized in ozone gas, the increased oxygen concentration in surface layer was found. Taking all this into account and considering the peculiarities of sample treatment we shall assume in the following that the surface region of the sample is enriched with oxygen.[2)] Based on this, it is possible to give a reasonable explanation of all obtained results.

The oxygen-enriched surface layer of sample can undergo a phase separation[1,5,6–10] with the resulting formation of considerable volume fraction of superconducting phase. In this case the surface layer would consist of disconnected superconducting regions in a poorly conducting (dielectric) matrix. We believe, that the critical temperature T_c of superconducting phase is about 20 K in the case being considered. It is at this temperature that the radical change in the nonlinear behavior of conduction takes place (Figs. 5 and 6).[3)] Consider, at first, the conduction below $T\simeq 20$ K. In the specified conditions, for driving electric field the system provides at least two main channels for the response: the low-resistive surface layer (with disconnected superconducting regions) and high-resistive core. The measured conductivity of these composite system should be much higher than the ''intrinsic'' conductivity of the core. The increasing U leads

to the increase in the current and this must induce the depression of the surface superconductivity and, hence, the increasing of the sample resistance. This corresponds to the observed $R(U)$ behavior in low-voltage range (Figs. 3, 5, and 6).

One of the obvious reasons for the superconductivity depression at increasing U is the increase in the current density (this leads to a reduction in T_c). However, in this case the possible influence of Joule heating in low-resistive surface layer on the conductivity of whole system must not be ruled out since the Joule heat (as well as current) is much more in this layer than in the core. It is known that Joule heating plays a crucial role in the breakdown of superconductivity in composite or inhomogeneous superconductors.[24] The Joule heating may result (among other things) in resistive domains and negative differential conductance.[24] The latter can be actually seen in the measured $I-V$ characteristics at low enough temperatures (Fig. 5). It cannot be excluded that the observed negative differential conductance is connected with some of the mechanisms of heat breakdown of superconductivity described in Ref. 24. The results obtained do not provide reason enough to consider this question in detail. In any case, however, we believe that increasing U leads to superconductivity depression and, hence, to the resistance increase.

The magnetic field should also reduce the superconductivity. In this connection the observed positive MR at low-voltage range and the transition to negative MR with increasing U (Fig. 9) can be considered as an important argument to support the existence of oxygen-enriched surface layer (with superconducting inclusions) in the sample. A close look at Fig. 9,c shows that when the temperature drops, the MR is first negative and then becomes positive. It is significant that the positive MR is combined with decreasing resistance with decreasing temperature at $H=0$, whereas the negative MR is combined with increasing resistance as the temperature decreases. The resistance decrease with decreasing temperature takes place only at low-voltage range where surface superconductivity is not depressed (Fig. 9, see also Fig. 4). This decrease can be explained by enhancing of Josephson coupling within some confined groups of superconducting regions with decreasing temperature. Such an effect is quite typical for granular metals in which the competition of the hopping conduction and Josephson coupling takes place.[25] All these effects (especially, the positive MR combined with resistance decreasing with decreasing temperature) can be considered as a direct evidence of superconductivity effect in the sample studied.

It is reasonable to expect that at high enough voltage the surface superconductivity will be depressed completely after which the non-linear conductance of the whole system would change over to Ohmic behavior (Figs. 5 and 6). At the highest applied voltage the non-linear behavior appears again for the reasons that we have mentioned above.

Above $T\simeq 20$ K, where the superconductivity effect should not take place, the non-linear behavior of conduction at low-voltage range still remains. It is weaker than at $T<20$ K, and appears in radically changed form: the resistance decreases with increasing U (Figs. 6 and 7), at high enough voltage the resistance seems to saturate, that is, the transition to Ohmic behavior occurs (Fig. 5). This type of non-linearity can also be adequately explained in the context of our main conjecture (oxygen-enriched surface layer). The low-resistive surface layer is inhomogeneous. It consists of disconnected (dispersed) high-conducting regions in dielectric matrix. Generally the surface layer would constitute a percolation system with tunneling (or hopping) between disconnected conducting regions. It is just the tunneling that is responsible for the non-linearity of this type of composite system.[26,27] The distinctive feature of these systems is the transition from non-Ohmic to Ohmic behavior of conduction at increasing applied electric field (or temperature). The transition of this type was observed on Ag particles in KCl matrix [28] and in a semicontinuous gold film near the percolation threshold [29]. In Ref. 29 such behavior was attributed (in line with theory of Ref. 30) to an increase in the probability of tunneling with increasing applied voltage U or temperature. The percolation approach of Refs. 26 and 27 leads to essentially the same result. Thus we believe that the observed change-over from non-linear conductance to Ohmic behavior at low-voltage range (Fig. 5–7) with increasing U is connected with the percolating structure of the oxygen-enriched surface layer and should be attributed to theoretical mechanisms similar those of Refs. 26, 27, and 30. Once the conduction of this layer becomes Ohmic beyond some voltage, the behavior of the whole sample also becomes Ohmic up to the highest voltage, where the influence of electric field (or Joule heating) on hopping conduction becomes perceptible.

In conclusion, it may be said that our conjection about the oxygen-enriched surface layer enables us to explain all the observed unusual non-linear effects and magnetoresistance behavior of studied sample of $La_2CuO_{4+\delta}$. The results obtained demonstrate that the transport properties of cuprate oxides may be determined to an essential degree by structural or stoichiometric inhomogeneities. This circumstance should be taken into account at evaluation of ⟨quality⟩ of high-temperature superconductors on the basis of transport properties.

We are very grateful to S. I. Shevchenko for critical reading of the manuscript and helpful comments.

*E-mail: belevtsev@ilt.kharkov.ua

[1)] Owing to the logarithmic scales in Fig. 6 the important peculiarities of the $R(U)$ behavior at temperatures above 100 K cannot be seen. Because of this, some examples of $R(U)$ dependences in this temperature range are shown more clearly in Fig. 7 using semilogarithmic coordinates.

[2)] The possible influence of this type of inhomogeneity on the conduction will be considered below. We exclude the phase separation in the inner part of sample as other source of inhomogeneity. Indeed, the Néel temperature $T_N\approx 290$ K for the sample studied means that $\delta\leqslant 0.003$.[10,23] This value of δ is far outside of the δ range (between $\delta=0.01$ and $\delta=0.055$) in which the phase separation occurs[1,5,7–10,23].

[3)] The stable superconducting phase with $T_c=20$ K can emerge due to phase separation of $La_2CuO_{4+\delta}$ at rather low oxygen doping level ($\delta=0.01$).[11]

[1] *Phase Separation in Cuprate Superconductors*, E. Sigmund and K. A. Müller (Eds.), Springer-Verlag, Heidelberg (1994).

[2] V. M. Browning, E. F. Skelton, M. S. Osofsky, S. B. Qadri, J. Z. Hu, L. W. Finger, and P. Caubet, Phys. Rev. B **56**, 2860 (1997).

[3] D. C. Johnston, J. P. Stokes, D. P. Goshorn, and J. T. Lewandowski, Phys. Rev. B **36**, 4007 (1987).
[4] R. J. Birgeneau and G. Shirane, in *Physical Properties of High Temperature Superconductors I*, D. M. Ginsberg (Ed.), World Scientific, Singapore (1989), Ch. 4, 151.
[5] R. K. Kremer, A. Simon, E. Sigmund, and V. Hizhnyakov, in *Phase Separation in Cuprate Superconductors*, E. Sigmund and K. A. Müller (Eds.), Springer-Verlag, Heidelberg (1994), pp. 66–81.
[6] H. Sato, M. Naito, and H. Yamamoto, Physica C **280**, 178 (1997).
[7] J. D. Jorgensen, B. Dabrowski, S. Pei, D. G. Hinks, L. Soderholm, B. Morosin, J. E. Schirber, E. L. Venturini, and D. S. Ginley, Phys. Rev. B **38**, 11337 (1988).
[8] M. F. Hundley, R. S. Kwok, S.-W. Cheong, J. D. Thompson, and Z. Fisk, Physica C **172**, 455 (1991).
[9] J. Ryder, P. A. Midgley, R. J. Beynon, D. L. Yates, L. Afalfiz, and J. A. Wilson, Physica C **173**, 9 (1991).
[10] A. A. Zakharov and A. A. Nikonov, Pis'ma Zh. Éksp. Teor. Fiz. **60**, 340 (1994) [JETP Lett. **60**, 348 (1994)].
[11] E. L. Vavilova, N. N. Garif'yanov, E. F. Kukovitsky, and G. B. Teitel'baum, Physica C **264**, 74 (1996).
[12] M. A. Kastner, R. J. Birgeneau, C. Y. Chen, Y. M. Chiang, D. R. Gabbe, H. P. Jenssen, T. Junk, C. J. Peters, P. J. Picone, Tineke Thio, T. R. Thurston, and H. L. Tuller, Phys. Rev. B **37**, 111 (1988).
[13] A. A. Zakharov, E. P. Krasnoperov, B. I. Savel'ev, A. A. Teplov, M. B. Tsetlin, and A. A. Shikov, Sverkhprovodimost: Fiz., Khim., Tekh. **4**, 1906 (1991).
[14] B. I. Belevtsev, N. V. Dalakova, and A. S. Panfilov, Low Temp. Phys. **23**, 274 (1997).
[15] B. I. Belevtsev, N. V. Dalakova, and A. S. Panfilov, Physica C **282–287**, 1223 (1997).
[16] N. F. Mott and E. A. Davis, *Electron Processes in Noncrystalline Materials*, Clarendon Press, Oxford (1979).
[17] Y. Iye, in *Physical Properties of High Temperature Superconductors III*, D. M. Ginsberg (Ed.), World Scientific, Singapore (1992), Ch. 4, p. 285.
[18] L. Forro, Int. J. of Mod. Phys. **8**, 829 (1994).
[19] V. M. Loktev, Fiz. Nizk. Temp. **22**, 3 (1996). [Low Temp. Phys. **22**, 1 (1996)].
[20] C. Y. Chen, R. J. Birgeneau, M. A. Kastner, N. W. Preyer, and T. Thio, Phys. Rev. B **43**, 392 (1991).
[21] T. Thio, C. Y. Chen, B. S. Freer, D. R. Gable, H. P. Jenssen, M. A. Kastner, P. J. Picone, and N. W. Preyer, Phys. Rev. B **41**, 231 (1990).
[22] B. I. Shklovskii and A. L. Efros, *Electronic Properties of Doped Semiconductors*, Springer-Verlag, New York (1984).
[23] R. J. Birgeneau, F. C. Chou, Y. Endoh, M. A. Kastner, Y. S. Lee, G. Shirane, J. M. Tranquad, B. O. Wells, and K. Yamada, in *Proceedings of the 10th Anniversary HTS Workshop on Physics, Materials and Applications*, March 12–16, 1996, Houston, Texas, USA, B. Batlog, C. A. Chu, W. K. Chu, D. U. Gubster, and K. A. Müller (Eds.), World Scientific, Singapore (1996), P. 421.
[24] A. V. Gurevich, R. G. Mints, and A. L. Rakhmanov, Fizika kompozitnykh svekhprovodnikov (Physics of Composite Superconductors), Nauka, Moscow (1987).
[25] B. I. Belevtsev, Sov. Phys. Usp. **33**, 36 (1990).
[26] A. K. Sen and A. Kar Gupta, in *Non-linearity and Breakdown in Soft Condensed Matter*, K. K. Bardhan, B. K. Chakrabarti and A. Hansen (Eds.), *Lecture Notes in Physics*, 437, Springer-Verlag, Berlin (1994), p. 271.
[27] A. Kar Gupta and A. K. Sen, Phys. Rev. B **57**, 3375 (1998).
[28] I.-G. Chen and W. B. Johnson, J. Mater. Sci. **27**, 5497 (1992).
[29] B. I. Belevtsev, E. Yu. Belyaev, Yu. F. Komnik, and E. Yu. Kopeichenko, Low Temp. Phys. **23**, 724 (1997).
[30] M. Mostefa, D. Bourbie, and G. Olivier, Physica B **160**, 186 (1989).

This article was published in English in the original Russian journal. It was edited by R. T. Beyer.

LOW-DIMENSIONAL AND DISORDERED SYSTEMS

On the existence of long-range magnetic order in two-dimensional easy-plane magnets

B. A. Ivanov and E. V. Tartakovskaya

Institute of Magnetism, National Academy of Sciences of the Ukraine, 252142 Kiev, Ukraine)*
(Submitted June 22, 1998)
Fiz. Nizk. Temp. **24**, 1095–1104 (November 1998)

A consistent phenomenological approach is used to show that a true long-range order can exist in two-sublattice two-dimensional antiferromagnets (AFM) and ferrites closed to the compensation point. The effect is due to the long-range component of dipole forces. A similar result was obtained earlier for ferromagnets by Maleev [Sov. Phys. JETP **43**, 1240 (1976)], who suggested that the Mermin–Wagner theorem may not be valid for interactions decreasing in proportion to $1/R^3$ or more slowly. It is found that the effect exists in the case of magnets with completely identical sublattices (AFM) only due to some types of the Dzyaloshinskii–Moriya interaction. For example, it is observed for AFM with an even (in Turov's sense) principal axis and is absent otherwise. For a magnet with nonidentical sublattices, the effect can take place only for ferrites, i.e., for sublattices that are not compensated in the exchange approximation. The effect of stabilization of long-range order disappears at the point of compensation of magnetic moment. If this point does not coincide with the point of compensation of spin angular momentum, the intensities of fluctuations are nonmonotonic functions of temperature. The obtained estimates for the phase transition temperature are compared with experimental results.
 [S1063-777X(98)00811-1]

It was shown in the classical works by Bloch[1] and by Mermin and Wagner[2] that, in two-dimensional magnets whose ground state is characterized by continuous degeneracy (as, for example, in isotropic and easy-plane models of magnets), thermal fluctuations violate the long-range magnetic order at indefinitely small but finite temperatures. Berezinskii,[3] as well as Kosterlitz and Thouless[4] proved that such systems can exhibit only quasi-long-range order at temperatures $T<T_{BKT}$, where $T_{BKT}\propto S^2J$ is the phase-transition temperature, J the exchange integral, and S atomic spin.

However, the conclusion on the impossibility of a true long-range order in two-dimensional magnets was drawn only for short-range potentials decreasing with distance at a rate higher than $1/R^3$. The magnetic dipole–dipole interaction whose energy decreases with distance as $1/R^3$ does not satisfy the conditions of the Mermin–Wagner theory. Maleev[5] was the first to pay attention to this circumstance. He proved that consistent inclusion of the dipole–dipole interaction in isotropic ferromagnets (FM) leads to a root dispersion relation for magnons ($\omega\propto\sqrt{k}$), and hence to stabilization of the long-range magnetic order at finite temperatures.

The interest in two-dimensional magnetism increased considerably after the refinement of the technology for obtaining monolayered structures with a high structural accuracy.[6–8] The Langmuir–Blodgett method was used to obtain true two-dimensional antiferromagnetic (AFM) of the type of manganese stearate.[9] However, a theoretical description of two-dimensional magnetism was proposed only for FM.[5,6] It was noted above that this description is based to a considerable extent on the inclusion of the dipole–dipole interaction which is inherent in ferromagnets. The magnetic dipole–dipole interaction of spins naturally exists in AFM as well, but this interaction is usually neglected in an analysis of AFM since the spins of the sublattices in AFM are compensated in the exchange approximation.[10–13,15–18] On the other hand, the contribution of the dipole–dipole interaction can appear in AFM due to noncollinearity of sublattices, but direct analysis based on microscopic spin Hamiltonian[5,6] is quite cumbersome. A theoretical explanation of two-dimensional antiferromagnetism was proposed for the first time in our brief communication,[19] where it was proved that the long-range magnetic order in Langmuir–Blodgett films of the type of manganese stearate ($Mn(C_{18}H_{35}O_2)_2$) with an easy-plane anisotropy is stabilized due to the long-range component of dipole forces. It should be noted that this result was obtained only for a specific type of the Dzyaloshinskii–Moriya interaction typical of this material.

In this paper, we develop the simple phenomenological approach proposed earlier[19] to explain two-dimensional magnetism and the role of dipole–dipole interaction in establishing the long-range magnetic order in AFM and generalize it for several different magnetic models. In Sec. 1, we consider the simplest case of a two-dimensional easy-plane ferromagnet. A good agreement between the results obtained here on the basis of the phenomenological approximation and calculations using the exact method of spin Hamiltonian of the dipole–dipole interaction demonstrates the correctness of the phenomenological approach.

In the following sections, two-sublattice models are

analyzed for which the exact method is inapplicable. In Sec. 2, the model of a magnet with two compensated sublattices is considered (i.e., the case of antiferromagnetic ordering). The results of theoretical analysis of the phase transition temperature are compared with experimental data. In Sec. 3, similar results are obtained for a two-dimensional easy-plane ferrite close to the compensation point.

1. PHENOMENOLOGICAL ANALYSIS OF DIPOLE–DIPOLE INTERACTION. FERROMAGNET

The energy of magnetic dipole–dipole interaction in the phenomenological description can be presented as the sum of two terms. The first term associated with interaction between nearest neighbors gives in the case of a two-dimensional magnet only a positive correction to the constant of uniaxial anisotropy, i.e., forms anisotropy of the ''easy plane'' type.[6] The second term corresponding to the long-range component of magnetic dipole forces can be written in the phenomenological approximation in terms of the so-called demagnetizing field $\mathbf{H}_m$ as follows[10]:

$$W_d = -(1/2)a \int dxdy(\mathbf{M}\cdot\mathbf{H}_m), \tag{1}$$

where a is the film thickness, and integration is carried out in the plane of the film. The demagnetizing field $\mathbf{H}_m$ is defined by the magnetostatic equations

$$\text{div } \mathbf{H}_m = -4\pi \text{ div } \mathbf{M}, \quad \text{curl } \mathbf{H}_m = 0 \tag{2}$$

taking appropriate boundary conditions into account. In the three-dimensional case, the solution of Eqs. (2) is well known:

$$\mathbf{H}_m = -\nabla \int d\mathbf{r}'[\mathbf{M}(\mathbf{r}')\cdot\nabla'] \frac{1}{|\mathbf{r}-\mathbf{r}'|}, \tag{3}$$

where $d\mathbf{r}' = dx'dy'dz'$; ∇ and ∇' are the gradient operators in the variables $\mathbf{r}$ and $\mathbf{r}'$, respectively. Phenomenological analysis of the contribution from dipole–dipole interaction will be carried out on the basis of an approximate but simple and (which is most important) universal model. We consider a two-dimensional magnet in the form of a very thin continuous magnetic film of thickness a with the normal along the z-axis, in which magnetization is a function of only two variables x and y. In order to obtain the result in compact form, we introduce the following notation: $\mathbf{H}_m = (\mathbf{H}_m^{(s)}, H_m^z)$, $\mathbf{M} = (\mathbf{M}^{(s)}, M^2)$, where the vectors $\mathbf{H}_m^{(s)} = (H_m^x, H_m^y)$ and $\mathbf{M}^{(s)} = (M^x, M^y)$ lie in the plane of the film. Integrating in (3) with respect to the variable z from $-a/2$ to $+a/2$, we obtain the required result for the two-dimensional case, the demagnetizing field being expressed in terms of magnetization $\mathbf{M}$:

$$\mathbf{H}_m^{(s)}(x,y) = \nabla_i^{(s)} \int_{-\infty}^{\infty}\int_{-\infty}^{\infty} dx'dy'[M_i^{(s)}(x-x',\, y-y') \times \mathbf{f}_1(x',\, y')], \tag{4}$$

$$= \int_{-\infty}^{\infty}\int_{-\infty}^{\infty} dx'dy' M^{(z)}(x-x',\, y-y') f_2(x',\, y'),$$

where

$$\mathbf{r} = (x,y), \quad \mathbf{r}' = (x',y'),$$

$$\mathbf{f}_1(x,y) = a\mathbf{r}r^{-2}(r^2 + a^2/4)^{-1/2},$$

$$f_2(x,y) = -a(r^2 + a^2/4)^{-3/2},$$

$$\nabla^{(s)} = \left(\frac{\partial}{\partial x}, \frac{\partial}{\partial y}\right).$$

These expressions can be used in principle for an analysis of linear as well as nonlinear magnetization dynamics. These formulas were used by Kovalev *et al.*[13] for an analysis of small-amplitude solitons; in this case, integral equations must be analyzed in actual practice. In our case of linear oscillations, calculations can be carried out completely by using the spatial Fourier transform. Writing $\mathbf{M} = \mathbf{M}_0 + \delta\mathbf{M}$, where $\mathbf{M}_0$ corresponds to the ground state and $\delta\mathbf{M}$ to small deviations from it, we can easily write the energy of magnetic dipole– dipole interaction in terms of Fourier components $\delta\mathbf{M}_k$:

$$W = -\pi a \sum_k \frac{1}{|k|} (\mathbf{k}\cdot\delta\mathbf{M}_k)(\mathbf{k}\cdot\delta\mathbf{M}_{-k}). \tag{5}$$

The nonanalyticity appearing in this formula is due to the long-range nature of the magnetic dipole–dipole interaction. The physical reason behind the nonanalyticity is quite clear. Let us consider a spin wave in any magnet, which is accompanied by oscillations of total magnetization in the direction of the wave vector of the wave. In this case, the quantity $\text{div}(\delta\mathbf{M}) \neq 0$, and since div$\mathbf{M}$ plays the role of the source of the field $\mathbf{H}_m$ (''magnetic charge'') in magnetostatic equations, the wave is accompanied by oscillations of the field $\mathbf{H}_m$. The range of localization of the field along the z-axis is determined by the wavelength $\lambda \approx 2\pi/k$, and hence the corresponding energy contains the factor $1/|k|$. It should be noted that the z-component of magnetization does not lead to such a singularity since the corresponding field $\mathbf{H}_m$ for $\lambda \gg a$ is virtually localized within the film. It should also be emphasized that the form of expression (5) does not depend on the type of magnetic ordering; it is valid for ferromagnets as well as compensated antiferromagnets or weak ferromagnets. Only the notation for the total magnetization $\delta\mathbf{M}$ with a corresponding dynamic variable changes (see Sec. 2).

In order to verify the approximation introduced above and to compare the result with the available exact data,[5,6] we obtain the magnon spectrum in a ferromagnet. Taking into account (5) and ordinary terms, viz., the exchange energy $A(\nabla\mathbf{M})^2$ $(A \propto JS^2)$ and the easy-plane anisotropy energy KM_z^2, we can write the Hamiltonian of a two-dimensional easy-plane ferromagnet in the quadratic approximation in the form

$$H = \sum_k \{Ak^2 \delta\mathbf{M}_k\delta\mathbf{M}_{-k} + K(\delta M_z)_k(\delta M_z)_{-k} - a(\pi/k)(\mathbf{k}\cdot\delta\mathbf{M}_k)(\mathbf{k}\cdot\delta\mathbf{M}_{-k})\}.$$

Using this expression, we can obtain the dispersion relation for spin waves in the standard manner (using the Landau–Lifshitz equation or the expression for $\delta\mathbf{M}_k$ in terms of spin

wave operators, see Refs. 10 and 11). The root modification of the dispersion relation for $k \to 0$ is due to corrections associated with nonlocal dipole–dipole interaction (5):

$$\varepsilon_k \to 2\mu_0[(H_K H_{\rm dip}/4)ka\ \sin^2\ \varphi_k + (2A/M_0)k^2]^{1/2}, \quad (6)$$

where $H_K = 2K/M_0$ is the anisotropy field, $H_{\rm dip} = 4\pi M_0$ indicated the field of dipole forces, and φ_k the angle between the wave vector and the equilibrium direction of magnetization.

This result coincides (to within a factor close to unity, appearing in formulas when the lattice discreteness is taken into consideration) with the exact result obtained by Maleev[5] and Bruno[6] on the basis of the microscopic Hamiltonian of dipole– dipole interaction in the two-dimensional discrete spin lattice.

With account of the root modification of the dispersion relation for magnons, the average fluctuation of magnetization $\Delta M(T)$ becomes finite, indicating the stabilization of the long-range magnetic order. In order to calculate the value of this quantity, we must know the coefficient D_k of spin deviation for a ferromagnet, which can be easily obtained from the coefficients of the $u-v$ transformation.[5,6] However, we shall describe another method of calculation of D_k, which is simpler for an analysis of multisublattice magnets and will be required in subsequent analysis.

We supplement the Hamiltonian with the term $\Delta = -\mathbf{M}\cdot\mathbf{H}^{\rm ext}$ corresponding to the energy of a ferromagnet in an external field. (It should be emphasized that we are speaking only of a formal approach simplifying calculations. Accordingly, we must make $\mathbf{H}^{\rm ext}$ tend to zero in final results.) We shall use the formula for the average thermal fluctuation of magnetic moment which is well known from the FM thermodynamics,[10] i.e.,

$$\Delta M(T) = -\frac{1}{(2\pi)^2}\sum_i \int d\mathbf{k}\ \frac{\partial \varepsilon_i(k,H^{\rm ext})}{\partial H^{\rm ext}} \times [\exp(\varepsilon_i(k)/T)-1]^{-1} \quad (7)$$

(in the case of multisublattice magnets, summation is carried out over all branches of spin waves). Comparing the above expression and formula (23) from Ref. 6, it can be readily seen that the coefficient D_k is defined by the quantity $\partial\varepsilon_i(k,H^{\rm ext})/\partial H^{\rm ext}$ whose value can be calculated easily. This approach is very productive in a more complex case of multisublattice magnets, when the alternative calculations of the coefficients of the generalized Bogoliubov $u-v$ transformation is very cumbersome.[11]

Thus, the phenomenological approach can be regarded as quite adequate for the microscopic approach for the given type of problems. The application of the phenomenological approximation becomes necessary in more complex two-sublattice models. The calculation of $\Delta M(T)$ by formula (7) can be carried out analytically only to logarithmic accuracy in the small parameter $M_0 H_{\rm dip}/A$. In this approximation, the exact value of the coefficient of $\sqrt{ka}$ is immaterial since the results calculated by using the phenomenological approach literally coincide with those obtained earlier.[5,6]

2. THE ROLE OF DIPOLE–DIPOLE INTERACTION IN ESTABLISHING LONG-RANGE MAGNETIC ORDER IN TWO-DIMENSIONAL EASY-PLANE ANTIFERROMAGNETS

In the description of AFM, it is convenient to introduce the normalized vectors of magnetization **m** and antiferromagnetism **l**:

$$\mathbf{m} = \frac{\mathbf{S_n} + \mathbf{S_{n+a}}}{2S}, \quad \mathbf{1} = \frac{\mathbf{S_n} - \mathbf{S_{n+a}}}{2S},$$

where the translation vector **n** defines spins of only one sublattice, and **a** is the set of minimum vectors of translation between atoms of the first and second sublattices. The vectors **m** and **l** satisfy the conditions $\mathbf{m}\cdot\mathbf{l} = 0$, $m^2 + l^2 = 1$. In the continual approximation, these vectors depend on continuous spatial variable, while the total magnetization of the AFM is defined by the formula $\mathbf{M} = 2M_0\mathbf{m}$, where M_0 is the magnetization of one sublattice.

The presence of two sublattices creates the main difficulty in the description of AFM (as compared to FM). In the semiclassical approach, we must consider equations for two dynamic vectors $\mathbf{S}_n$, $\mathbf{S}_{n+a}$ or **m, l**. In the standard method of introduction of magnon operators, we have to use the generalized $u-v$ transformation containing four operators. Many difficulties can be avoided by going over to the σ-model for the vector **l** (see reviews in Ref. 12). The Lagrangian in the σ-model for a two-dimensional easy-plane AFM has the form $L = L_0 - W_d$, where W_d has the meaning of the long-range component of the dipole–dipole interaction energy, as before, and L_0 is the standard Lorentz-invariant Lagrangian

$$L_0 = \int dxdy\left\{A\left[\frac{1}{c^2}\left(\frac{\partial \mathbf{l}}{\partial t}\right)^2 - (\nabla \mathbf{l})^2\right] - Kl_z^2\right\}.$$

In this formula, xy is the plane of the film coinciding with the easy plane of the AFM, c the velocity of spin waves ($c^2 = 2g^2A/\chi$, where χ is the magnetic susceptibility of the AFM), and the easy-plane anisotropy constant $K > 0$ is renormalized taking into account the short-range component of the dipole–dipole interaction. In the σ-model, the magnetization **M** in the AFM is not an independent dynamic variable and can be expressed in terms of **l** and its time derivatives:

$$\mathbf{M} = -\frac{\chi}{g}\left[\mathbf{l}\times\frac{d\mathbf{l}}{dt}\right] + \chi[\mathbf{H}_0 + \mathbf{H}_D - \mathbf{l}\{(\mathbf{H}_0 + \mathbf{H}_D)\cdot\mathbf{l}\}]. \quad (8)$$

Here $\mathbf{H}_0$ is the external magnetic field, $\mathbf{H}_D$ the Dzyaloshinskii field, $H_D^i = D_{ik}l_k$; $g = 2\mu_0/\hbar$ the gyromagnetic ratio, and the form of the tensor D_{ik} is determined by the magnetic symmetry of the crystal.

Formula (8) is written taking into account the general form of the Dzyaloshinskii– Moriya energy which is chosen in the form

$$W_D = -M_0\int dxdy D_{ik}M_i l_k. \quad (9)$$

Let us go over to the angles characterizing the direction of the vector **l**: $l_z = \cos\theta$, $l_x + il_y = \sin\theta\exp(i\varphi)$. Assuming that $\theta = \pi/2$ and $\varphi = 0$ in the ground state, we can introduce the field variables ϑ and φ, where $\vartheta = \pi/2 - \theta$, $\vartheta \ll 1$, and $\varphi \ll 1$. In order to analyze thermal fluctuations of the moment

in the approximation of noninteracting spin waves, we introduce canonic field pairs: (ϑ,φ) and conjugate field momenta (P_ϑ,P_φ), respectively. Taking into account only quadratic terms, we can easily obtain from the Lagrangian L_0

$$P_\vartheta=(2A/c^2)\partial\vartheta/\partial t, \quad P_\varphi=(2A/c^2)\partial\varphi/\partial t. \tag{10}$$

Using these formulas, we can determine the Hamiltonian H_0 corresponding to the Lagrangian L_0. The small correction term H_d in the total Hamiltonian $H=H_0+H_d$ of spin waves is due to the dipole–dipole interaction and is equal to the energy W_d expressed in terms of canonic variables (10).[14]

Let us first consider the spectrum of spin waves and calculate the rms fluctuations of the antiferromagnetism vector disregarding W_d. Carrying out the two-dimensional Fourier transformation in the wave vector $\mathbf{k}=(k_x,k_y)$, i.e.,

$$(\vartheta,\varphi)=\frac{1}{\sqrt{V}}\sum_{\mathbf{k}}(Q_{\mathbf{k}},q_{\mathbf{k}})e^{i\mathbf{k}\cdot\mathbf{r}},$$

$$(P_\vartheta,P_\varphi)=\frac{1}{\sqrt{V}}\sum_{\mathbf{k}}(P_{\mathbf{k}},p_{\mathbf{k}})e^{i\mathbf{k}\cdot\mathbf{r}},$$

we obtain the Hamiltonian H_0 in canonic form:

$$H_0=\sum_{\mathbf{k}}\frac{c^2}{2A}(P_{\mathbf{k}}P_{-\mathbf{k}}+p_{\mathbf{k}}p_{-\mathbf{k}}) + \sum_{\mathbf{k}}\frac{A}{c^2}(\Omega_{\mathbf{k}}^2Q_{\mathbf{k}}Q_{-\mathbf{k}}+\omega_{\mathbf{k}}^2q_{\mathbf{k}}q_{-\mathbf{k}}). \tag{11}$$

Here V is the volume of the system, and $\Omega_k=c\sqrt{k^2+K/A}$ and $\omega_k=c|k|$ are the frequencies of two spin branches, the first branch corresponding to oscillations of $\mathbf{l}$ perpendicular to the plane of the film, and the second—to oscillations of $\mathbf{l}$ in the plane of the film. Since the Hamiltonian is written in canonic form, we can easily find mean fluctuations of field variables ϑ and φ. For this purpose, we use the standard formulas for averaging Bose operators:

$$\begin{aligned}
&\langle q_1q_2\rangle=\hbar c^2n_1\delta(1+2)/2A\omega_1,\\
&\langle Q_1Q_2\rangle=\hbar c^2N_1\delta(1+2)/2A\Omega_1,\\
&\langle p_1p_2\rangle=2A\hbar n_1\delta(1+2)\omega_1/c^2,\\
&\langle P_1P_2\rangle=2A\hbar N_1\delta(1+2)\Omega_1/c^2.
\end{aligned} \tag{12}$$

Here N_1 and n_1 are Bose distribution functions for the first and second magnon branches, respectively, $1\equiv\mathbf{k}_1$, while the remaining average values are obviously equal to zero. Going over from summation over $\mathbf{k}$ to integration, we can easily find that the fluctuation of ϑ is finite at finite temperatures: $\langle(\Delta\vartheta)^2\rangle=(T/A)\ln(T/\hbar\Omega_0)$, where $\hbar\Omega_0$ is the activation energy. On the other hand, the corresponding integral for the activationless branch diverges logarithmically as $k\to0$. Since $\langle(\varphi)^2\rangle$ defines thermal fluctuations of magnetization in the easy plane, the divergence of this quantity indicates the absence of a long-range order at finite temperatures. However, the situation changes radically if we take into account the energy W_d of dipole–dipole interaction.

The Hamiltonian H_d expressed in terms of canonic operators is much more cumbersome than H_0. It generally contains almost all bilinear combinations of the variables Q_k, q_k, P_k, and p_k. But since we are interested only in the possible singular contribution of this term for $k\to0$, the expression for H_d can be simplified significantly.

First, we can calculate H_d by taking into account only the variables q and p since the magnon frequency of the branch with P and Q is finite for $k\to0$ and makes zero contribution to divergence. Second, we can ignore the dynamic contribution to magnetization since it obviously contains the magnon frequency and is small for $k\to0$. Consequently, we are obviously interested only in terms proportional to q_k.

We can write $\mathbf{l}=\mathbf{l}_0+\delta\mathbf{l}$, $\mathbf{m}=\mathbf{m}_0+\delta\mathbf{m}$, where $\mathbf{l}_0$ and $\mathbf{m}_0$ are equilibrium values of the vectors $\mathbf{l}$ and $\mathbf{m}$, and $\delta\mathbf{l}$ and $\delta\mathbf{m}$ describe their oscillations in the wave. It can easily be verified that the component $\delta\mathbf{l}$ linear in Ψ can be written in the form $\delta\mathbf{l}\propto(\mathbf{e}_z\times\mathbf{l}_0)\Psi$. In the approximation linear in $\Psi,\delta\mathbf{m}$, and $\delta\mathbf{l}$, we can easily find from the relations $\mathbf{l}\cdot\mathbf{m}=0$, $\mathbf{l}^2+\mathbf{m}^2=1$ that $\delta\mathbf{m}=-\mathbf{l}_0(\mathbf{m}_0,[\mathbf{e}_z\times\mathbf{l}_0])\Psi$. Using expression (8) for $\mathbf{m}$ in the static limit, we can present the magnetization component in the plane of the film in the form

$$\delta\mathbf{M}=2M_0\cdot\delta\mathbf{m}=-\mathbf{l}_0((\mathbf{H}+\mathbf{H}_D),[\mathbf{e}_z\times\mathbf{l}_0])\chi\Psi.$$

This leads to the following simple universal expression for the singular component of dipole energy:

$$H_d=\frac{\pi aH_{D_0}^2\chi^2}{4}\sum_k q_kq_{-k}a|k|\cos^2\varphi_0.$$

Here $\cos\varphi_0=(\mathbf{k}\cdot\mathbf{l}_0)/|k|$, and the following notation is introduced:

$$H_{D_0}=((\mathbf{H}+\mathbf{H}_D),[\mathbf{e}_z,\mathbf{l}_0]). \tag{13}$$

The quantity H_{D_0} introduced here plays the leading role in the modification of the dispersion relation for the activationless branch of spin waves. If $H_{D_0}\neq0$, a root modification of the same type as for FM appears, and hence the long-range magnetic order is stabilized. This term appears in the Hamiltonian of the long-range component of the dipole–dipole interaction only if the magnetization $\mathbf{M}$ has a component parallel to the plane of the film. It can be seen from formula (13) that, if the direction of the external field $\mathbf{H}$ is perpendicular to the film, i.e., is such that the isotropy of the easy plane is not violated, the required contribution to $\mathbf{M}$ can come only from the Dzyaloshinskii–Moriya interaction.

We begin with an analysis of the most standard form of the Dzyaloshinskii–Moriya interaction with the antisymmetric tensor D_{ik}:

$$D_{ik}=\varepsilon_{ikj}H_D^{(j)},$$

and do not fix the direction of the vector $\mathbf{H}_D$ at this stage. It is well known that such an interaction is of the exchange-relativistic origin,[15] $H_D=\sqrt{H_KH_e}$ (H_K and H_e are the anisotropy and exchange fields), and does not disturb the Lorentz-invariance of the σ-model. Simple calculations show that the parameter $H_{D_0}=-(\mathbf{e}_z\cdot\mathbf{H}_d)$, i.e., $H_{D_0}\neq0$ only if the chosen axis of the Dzyaloshinskii–Moriya interaction is perpendicular to the plane of the two-dimensional magnet. This exactly corresponds to the situation when the Dzyaloshinskii–Moriya interaction does not violate the exact easy-plane

anisotropy and continuous degeneracy of the ground state of the magnet. In this case, the long-range order can be stabilized only due to the root modification of the dispersion relation for the lower magnon branch.

Thus, we arrive at the conclusion that in an analysis of the stabilization of the long-range magnetic order in two-dimensional easy-plane AFM we must take into account the long-range component of the magnetic dipole–dipole interaction as well as the Dzyaloshinskii–Moriya interaction with an invariant of the form $(m_x l_y - m_y l_x)$. The dispersion relation for the upper branch Ω_k changes insignificantly in this case. The energy of the lower branch in the main approximation in the small parameters χ and ak assumes the form

$$\hbar\omega_k = \hbar c\left(k^2 + \frac{\pi a \chi^2 H_D^2}{4A}\, a|k|\cos^2\varphi_0\right)^{1/2}. \tag{14}$$

Thus, this dispersion relation for small k has a root modification $\omega_k \approx c\sqrt{|k|\cdot k^*}$ and remains linear $\omega_k \approx c|k|$ for $k \gg k^*$, where

$$k^* = \frac{\chi^2 H_D^2 a}{4A}\,\pi\cos^2\varphi_0.$$

It should be noted that these results are in accord with those obtained earlier for FM,[5] but the value of k^* for AFM is considerably smaller than the corresponding parameter for FM.

Let us estimate the value of $\langle(\Delta\varphi)^2\rangle$ which does not diverge in the root modification of the dispersion relation. For this purpose, we use the method proposed in Sec. 1 in similar calculations for a two-dimensional FM. Formally, we supplement the Hamiltonian for AFM with the term $\Delta = -l_x \cdot M_0 H_l^{\rm ext}$. In contrast to ferromagnets, this term in the Hamiltonian of AFM cannot be interpreted as the energy in an external magnetic field. The dispersion relation (14) for spin waves is modified as follows:

$$\hbar\omega_k \to \hbar c\left(k^2 + \frac{H^{\rm ext}}{2A} + \frac{\pi a \chi^2 H_D^2}{4A}\, a|k|\cos^2\varphi_0\right)^{1/2}$$

(the dispersion relation for the upper branch also changes in the same way). Since the equilibrium direction of the antiferromagnetism vector was chosen by us in the plane of the film along the x-axis, the average fluctuation of $\mathbf{l}$ can be expressed in terms of mean fluctuations of field variables: $\langle\Delta l_x\rangle = -(1/2)\langle(\Delta\varphi)^2\rangle - (1/2)\langle(\Delta\vartheta)^2\rangle$. On the other hand, we can present $\langle\Delta l_x\rangle$ in the form

$$\langle\Delta l_x\rangle = -\frac{1}{(2\pi)^2}\int d\mathbf{k}\,\frac{\hbar}{2M_0} \times\left(\frac{\partial\omega_k(H^{\rm ext})}{\partial H^{\rm ext}}\, n_k + \frac{\partial\Omega_k(H^{\rm ext})}{\partial H^{\rm ext}}\, N_k\right),$$

where the first term corresponds to the fluctuation $\langle(\Delta\varphi)^2\rangle$ and the second term to the fluctuation $\langle(\Delta\vartheta)^2\rangle$. Since $(\partial\omega_k/\partial H_l^{\rm ext}) \propto 1/\omega_k$, we again arrive at the formula following from (12).

Taking into account (14), we obtain for $T \gg (\hbar c)\chi^2 H_D^2 a^2/4A$

$$\langle(\Delta\varphi)^2\rangle \approx \frac{2T}{A}\ln\left(\frac{TA}{\pi a^2 \hbar c \chi^2 H_D^2}\right).$$

This expression can readily be used for estimating the temperature T_C corresponding to violation of the long-range magnetic order if we assume qualitatively that $\langle(\Delta\varphi)^2\rangle \propto 1$ for $T = T_C$.[5,6] This leads to the following estimate for T_C: $T_C \approx A\ \ln^{-1}(A^2/\pi\hbar a^2 c\chi^2 H_D^2)$. This temperature for the same value of exchange integral is much lower than the corresponding parameter for FM; its estimated value for $Mn(C_{18}H_{35}O_2)_2$ leads to the result matching with the experimental values ($T_C \approx 0.5$ K).[9]

Concluding the section devoted to antiferromagnets, let us consider the general case of the Dzyaloshinskii–Moriya interaction leading to the emergence of the terms W_D in the energy of the magnet, which is linear in magnetization[15] ($W_D = D_{ik} M_i l_k$), where the tensor $D_{ik} = D_{ik}(\mathbf{l})$ is determined by the magnetic crystal symmetry of the magnet. If we consider only such a form of the tensor D_{ik} for which the continuous degeneracy of the ground state (i.e., the isotropy of the easy plane corresponding to the symmetry C_∞) is not violated, we can prove that the case of $W_D = H_D(M_x l_y - M_y l_x)$ analyzed above is the only case in which the stabilization of the long-range order due to the nonanalyticity (root modification) of the dispersion relation is manifested in pure form. Indeed, this condition corresponds to the tensor D_{ik} including only three different components:

$$D_{ik} \propto \begin{pmatrix} D_2 & -D_1 & 0 \\ D_1 & D_2 & 0 \\ 0 & 0 & D_3 \end{pmatrix},$$

where D_1, D_2 and D_3 are independent of $\mathbf{l}$.

The corresponding terms in the expression for energy can be written as the sum of two invariants: $W_D = I_1 + I_2$, $I_1 = D_1(M_y l_x - M_x l_y)$, $\quad I_2 = D_2(M_x l_x + M_y l_y) + D_3 M_z l_z$. The first invariant was considered in this section, while the second can exist only for two-sublattice AFM with nonequivalent sublattices. Examples of such magnets are ferrites at the point of compensation or so-called weak longitudinal ferromagnets,[15] in which the atomic spins in different sublattices are equal, but their crystal environments are nonequivalent. Strictly speaking, these magnets are not AFM even when the magnetizations of the sublattices are equal exactly $|M_1| = |M_2|$ since their crystal symmetry group does not contain an odd element transposing the sublattices (see Ref. 15). In the pure easy-plane model, the only symmetry axis is C_∞ which cannot be odd by definition. In this case, the expression $L_z M_z$ changes sign and is not invariant in the presence of some other odd symmetry element. The inclusion of other invariants in the Dzyaloshinskii–Moriya interaction, which are manifested for ''true'' AFM with an odd principal axis is a quite complicated problem. First, the inclusion of such invariants violates the initial Lorentz-invariance of the Lagrangian L_0 of the σ-model. Second, in the case of a consistent exclusion of $\mathbf{M}$ and a transition to the σ-model, these invariants lead to anisotropy in the basal plane with a constant of the order of D^2/δ (see for details the analysis of these problems in Refs. 12 and 16). An analysis of AFM

should actually be carried out by taking into account these two factors. Simple calculations show that the constant H_{D_0} in (13) for some classes of magnets differs from zero, and the frequency acquires a nonanalytic term of the type $H_{D_0}^2|k|\cos^2\varphi_0$. Foe example, this is true of AFM with the symmetry $4_z^{(-)}2_x^{(-)}2_{xy}^{(+)}$ (this symmetry is inherent in MnF_2, CoF_2, and other magnets). In this case, $W_D = D(M_x l_y + M_y l_x)$, and the constant H_{D_0} can be written in the form

$$H_{D_0} = D[\mathbf{l}_0, (\mathbf{e}_x - \mathbf{e}_y)].$$

Thus, the quantity H_{D_0} is determined by the type of the ground state: $H_{D_0}=0$ for $\mathbf{l}$ oriented along the odd axes $\mathbf{e}_x$ and $\mathbf{e}_y$, while $H_{D_0}=\pm D\sqrt{2}$ and differs from zero for $\mathbf{l}$ oriented along the diagonal of the square. The same regularity is also typical of other AFM: for $D_{ik}\neq\varepsilon_{ikj}H_D^j$: the constant H_{D_0} is determined by the orientation of the vector $\mathbf{l}$ in the easy plane.

The lowering of symmetry (both crystal and dynamic; the latter is manifested in the violation of the Lorentz invariance) complicates the calculation of Δl_x. Lorentz invariance is violated due to the emergence in the Lagrangian of the terms linear in $\partial\theta/\partial t, \partial\varphi/\partial t$ of the type $\Delta_1(\theta,\varphi)(\partial\theta/\partial t) + \Delta_2(\theta,\varphi)(\partial\varphi/\partial t)$ (see the table in Ref. 16). If these invariants are taken into consideration, the transition to canonic variables becomes quite complicated, and the simple formulas (11) and (12) are no longer applicable. However, this does not complicate significantly the calculations of Δl_x using the above-described approach with the introduction of $H_l^{\exp}$.

It can be proved, however, that the main factor in these cases is the anisotropy in the basal plane which inevitably appears for AFM with $D_{ik}\neq\varepsilon_{ikj}H_{Dj}$. It leads to the emergence of activation in the spectrum of the lower branch and to a deviation of the dispersion relation from the linear form for $k<k_*^A$, where the quantity $(ak_*^A)\propto(agH_{D_0}/c) \propto(ak_*)^{1/2}\gg(ak_*)$. It follows hence that the inclusion of the magnetic dipole–dipole interaction for such AFM is immaterial. The main source for the existence of a long-range magnetic order in such materials is that the degeneracy of the ground state can also be discrete when anisotropy in the basal plane is taken into account.

Thus, the case when the Dzyaloshinskii–Moriya energy has the simplest form $D(M_x l_y - M_y l_x)$ is the only nontrivial case for ''pure'' AFM with equivalent sublattices considered here.

3. MAGNETS WITH NONEQUIVALENT SUBLATTICES. TWO-DIMENSIONAL FERRITE NEAR THE COMPENSATION POINT

We shall consider peculiarities of a magnet with two nonequivalent sublattices on the basis of the model of a two-sublattice easy-plane ferrite film whose state is determined by two vectors $\mathbf{M}_1$ and $\mathbf{M}_2$ of magnetization of sublattices. For definiteness, we choose $\Delta M = M_1 - M_2 > 0$. If the values of M_1 and M_2 differ significantly, the dynamics of such a magnet is completely equivalent to the dynamics of a ferromagnet and is described by the Landau–Lifshitz equation for the total magnetization $\mathbf{M}=\mathbf{M}_1+\mathbf{M}_2$. If, however, $|M_1| \approx |M_2|$, it can be described on the basis of the modified σ-model.[17,18] The normalized antiferromagnetism vector can be determined in the standard manner:

$$\mathbf{l} = \frac{\mathbf{M}_1 - \mathbf{M}_2}{|\mathbf{M}_1 - \mathbf{M}_2|} \quad \text{for} \quad |M_1| \approx |M_2|$$

As in the case of AFM, the magnetization $\mathbf{M}=\mathbf{M}_1+\mathbf{M}_2$ is a dependent variable that can be expressed in terms of the antiferromagnetism vector $\mathbf{l}$. In the static case, we have

$$\mathbf{M} = \Delta M \mathbf{l} + (D_3 - D_2)(l_z^2 \mathbf{l} - l_z \mathbf{e}_z). \tag{15}$$

The dynamic term has the same form as for AFM and is not given here. The second term is due to the invariants $D_2(M_x l_x + M_y l_y)$ and $D_3 M_z l_z$. The fact that this contribution is proportional to $(D_3 - D_2)$ is obvious since it does not depend on the relation between $|M_1|$ and $|M_2|$; $\mathbf{M}\cdot\mathbf{l}=0$ for $|M_1|=|M_2|$, and for $D_3=D_2$ these two invariants cancel out.

It should be emphasized that a magnet with nonequivalent sublattices cannot have other invariants bilinear in M_i and M_k. The emergence of terms of the type of W_D in pure AFM is due to the presence of odd (in Turov's sense[15]) elements of the crystal group, which are absence in the present case.

It was mentioned earlier for two-dimensional easy-plane antiferromagnets that the root modification of the dispersion relation, taking into account the magnetic dipole–dipole interaction is observed only provided that the nondynamic part of magnetization $\mathbf{M}$ in equilibrium has a component parallel to the easy plane. The corresponding component of $\mathbf{M}$ in AFM appears as a result of the Dzyaloshinskii–Moriya interaction. It can be seen from formula (15) that this component for ferrites is equal to $\Delta M\mathbf{l}$, and hence appears due to nonidentity of the sublattices. The term with $(D_3 - D_2)$ is such that it gives a nonzero magnetization only when $\mathbf{l}$ forms an angle with the easy plane other than 0 or 90°.

The Lagrangian of the system in terms of the field variables ϑ and φ has the form

$$L = \int dxdy \left\{ \frac{a}{g}\left[\frac{\Delta M}{2}(1-\sin\vartheta) + \chi(D_2 - D_3) \times \sin\vartheta\cos^2\vartheta \right] \frac{\partial\varphi}{\partial t} - A[(\nabla\vartheta)^2 + \cos^2\vartheta(\nabla\varphi)^2] + \frac{A}{c^2}\left[\left(\frac{\partial\vartheta}{\partial t}\right)^2 + \cos^2\vartheta\left(\frac{\partial\varphi}{\partial t}\right)^2 \right] - K\sin^2\vartheta - W_d \right\},$$

where the constants A and K of nonuniform exchange and anisotropy are defined in the same way as in AFM, and c is the velocity of spin waves in the ferrite. In addition to the term which is standard in Lorentz-invariant models, this Lagrangian contains terms linear in $\partial\varphi/\partial t$. These terms appear due to the difference between $|M_1|$ and $|M_2|$ (''ferromagnetic'' term)[17] as well as due to an invariant with D_2, D_3.[18] If we take into account the dipole–dipole interaction, the Hamiltonian of the problem acquires an additional term

$$H_d = a(M_1 - M_2)^2 \sum_k \Psi_k \Psi_{-k} a|k| \sin^2 \varphi_0 .$$

As in the case of static magnetization,, the invariant with $(D_3 - D_2)$ makes no contribution to the quadratic Lagrangian for an easy-plane magnet. Consequently, its inclusion is immaterial for the calculation of the spectrum of spin waves. As regards the ''ferromagnetic'' term, it plays the leading role for all values of ΔM except very small values ($\Delta M < (H_K/H_e)^{1/2} \cong 10^{-2}$, where H_e is the exchange field) (see estimates obtained in Ref. 17).

The frequencies of the two magnon branches are defined by the equation

$$[\Omega_0^2(k) - \omega^2][\omega_0^2(k) - \omega^2] = \omega^2 (g\Delta M/\chi)^2,$$

where $\Omega_0(k)$, $\omega_0(k)$ are the frequencies in the ''antiferromagnetic'' limit for $\Delta M = 0$. Taking into account the contribution of the long-range component of the dipole–dipole interaction and the fictitious field H_l^{ext}, these frequencies are defined as

$$\Omega_0(k) = c[k^2 + K/A + (1/2)H_l^{\text{ext}}]^{1/2};$$

$$\omega_0(k) = c[k^2 + \pi(\Delta M)^2 |k| \sin^2 \varphi_0 / A + (1/2)H_l^{\text{ext}}]^{1/2},$$

where $\sin^2 \varphi_0 = [k^2 - (\mathbf{k}\cdot\mathbf{l})^2]/k^2$. If, however, $\Delta M \neq 0$, the formulas for the magnon frequencies $\omega_1(k)$ and $\omega_2(k)$ become more cumbersome. The ''ferromagnetic'' limit corresponds to the inequality $\Delta M \gg \sqrt{\chi K}$; in this case, the frequency of the lower branch $\omega_{1(k)} \cong (\chi/g\Delta M)\omega_0(k)\Omega_0(k)$ and has a root dispersion relation for $H_l^{\text{ext}} = 0$. In this limit, the frequency of the upper branch $\omega_2(k)$ has a very large activation energy (of the order of the exchange integral) and can be ignored here. Consequently, the specific behavior associated with the presence of two sublattices is observed only in a narrow range of ΔM for

$$|M_1 - M_2| \leqslant \sqrt{\chi K} \cong 10^{-2} - 10^{-3}.$$

In this region, the standard procedure of separation of canonic variables is quite cumbersome, but the introduction of H_l^{ext} leads to a general formula for the contribution from both magnon branches to the fluctuation $\langle \Delta l \rangle$. Differentiating $\omega_{1,2}$ with respect to H_l^{ext} and considering that $(\partial\omega_0/\partial H_l^{\text{ext}}) \propto 1/\omega_0$, $(\partial\Omega_0/\partial H_l^{\text{ext}}) \propto 1/\Omega_0$, we can easily write

$$\langle \Delta l \rangle = \frac{\hbar c^2}{4A} \sum_k \left\{ \left[1 - \frac{(g\Delta M/\chi)^2}{F} \right] N(\omega_1) \frac{1}{\omega_1} + \left[1 + \frac{(g\Delta M/\chi)^2}{F} \right] N(\omega_2) \frac{1}{\omega_2} \right\},$$

where ω_1 and ω_2 are the magnon frequencies, $\omega_1 < \omega_2$; $F^2 = [\Omega_0^2(k) + \omega_0^2(k) + (g\Delta M/\chi)^2]^2 - 4\Omega_0^2(k)\omega_0^2(k)$; and $N(\omega)$ are occupation numbers for magnons from the two branches. It should be noted that the two contributions in this case cannot be interpreted simply as the contributions from the variables $\langle (\Delta\varphi)^2 \rangle$ and $\langle (\Delta\vartheta)^2 \rangle$. For small k, the value of $\omega_0 \ll \Omega_0$, and the formula for F is simplified ($F = (g\Delta M/\chi)^2 + c^2 K/A$).

Thus, the coefficients of $N(\omega_{1,2})$ contain only the standard singularity $(1/\omega_{1,2})$ for $\omega_{1,2} \to 0$ in this case also. Clearly, the main contribution to $\langle \Delta l \rangle$ is due to the first term associated with the activationless mode, whose frequency can be written in the form

$$\omega_1^2(k) = \frac{2K\chi\omega_0^2(k)}{2K\chi + (\Delta M)^2}.$$

In the main approximation in k, this term can we written in the form of the same integral as in the case of AFM, but with an additional factor

$$\langle \Delta l \rangle = \frac{T}{A} \frac{2K\chi}{2K\chi + (\Delta M)^2} \ln \left| \frac{\chi T [2K\chi + (\Delta M)^2]^{1/2}}{g\hbar (2K\chi)^{1/2} (\Delta M)^2} \right| . \tag{16}$$

Thus, thermal fluctuations of the vector **l** increase with decreasing ΔM due to the prelogarithmic factor as well as due to the logarithm itself. As $\Delta M \to 0$, $\langle \Delta l \rangle \to \infty$ due to the divergence of the logarithm, i.e., the long-range order is violated. This is clear since the dipole–dipole interaction ''does not operate'' for $\Delta M \to 0$.

It is appropriate to note here that the points of compensation of the mechanical moment $\Delta I = I_1 - I_2 = (M_1/g_1) - (M_2/g_2)$ and the magnetic moment ΔM in real ferrites with nonequivalent atoms in sublattices do not coincide in view of the difference in g-factors. In this case, formula (16) should be modified as follows: ΔM must be replaced by $\overline{g}(\Delta I)$, where $\overline{g} = (g_1 + g_2)/2$ (see Ref. 18) everywhere except in the denominator of the argument of the logarithm. The dependence of $\langle \Delta l \rangle$ on ΔM may not be monotonic in this case. The minimum value of $\langle \Delta l \rangle$ exists between the points of compensation of the magnetic and mechanical moments.

The authors are grateful to V. G. Bar'yakhtar and V. Kambersky for fruitful discussions.

This research was partly supported by grants of the Ukrainian Center of Science and Technology (Grant No. 300) and the Ukrainian Foundation for Fundamental Studies (Grant 2.4/27). B. Ivanov was also sponsored by the Soros Program Supporting Education in Science, Grant SPU 072025.

*)E-mail: vbaryakhtar@gluk.apc.org

[1] F. Bloch, Z. Phys. **61**, 206 (1930).
[2] N. D. Mermin and H. Wagner, Phys. Rev. Lett. **17**, 1133 (1966).
[3] V. L. Berezinskii, Zh. Eksp. Teor. Fiz. **61**, 1144 (1971) [Sov. Phys. JETP **34**, 610 (1971)].
[4] J. M. Kosterlitz and D. J. Thouless, J. Phys. **6**, 1181 (1973).
[5] S. V. Maleev, Zh. Eksp. Teor. Fiz. **70**, 2374 (1976) [Sov. Phys. JETP **43**, 1240 (1976)].
[6] P. Bruno, Phys. Rev. **43**, 6015 (1991).
[7] Y. Yafet, J. Kwo, and E. M. Jyorgy, Phys. Rev. B **33**, 6519 (1986).
[8] R. P. Ericson and D. L. Mills, Phys. Rev. B **46**, 861 (1992).
[9] M. Pomerants, Surf. Sci. **142**, 556 (1984).
[10] A. I. Akhiezer, V. G. Bar'yakhtar, and S. V. Peletminskii, *Spin Waves*, No. Holland, Amsterdam, 1968.
[11] V. N. Krivoruchko and D. A. Yablonskii, Phys. Status Solidi B **104**, K41 (1981).
[12] B. A. Ivanov and A. K. Kolezhuk, Fiz. Nizk. Temp. **21**, 355 (1995) [Low Temp. Phys. **21**, 375 (1995); H. J. Mikeska and M. Steiner, Adv. Phys. **40**,

191 (1991); A. F. Andreev and V. I. Marchenko, Usp. Fiz. Nauk **130**, 39 (1980) [Sov. Phys. Usp. **23**, 21 (1980)].
[13] A. S. Kovalev, A. M. Kosevich, I. V. Manzhos, and K. V. Maslov, Pis'ma Zh. Éksp. Teor. Fiz. **44**, 174 (1986) [JETP Lett. **44**, 222 (1986)].
[14] L. D. Landau and E. M. Lifshitz, *Mechanics* [in Russian], Nauka, Moscow (1988).
[15] E. A. Turov, *Physical Properties of Magnetically Ordered Crystals*, Academic Press, New York, 1965.
[16] E. V. Gomonai, B. A. Ivanov, V. A. L'vov, and G. K. Oksyuk, Zh. Éksp. Teor. Fiz. **97**, 307 (1990) [Sov. Phys. JETP **70**, 174 (1990)].
[17] B. A. Ivanov and A. L. Sukstanskii, Zh. Éksp. Teor. Fiz. **84**, 371 (1983) [Sov. Phys. JETP **57**, 214 (1983)].
[18] A. A. Zhmudskii, B. A. Ivanov, G. K. Oksyuk, and A. L. Sukstanskii, Fiz. Nizk. Temp. **16**, 1439 (1990) [Sov. J. Low Temp. Phys. **16**, 814 (1990)].
[19] B. A. Ivanov and E. V. Tartakovskaya, Phys. Rev. Lett. **77**, 386 (1996).

Translated by R. S. Wadhwa

SUPERLOW TEMPERATURE TECHNIQUES

Dynamic characteristics of adsorbents for adsorption pumps of dilution refrigerators

R. I. Shcherbachenko and V. N. Grigor'ev

*B. Verkin Institute for Low Temperature Physics and Engineering, National Academy of Sciences of the Ukraine, 310164 Kharkov, Ukraine**

(Submitted June 4, 1998)
Fiz. Nizk. Temp. **24**, 1105–1109 (November 1998)

The data on adsorption isotherms of ^{4}He in synthetic adsorbents are obtained at 4.2 K in the pressure range $1–10^{-2}$ torr. The dependence of pressure on the amount of adsorbed gas in adsorption pumps is studied under conditions simulating the pump operation in dilution refrigerators. It is found that the pressure in the pump is practically independent of the amount of adsorbed helium for a constant pumping rate in the interval $10^{-6}-10^{-4}$ mole/s, over a wide pressure range. The obtained characteristics can be used for designing and developing pumps for dilution refrigerators. © *1998 American Institute of Physics.* [S1063-777X(98)00911-6]

Adsorption pumps, which are used quite frequently in vacuum technology,[1] have found a new application recently following the development of ^{3}He–^{4}He dilution refrigerators with cryogenic circulation cycles.[2–4] Interest has been growing in the new information concerning the characteristics of such pumps in view of the peculiarities of their operation in dilution refrigerators. In vacuum technology, the mass flux is not large during pumping in most cases of evacuation, and hence the construction of adsorption pumps requires just a knowledge of the limiting values of pressure for a given level of adsorbent filling, i.e., adsorption isotherms measured under static conditions. Dynamic characteristics, which determine the possibility of a constant pumping rate for prolonged durations under considerable mass fluxes, are also significant for dilution refrigerators. Information about the pump operation under such conditions is quite scarce and even contradictory (see, for example, Ref. 5). it was found by Wiedemann *et al.*[6] that the pumping rate remains practically unchanged as long as the amount of adsorbed helium is less than about two thirds of the equilibrium volume of the adsorbent defined by the adsorption isotherm. At the same time, Amamchan *et al.*[7] discovered a decrease in the pumping rate upon an increase in the adsorbent filling, starting from the smallest values. An identical result was also reported in a subsequent publication by Kolobrodov *et al.*[8]

In order to ensure a stable operation of dilution refrigerators with a cryogenic circulation cycle, we must find the conditions under which the pumping rate can remain constant over a quite long time. Otherwise, either the temperature regime of operation of the refrigerator will be violated, or at least its operation will be considerably complicated. The present work is devoted to an analysis of such problems. Moreover, we also continue our studies of the properties of new adsorbents.

First of all, we studied the adsorption isotherms of a number of new synthetic adsorbents. Measurements were made at 4.2 K according to the technique described by Dikina *et al.*[9] by using liquid helium in a standard dewar containing the sample under investigation. Pressures P in the interval $1–10^{-2}$ mmHg corresponding to the working pressures in the dilution refrigerators were measured by a thermocouple vacuum gauge calibrated for helium with the help of a McLeod gauge. Figure 1 shows the adsorption isotherms of ^{4}He at 4.2 K for carbons SKN and KAU under normal conditions.

Within the limits of the spread of data, the adsorption isotherms are described by the dependence

$$V_\alpha = A + BV^0 gP. \tag{1}$$

The parameters of this dependence for the investigated samples are given in Table I.

In addition to the values of A and B corresponding to the pressure P in mm Hg, Table I also contains data about the absorbability V_0 of the adsorbents for the highest characteristic value of pressure 7.5×10^{-2} mm Hg in the evaporation chamber of the dilution refrigerator.

The difference in the results for SKNP-4 can be attributed to different batches of the adsorbents used by us and by the authors of Ref. 9.

Subsequent investigations were carried out by using carbons SKN and KAU. The carbon SKN has the best adsorption isotherm, while KAU is characterized by the shortest period in which equilibrium pressure is established. This circumstance envisages the existence of optimal characteristics of adsorbents under dynamic conditions in spite of the relatively small absorbability under equilibrium conditions. Hence the carbon KAU was chosen as the material for the most comprehensive studies in our experiments.

Measurements were made by using a pump whose construction is shown in Fig. 2. The adsorbent was placed in a single layer on plates fitted on a tube passing through the center of the cylindrical casing. All components of the pump

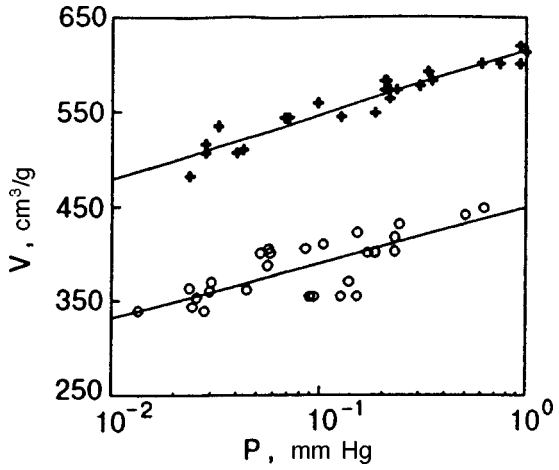

FIG. 1. Isotherms of ^{4}He adsorption by SKN (crosses) and KAU (circles) at $T=4.2$ K.

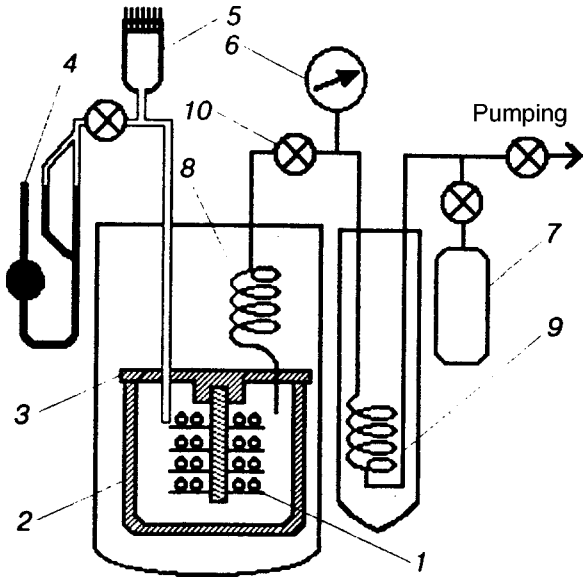

FIG. 2. Schematic diagram of the adsorption pump: *1*—adsorbent, *2*—pump casing, *3*—lid, *4*—McLeod gauge, *5*—thermocouple vacuum gauge, *6*—mechanical pressure gauge, *7*—calibrated volume, *8*—condenser coil, *9*—nitrogen trap, *10*—inlet valve.

were made of copper. In most experiments, 13 plates containing 8.73 g carbon KAU and 14.35 g carbon SKN were used. Gaseous helium was supplied through a tube in the form of a spiral *8* immersed in liquid helium to ensure cooling of the gas being supplied. Another tube was used for connection with the manometer. The lid *3* was connected with the casing through an indium seal ensuring a convenient replacement of samples.

In our experiments, we measured the dependence of the pressure P in the pump on the amount of adsorbed helium under a constant injection rate. The injection rate $\dot{V}$ varied in the interval $(10^{-6}-10^{-4})$ mole/s. Figure 3 shows some of the obtained dependences. It can be seen that the pressure in the pump in the initial stage in almost all cases does not depend on the amount of the adsorbed gas, the plateau being observed at low injection rates up to $0.9V_a$ (V_a corresponds to the adsorption isotherm at a given pressure). The length of the plateau decreases upon an increase in the injection rate. (Note that the data corresponding to an increase in the pressure are only qualitative since a constant injection rate cannot be ensured under these conditions.)

Figure 4 shows such dependences obtained under the conditions when the injection rate changes stepwise in the course of the experiment. It can be seen that under such conditions, a plateau is also observed on the dependence $P(V)$. In our experiments, the plateau was observed for all

TABLE I. Values of parameters A and B in Eq. (1) for different adsorbents.

		A	B	V_0
Adsorbent	ρ, g/cm^3	cm^3/g		
SKF	0.35	719	77.2	628
SKT	0.39	644	77.1	560
KAU	0.58	437	59.7	361
SKT	0.49	440	41.0	394
SKN	0.40	613	59.4	546
UST	0.64	78	12.5	64
SKNP-4	0.34	579	67.8	502
SKNP-4*	0.34	790	97.2	680

*data from Ref. 10.

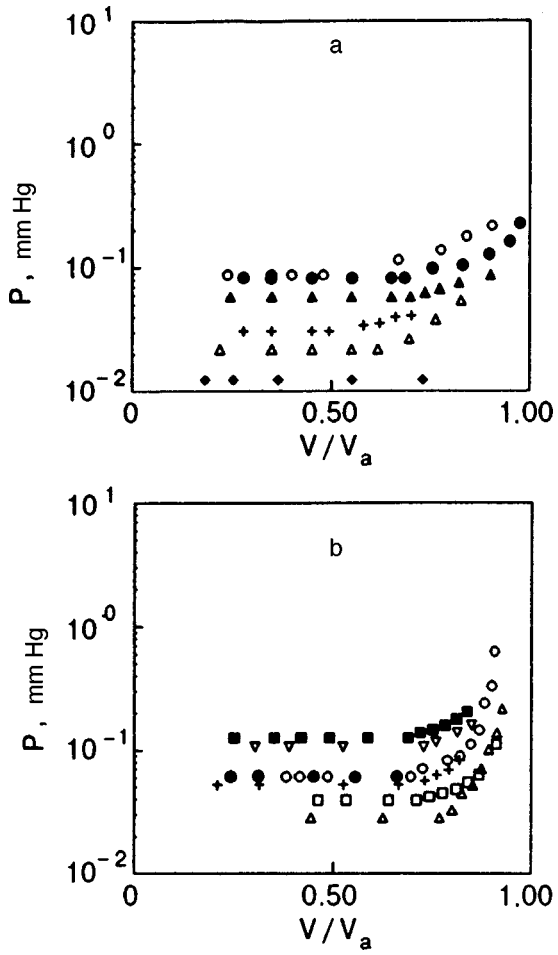

FIG. 3. Dependence of pressure on the degree of filling for various injection rates $\dot{V}$ (in micromole/s): (a) adsorbent KAU: 9,6 (♦); 18 (△); 40 (+); 78 (▲); 110 (●); 120 (○) (b) adsorbent SKN: 57 (△); 79 (□); 140 (+); 150 (●), (○) (data obtained in different experiments); 230 (▽); 290 (■).

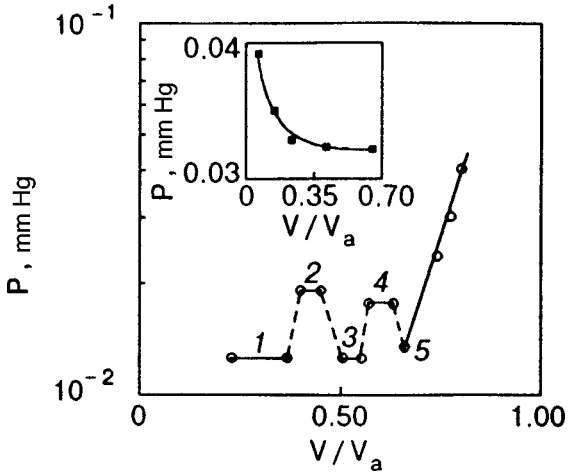

FIG. 4. Dependence of pressure in the pump on the degree of filling of the adsorbent KAU during a stepwise variation of the gas flow rate $\dot{V}$ (in micromole/s): 10 (*1*), 18 (*2*), 10 (*3*), 12 (*4*), 9.5 (*5*). The inset shows the dependence of pressure for silica gel in the initial stage of the experiment.

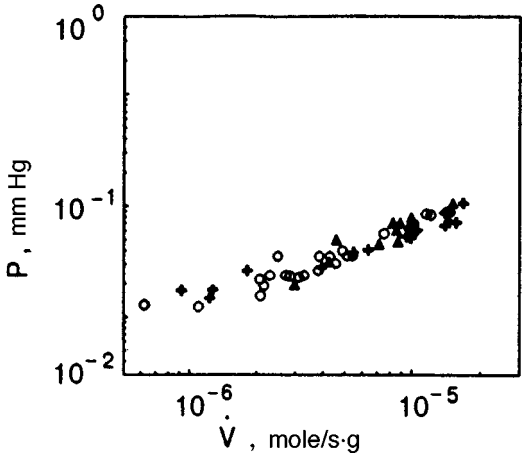

FIG. 5. Dependence of pressure in the pump in the plateau region on the gas injection rate per unit mass of the sample: SKNP-4 (triangles); KAU (circles), SKN (crosses).

the investigated adsorbents. This is in qualitative agreement with the data of Ref. 6. At present, it is not possible to explain unambiguously the absence of a plateau in the experimental data presented in Refs. 7 and 8. This can hardly be associated with high pumping rates since indirect estimates indicate that values of $\dot{V}$ of the order of 10^{-4} mole/s were used in both cases (the exact data are not presented in either of the above-mentioned works). Hence the absence of a plateau is most probably associated with the construction of the pumps. In particular, one can also expect the detrimental effect of multilayer arrangement of adsorbents on pump characteristics. In this connection, it should also be recalled that the data presented in Ref. 8 correspond to a lower pressure $P=5\times10^{-3}$ mm Hg than in our case (the value of P presented in Ref. 7 is $P\simeq10^{-2}$ mm Hg).

An interesting peculiarity was observed in the initial stage of the experiment. As a rule, the pressure in the pump decreases in such cases upon an increase in the amount of adsorbed helium, the decrease being especially noticeable at low injection rates. This circumstance is illustrated in the inset to Fig. 4 showing the initial experimental stage with silica gel at an injection rate of 10^{-6} mole/s. Apparently, such a behavior can be explained by the fact that the adsorbed helium facilitates a more effective cooling of the adsorbent.

The data presented in Fig. 3 were used to construct the most representative (from the point of view of practical application) dependence of pressure ensured by the pump in the region of the plateau on the pumping rate (Fig. 5). In addition to the data for KAU and SKN, the figure also contains points obtained in analogous experiments with the adsorbent SKNP-4 which has been used in dilution refrigerators.[4] In order to take into consideration the difference in the masses of the investigated samples, the pumping rate divided by the mass of the sample is laid along the abscissa axis in Fig. 5 (preliminary experiments with a lower concentration of the adsorbent showed that $\dot{V}$ in the plateau region is proportional to the mass under identical pressures). It was found that, within the spread of experimental points, the obtained dependence in these coordinates is universal for all three adsorbents and is practically linear.

The comparatively weak increase in pressure upon an increase in the pumping rate is apparently due to the fact that the increase in heat removal during absorption is compensated by an increase in the thermal conductivity of the gas. Apparently, the thermal conductivity of a gas is the main mechanism for removal of the heat of adsorption and ensures the universal nature of the obtained dependence under conditions when the pumping rate for the adsorbent is determined by the intensity of its cooling.

It should be emphasized that the dependences $P(\dot{V})$ are almost identical in spite of the fact that the adsorption isotherms of KAU differ significantly from those of SKNP-4 and SKN (see Fig. 1). This confirms the idea put forth in the Introduction that the adsorption isotherm is not a sufficiently reliable characteristic of the quality of the adsorbents used in dilution refrigerator pumps, and also supports the assumption that there exists a correlation between the speed at which equilibrium pressure is established in the adsorbent and the possibility of ensuring a fast pumping rate. However, the role of the absorbability can by no means be disregarded since it determines the required amount of the adsorbent.

The obtained dependences allow us to carry out quantitative analysis of adsorption pumps used in low-temperature dilution and evaporation refrigerators. Naturally, in order to make the calculations reliable, we must carry out measurements in a wider range of parameters and, above all, of the pumping rates. We must also clarify the role of construction details of the pumps and determine the ways of improving the cooling of the adsorbents. It should also be interesting to determine the extent to which the dependence $P(\dot{V})$ is universal. We plan to carry out these investigations and to search for new adsorbents. This research was carried out by using ordinary helium while dilution refrigerators use ^{3}He as a rule. One can hope that the difference will turn out to be just quantitative as was found during a comparison of the

adsorption isotherms of ^{3}He and ^{4}He.[10,11] However, this conclusion needs to be verified.

*E-mail: grigor'ev@ilt.kharkov.ua

[1] A. N. Volkevich, *High-Vacuum Adsorption Pumps* [in Russian], Mashinostroyeniye, Moscow (1973).
[2] V. A. Mikheev, V. A. Maidanov, and N. P. Mikhin, Cryogenics **14**, 190 (1984).
[3] V. E. Sivokon', V. V. Dotsenko, L. A. Pogorelov, and V. I. Sobolev, Fiz. Nizk. Temp. **19**, 444 (1993) [Low Temp. Phys. **19**, 312 (1993)].
[4] V. A. Maĭdanov, N. P. Mikhin, N. F. Omelaenko *et al.*, Fiz. Nizk. Temp. **20**, 672 (1994) [Low Temp. Phys. **20**, 527 (1994)].
[5] B. I. Verkin, V. N. Grigor'ev, V. G. Ivantsov *et al.*, *Methods of Attaining and Measuring Low and Ultralow Temperatures* [in Russian], Naukova Dumka, Kiev (1987).
[6] W. Wiedeman and E. Smolic, in *Proceedings of the 11th Int. Conf. Cryogen. Eng.*, Brighton, UK (1968), p. 59.
[7] R. G. Amamchan, S. V. Favorskaya, and S. T. Boldarev, in *Abstracts of papers to the 21st All-Union Conf. Low Temp. Phys.*, Kharkov (1980), p. 220.
[8] V. G. Kolobrodov, L. V. Karnatsevich, T. K. Grigorova, and A. N. Skomorokhov, Fiz. Nizk. Temp. **19**, 331 (1993) [Low Temp. Phys. **19**, 234 (1993)].
[9] L. S. Dikina, V. G. Ivantsov, N. T. Kartel' *et al.*, Fiz. Nizk. Temp. **15**, 532 (1989) [Sov. J. Low Temp. Phys. **15**, 300 (1989)].
[10] P. Roubean, G. Nigohossian, and D. Avenel, in *Proceedings Colloque. Int. ''Le vide at le froid''*, Grenoble, France (1969), 49 pp.
[11] C. Menetrier and P. Roubean, Rev. Phys. Appl. **14**, 131 (1979).

Translated by R. S. Wadhwa

BRIEF COMMUNICATIONS

Did Ogg really observe high-temperature superconductivity in metal-ammonia solutions?

É. A. Pashitskiĭ

Institute of Physics, National Academy of Sciences of the Ukraine, 252650 Kiev, Ukraine[*)]

(Submitted June 22, 1998)
Fiz. Nizk. Temp. **24**, 1110–1112 (November 1998)

An empirical analysis of the results of time- and temperature dependences of the electrical resistance R of metal-ammonia solutions NH_3:Na with different Na concentrations quenched in liquid nitrogen point towards an anomalously high but finite conductivity rather than superconductivity. In particular, the time dependence $R(t)$ of solutions NH_3:Na quenched rapidly at $T<80$ K can be described correctly by a ''logistic curve'' with a nonzero initial value $R(0)\neq 0$ (at $t=0$). © *1998 American Institute of Physics.* [S1063-777X(98)01011-1]

1. The experimental results obtained by Ogg[1] from resistance measurement of metal–ammonia solutions quenched in liquid nitrogen (at $T=78$ K) have remained enigmatic for over half a century. These investigations were the first to arouse the interest of researchers in the problem of high-temperature superconductivity (HTSC) and stimulated experimental and theoretical quest for nontraditional superconductors which culminated in a resounding success after 40 years when Bednorz and Müller[2] discovered HTSC in cuprate metal-oxides in 1986.

However, the main (foremost) question as to whether Ogg[1] observed ''nitrogen-temperature'' superconductivity for the first time or an anomalously high ''normal'' conductivity in frozen NH_3:Na solutions remains unanswered so far. For example, Verkin *et al.*[3] suggested that the high conductivity of metal–ammonia solutions is due to the precipitation of whiskers of chemically pure sodium as a result of quenching of solutions in liquid nitrogen. However, the reasons behind a low initial resistance of solutions with low Na concentration of the order of 2–3 at. %, and a subsequent increase in the resistance of metallic Na filaments with time are not clear so far.

Dmitrenko and Shchetkin[4] carried out the most comprehensive investigations of temperature- and time dependences of the resistance R of metal–ammonia solutions with various sodium concentrations (1–12 at. %) over a wide temperature interval $T=20-240$ K. These experiments showed that in addition to the low-temperature phase with an anomalously high conductivity in the temperature range $T<80$ K, quenched solutions NH_3:Na also contain a conducting phase with a higher resistance in the interval 80 K$<T<$120 K, a dielectric phase in the interval 120 K$<T<$160 K, and a high-temperature conducting phase in the interval 160 K$<T<$195 K, a transition to which from the dielectric phase is accompanied by a hysteresis of width about 5 K. In order to describe the $R(T)$ dependence in the entire temperature range, Dmitrenko and Shchetkin[4] proposed an empirical interpolation relation:

$$R(T)=A\ \exp(-T_0/T), \tag{1}$$

which can be treated as an inversion of the temperature dependence of activation conductivity $\sigma(T)=\sigma_0\ \exp(-T_0/T)$ and corresponds to zero (exponentially low) resistance $R(0)=0$ for $T=0$. However, formula (1) does not describe a sharp increase in resistance ($R\to\infty$) upon a transition to the dielectric phase, or the hysteresis phenomena in the vicinity of $T=160$ K.

Dmitrenko and Shchetkin[4] measured at low temperatures ($T<20$ K) the time dependence $R(t)$ of quenched NH_3:Na solution with a 2%-concentration of sodium which has the lowest initial resistance R_0. Using the obtained experimental data, they showed that under the assumption of precipitation of the entire sodium content into a single conducting filament of a uniform cross-section throughout its length, the resistivity ρ corresponds to the effective value $\rho\approx(10^{-7}-10^{-8})\Omega\cdot$cm which is about 3–4 orders of magnitude lower than the resistivity of metallic sodium. Hence the authors of Ref. 4 suggested that a transient superconducting state with zero resistance at the initial instant of quenching of the solution is formed in NH_3:Na, and proposed the following empirical exponential dependence of R on t:

$$R(t)=B\ \exp(-t_0/t), \tag{2}$$

which corresponds to the limiting value $R(0)=0$ at $t=0$.

2. In this communication, we wish to emphasize that for an appropriate choice of the parameters $R_0=R(0)$, $R_\infty=R(t\to\infty)$ and τ, the experimental data obtained by Dmitrenko and Shchetkin[4] on the time dependence $R(t)$ fit much better on the so-called ''logistic curve''

$$R(t)=\frac{R_\infty}{1+(R_\infty/R_0-1)\exp\{-t/\tau\}}, \tag{3}$$

than on the dependence described by formula (2).

Figure 1 shows the dependence $R(t)$ described by formula (3) plotted on semilogarithmic scale for various values of the parameters $R_\infty=1.2\ \Omega$, $R_\infty/R_0=10^4$, $\tau=2.2$ min

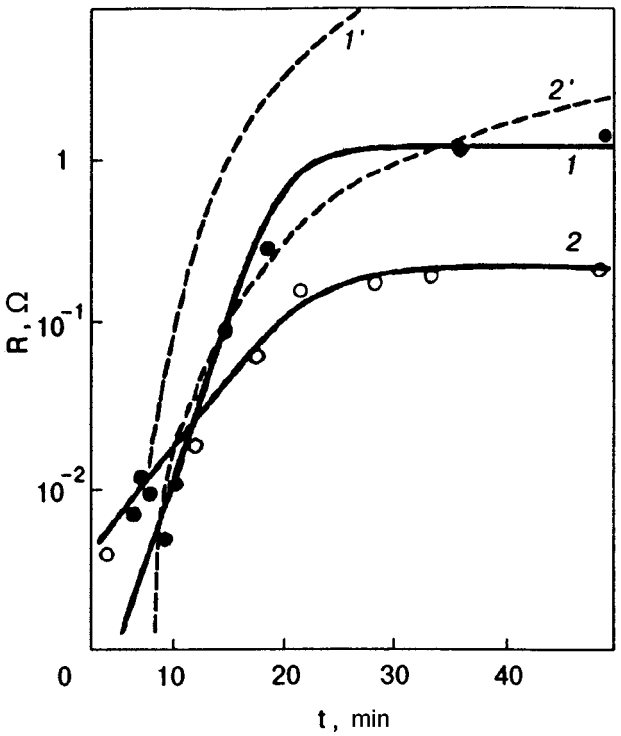

FIG. 1. Time dependence $R(t)$ of the resistance according to the experimental data of Ref. 4 (dark and light circles), and according to the ''logistic curve'' *3* for different values of the parameters (curves *1, 2*). The dashed curves show the exponential dependences (2) for $t_0=30$ min for $B=10^2$ Ω (curve *1′*) and 10 Ω (curve *2′*).

(curve *1*) and $R_\infty=0.2\ \Omega$, $R_\infty/R_0=10^2$, $\tau=4.4$ min (curve *2*). The dark and light circles reflect the experimental values of $R(t)$ taken from Ref. 4 for two different series of experiments. It can be seen that the theoretical curves are in good agreement with the experimental data. For comparison, the dashed curve *1′* in the figure shows the dependence (2) for parameters $B=10^2$ Ω and $t_0=30$ min used in Ref. 4. It can be seen that this curve does not match the experimental results. A slightly better agreement is attained for $B=10\ \Omega$ and the same value of t_0 (curve *2′*, but the saturation of the dependence $R(t)$ for $t>20$ min, which is described quite well by the ''logistic curves'' *1* and *2*, is not observed clearly in this case.

Let us consider the possible reasons behind the agreement between formula (3) and the experimental results obtained in Ref. 4. The dependence of type (3) is a solution of the first-order nonlinear differential equation

$$\frac{dR}{dt}=\frac{R(t)}{\tau}\left[1-\frac{R(t)}{R_\infty}\right] \tag{4}$$

with a nonzero initial condition $R(0)=R_0$ at $t=0$.

Since the resistance R is inversely proportional to the conductivity σ, and σ is proportional to the carrier concentration n, we obtain from Eq. (4) the following equation for n under the assumption $R(t)=C/n(t)$, where $C=$const:

$$\frac{dn}{dt}=-\frac{n(t)}{\tau}+\frac{C}{\tau R_\infty}. \tag{5}$$

The first term on the right-hand side of this equation describes the rate of decrease in the carrier concentration, which is proportional to n, while the second term describes the intensity of the n-independent source of charge carriers.

The majority carriers in the metal-ammonia solution NH_3:Na are electrons formed as a result of ionization of alkali metal atoms owing to large permittivity $\varepsilon=22$ of ammonia. Since electrons in liquid ammonia are surrounded by heavy solvate shells from NH_3 molecules with a large dipole moment, we can assume the following hypothetical mechanism of increase in the concentration of free charge carriers in the quenched solution: during quenching of the solution, the solvate shells are destroyed as a result of crystallization of NH_3, and a considerable fraction of electrons are liberated, thus ensuring a high initial conductivity (i.e., a low initial resistance R_0). With the passage of time, however, electrons are gradually captured in polar ''traps'' and are transformed into heavy polarons, which leads to a decrease in conductivity (i.e., an increase in the resistance). In the solid phase ($T<80$ K), the process of ''trap'' formation is much slower than the formation of solvate shells in the liquid phase, and is characterized by much longer times (of the order of several minutes). According to Eq. (5), the concentration of free electrons decreases according to an exponential law:

$$n(t)=(n_0-n_\infty)\exp\{-t/\tau\}+n_\infty, \tag{6}$$

where $n_0=n(0)$ and $n_\infty=C/R_\infty$. The limiting concentration n_∞ for $t\to\infty$ is mainly determined by the ejection of electrons from the cathode during the passage of current, and may be much lower than the initial concentration n_0 which is of the same order of magnitude as the concentration of Na atoms in the solution NH_3:Na. This accounts for the large value of the final resistance R_∞ as compared with the initial resistance ($R_\infty/R_0=10^2-10^4$), which led to the assumption about the zero value of R_0, i.e., about the superconductivity of quenched metal–ammonia solutions.[1,4]

Naturally, the confirmation of the above hypothesis requires a more detailed investigation of the processes of destruction of solvate shells and the formation of polarons in crystalline ammonia.

This research is dedicated to the 70th birth anniversary of Igor Mikhailovich Dmitrenko, member of the National Academy of Sciences of the Ukraine. The author was greatly benefited by the many years of his association with Academician Dmitrenko, which enriched him both as a scientist and as a human being.

*)E-mail: pashitsk@iop.kiev.ua

[1] R. A. Ogg, Phys. Rev. **69**, 243, 544, 559 (1946); *ibid.* **70**, 93 (1946).
[2] J. G. Bednorz and K. A. Müller, Z. Phys. B **44**, 189 (1986).
[3] B. I. Verkin, B. G. Lazarev, and V. I. Khotkevich, in *Proceedings of the Physics Faculty of Kharkov State University* [in Russian] (1952).
[4] I. M. Dmitrenko and I. S. Shchetkin, Pis'ma Zh. Éksp. Teor. Fiz. **18**, 497 (1973) [JETP Lett. **18**, 292 (1973)].

Translated by R. S. Wadhwa

LETTERS TO THE EDITOR

Linear electron chains on the surface of superfluid helium

Yu. Z. Kovdrya, V. A. Nikolaenko, S. P. Gladchenko, and S. S. Sokolov

B. Verkin Institute for Low Temperature Physics and Engineering, National Academy of Sciences of the Ukraine, 310164 Kharkov, Ukraine)*

(Submitted June 24, 1998)
Fiz. Nizk. Temp. **24**, 1113–1116 (November 1998)

A unique one-dimensional system of linear electron chains on the liquid helium surface is realized experimentally for the first time. This system is created by using the distortion of the helium surface and covering the profiled dielectric substrate in a confining electric field holding electrons in the liquid channels being formed. The carrier mobility in linear electric chains is measured in the temperature interval 0.5–1.8K in confining fields up to 1 kV/cm. It is shown that the electron mobility depends on the purity of the substrate surface. For clean substrates, the mobility increases with decreasing temperature in the entire investigated temperature range. The results of measurements are found to be in accord with the existing theory.
 [S1063-777X(98)01111-6]

Investigation of the one-dimensional ($1D$) systems is one of the most interesting problems in the physics of the condensed state. However, only quasi-one-dimensional systems have been created so far. In most cases, such low-dimensional systems were created by using thin metallic wires or semiconducting structures with a narrow field shutter (such systems contain several electrons across the channel). By using the high degree of homogeneity of the electron system on the surface of extremely pure helium, we can obtain a basically new one-dimensional electron system.

Earlier, we proposed[1] a method for realizing a one-dimensional electron system on the grooved surface of liquid helium on a dielectric substrate with parallel channels of given transverse dimensions ruled on its surface. The confining electric field drives the electrons to the channels formed on the liquid helium surface. The motion of electrons is free along the channels and quantized in the transverse direction. It was shown in Ref. 1 that the separation between energy levels corresponding to the motion of particles across the channels may attain values 0.1–0.3 K for reasonable values of the channel parameters and the confining electric field.

Such systems were obtained by us and by other authors[2–6] using optical gratings made of glass as substrates. The mobility and conductivity of charge carriers were studied. However, one-dimensional systems with a good conductivity could not be constructed: the channels with good conductivity created in Refs. 2–6 contained several electrons in a direction transverse to them.

In the present communication, we report on the first realization of conducting channels on liquid helium surface with a very small number of electrons forming a one-dimensional system, viz., linear electron chains.

For the insulating substrate, we chose a glass plate on which a nylon thread of diameter 0.1 mm was wound tightly (Fig. 1). The dielectric constant of nylon at helium temperatures, extrapolated from the measurements made by us at 80 K, is 1.5. The experimental cell (Fig. 1a) was analogous to the one described in Ref. 6. The substrate was placed over the measuring electrodes A, B and C of size 5.6×9.2, 2×9.2, and 15.6×9.2, respectively. The electrodes A, B and C were maintained at zero potential. A negative potential confining the electrons to the liquid helium surface was applied to the electrodes *2, 3* and the guard electrode *4*. The voltage from the generator was supplied to the electrode A, while the signal passing through the cell was recorded at the electrode C. The driving electric field was directed along the liquid channels.

Measurements of the 0°- and 90° components of the signal passing through the cell charged by electrons were made at a frequency of 100 kHz. The measured values were used to determine the real (G_r) and imaginary (G_i) parts of the conductance of the cell associated with electrons.

The experiments were carried out as follows. The liquid helium surface was charged by applying a small confining voltage $V_\perp = 0.5$ V by lighting a miniature incandescent filament for a very short time. The charging of helium surface was registered as the emergence of a signal from the electrons. The confining potential was then reduced to zero in order to remove the main part of electrons from the liquid surface. In this case, no signal was detected from the electrons. Without lighting the incandescent filament, a large confining potential was applied, which resulted in the reappearance of the signal from electrons with a magnitude smaller than the initial signal. This procedure makes it possible to select the required smallest number of electrons in the conducting channel. The electrons over the thin film in a zero confining potential were accumulated (by applying a high confining field in the grooves of the fluted surface of liquid helium) in deeper liquid channels. Their mobility

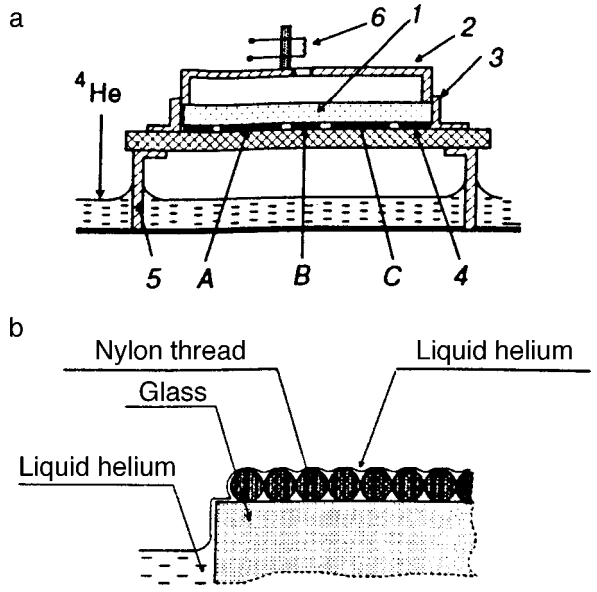

FIG. 1. (a) Schematic diagram of the measuring cell: *1* — substrate, *2, 3* — confining electrodes, *4* — guard electrode, *5* — copper supports, *6* — incandescent filament, and A, B, C are measuring electrodes. (b) Substrate.

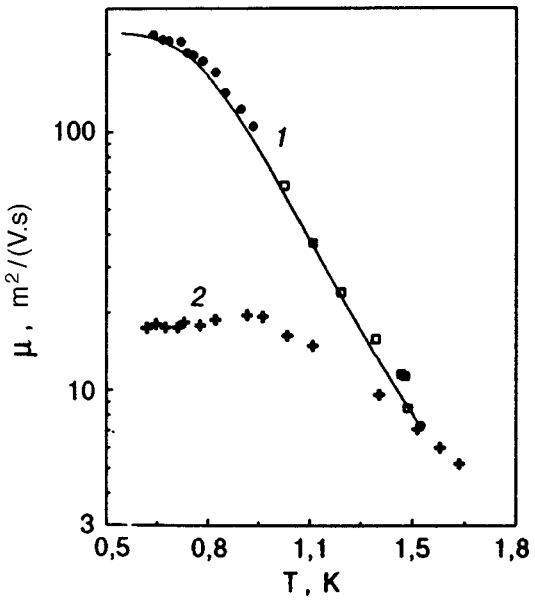

FIG. 2. Temperature dependence of the carrier mobility in linear electron channels over liquid helium: *1* — uncharged substrate, $a=5\times10^{-4}$ cm (squares), $a=7\times10^{-5}$ cm (circles). The solid curve describes the theoretical results;[7] dependence *2* corresponds to a charged substrate with $a=4\times10^{-5}$ cm.

increases sharply and hence a signal is detected from the electrons.

In this work, we calculated the real (G_r) and imaginary (G_i) parts of the conductance of the experimental cell containing a system of parallel conducting channels (in the same way as the calculations for a two-dimensional system made in Ref. 5). Calculations show that for the frequencies of the exciting signal used by us, the quantities G_r and G_i are defined by the real part ρ_r of the resistance of the conducting channels and by the frequency ω_p of plasma oscillations propagating along the channels. The obtained values of G_r and G_i can be used to determine the conductivity $\sigma=n_j e\mu$ of electrons in the conducting channel (μ is the mobility) as well as the frequency ω_p.

In order to determine the mobility of electrons in the one-dimensional system, we must know the linear density n_j of electrons in the channels. The method of computation of this quantity in the ''saturated'' case, when the electric field over the electron layer is compensated by the intrinsic field of the electron layer for a given value of $V_\perp$, was described in Ref. 5. For a small number of electrons in the ''unsaturated'' case, the value of n_j was determined at a relatively high temperature from the ratio of the channel resistances measured for different values of n_j. Another method of calculating the linear density of electrons in the channel involves the use of theoretical values of electron mobility in a one-dimensional system obtained by Sokolov *et al.*[7]. The value of n_j can be calculated from the known resistance of the channel. Both methods of calculating n_j led to nearly the same value. Estimates show that electron chains with a mean separation $a\approx(4-5)\times10^{-4}$ cm were obtained in the present work.

During charging of the liquid helium surface, the substrate (nylon thread) remained uncharged as a rule. However, in the case of a rapid variation of temperature of the cell, some electrons could pierce the liquid helium layer and charge the substrate due to uncontrollable variation of the film thickness. We could also carry out a limited charging of the substrate by heating the cell beyond the temperature of superfluid transition. The electron mobility is found to be different for charged and uncharged substrates.

Figure 2 shows typical temperature dependences of the electron mobility μ in one-dimensional channels on liquid helium surface. The experimental points on curve *1*, obtained for an uncharged substrate, are in good agreement with the theoretical results obtained by Sokolov *et al.*[7] in the absence of localization of carriers (solid curve). As in the case of a two-dimensional electron system over liquid helium, the electron mobility at $T>0.8$ K is determined by their interaction with helium atoms in the vapor, while the mobility at $T<0.8$ K is limited by the interaction with vibrations of the liquid helium surface, i.e., ripplons. The situation is quite different for a charged substrate (dependence *2*): the mobility at $T<1.2$ K is lower than for a ''clean'' (uncharged) substrate, and the nature of the temperature dependence changes. Among other things, it can be seen from the figure that a tendency towards a slight decrease in the value of μ is observed at $T<0.9$ K.

It can be assumed that the latter case is characterized by localization of charge carriers, which was observed earlier in Refs. 2–6 for quasi-one-dimensional electron systems. The electrons charging the substrate create a random potential in which charges move on the surface of liquid helium. This potential is responsible for electron localization in liquid channels. A very weak temperature dependence of mobility at $T<0.9$ K (dependence *2*) may point towards the quantum-mechanical nature of the motion of charge carriers. Apparently, tunneling of electrons between potential wells formed due to the presence of electrons localized on the substrate occurs in this temperature interval. It must be noted that even

a small random potential may lead to localization of charge carriers in a one-dimensional system. It should also be observed that localization of electrons in channels must lead to formation of cavities on the surface of liquid helium, which may complicate the nature of movement of these electrons.

We also determined the frequency ω_p of plasma oscillations in a system of parallel conducting channels, which was calculated as a fitting parameter from the values of G_r and G_i. It is interesting to note that the experimentally obtained value of ω_p in the absence of localization was found to be about an order of magnitude higher than the theoretical value. It was found that ω_p decreases with temperature. This result has not been explained so far. It is also worthwhile to note that in the case of localization, the value of ω_p for the dependence *2* increases in comparison with the case of an uncharged substrate, as was observed by us for quasi-one-dimensional electron systems.[5]

Thus, linear electron chains on the liquid helium surface are realized for the first time in this work, and the mobility of charge carriers in such a system is measured. As in two-dimensional systems, the mobility is determined by the interaction with gaseous helium atoms and with ripplons. A tendency towards localization is observed during charging of the substrate by electrons and the resulting variation of the potential in which the carriers move.

The above-mentioned chains can serve as a model for verifying and studying a number of properties of one-dimensional systems, e.g., transport properties, localization of charge carriers, and possible transitions to the ordered state.

The authors are obliged to V. N. Grigor'ev for his interest in this research and for fruitful discussions of the results.

*)E-mail: kovdrya@ilt.kharkov.ua

[1] Yu. Z. Kovdrya and Yu. P. Monarkha, Fiz. Nizk. Temp. **12**, 1011 (1986) [Sov. J. Low Temp. Phys. **12**, 571 (1986)].
[2] Yu. Z. Kovdrya and V. A. Nikolaenko, Fiz. Nizk. Temp. **18**, 1278 (1992) [Sov. J. Low Temp. Phys. **18**, 894 (1992)].
[3] O. I. Kirichek, Yu. P. Monarkha, Yu. Z. Kovdrya and V. N. Grigorev, Fiz. Nizk. Temp. **19**, 458 (1993) [Low Temp. Phys. **19**, 323 (1993)].
[4] H. Yayama and A. Tomokiyo, Czech. J. Phys. **46**, S1, 353 (1996).
[5] V. A. Nikolaenko, H. Yayama, Yu. Z. Kovdrya, and A. Tomokiyo, Fiz. Nizk. Temp. **23**, 642 (1997) [Low Temp. Phys. **23**, 482 (1997)].
[6] Yu. Z. Kovdrya, V. A. Nikolaenko, H. Yayama *et al.* J. Low Temp. Phys. **110**, 191 (1998).
[7] S. S. Sokolov, Guo-Giang Hai, and N. Studart, Phys. Rev. B **51**, 5977 (1995).

Translated by R. S. Wadhwa

Anomalously rapid transport of matter during dissolution of solid clusters of ^{3}He in separated ^{3}He–^{4}He mixtures

A. N. Gan'shin, V. A. Maidanov, N. F. Omelaenko, A. A. Penzev, E. Ya. Rudavskii, and A. S. Rybalko

B. Verkin Institute for Low Temperature Physics and Engineering, National Academy of Sciences of the Ukraine, 310164 Kharkov, Ukraine[*)]

(Submitted July 7, 1998)
Fiz. Nizk. Temp. **24**, 1117–1120 (November 1998)

The kinetics of growth and dissolution of a new phase during phase separation and homogenization of solid ^{3}He–^{4}He mixtures is studied experimentally. It is found that both these processes have different kinetics, while homogenization is ensured by an anomalously rapid transport of matter in the crystal. It is shown that the prevailing theories about diffusion processes in a quantum crystal cannot explain the obtained results. © *1998 American Institute of Physics.* [S1063-777X(98)01211-0]

The first-order phase transition leading to isotopic phase separation of solutions of quantum crystals of ^{3}He in ^{4}He was discovered by Edvards *et al.*[1] However, the kinetics of such a transition remains unclear so far. Peculiarities of phase transition kinetics in this system were studied in Refs. 2–12 using various experimental techniques. However, the results of measurements are not reproducible in most cases and depend on the past history of the sample.

A good reproducibility of the experimental data was attained quite recently,[11,12] and made it possible to connect the kinetics of phase transition with peculiar diffusion processes induced by delocalized impurity excitations. It should be noted that the inverse process of phase transition of separated solid solutions into a homogeneous state (homogenization) has practically not been studied so far.

In the present communication, we describe the results of a series of investigations started in Ref. 12. The main attention is paid to the process of homogenization and its comparison with the process of phase separation. The asymmetry of these processes was indicated earlier by us,[12] but the difference between them is manifested more clearly upon a rapid cooling and strong heating of the samples. Such conditions were created in our experiments.

The measuring cell and the experimental technique used by us were described earlier in Ref. 12. The sample was in the form of a cylinder of diameter 9 mm and height 1.5 mm, and the measuring cell did not contain any fine-pore sintered heat exchanger, which could distort the phase transition kinetics.

Phase separation was initiated by rapid cooling of the crystal from homogeneous state to phase separation region at a rate of 3 mK/min determined by the cooling capacity of the dilution refrigerator. The inverse transition to the homogeneous state is induced by a rapid heating (within 1–2 minutes), the bottleneck in this case being the Kapitza resistance between the crystal and the case of the cell. The time constant associated with the Kapitza resistance is estimated at 20–50 s.

In order to record the phase transition, we made precise measurements of the crystal pressure at constant volume in the course of the transition. The Stratis–Adams pressure gauge used for this purpose had a resolution of about 8 Pa. The obtained time dependence of the pressure reflects the kinetics of phase separation as well as homogenization of the solution.

We studied phase transition kinetics during several cooling-heating cycles for crystals with different densities corresponding to molar volumes 20.266 cm^3/mole (pressure in the homogeneous region was 35.99 bar) and 20.435 cm^3/mole (pressure in the homogeneous region was 33.445 bar).

Like any first-order phase transition, the isotopic phase separation for a homogeneous ^{3}He–^{4}He solid solution begins with the formation of stable critical nuclei of the new phase. This is followed by the second stage of the phase transition, viz., the growth of these nuclei and their transformation into bcc inclusions of the concentrated phase in the host hcp crystal. We studied only the second stage of the phase transition, which is ensured by a transport of impurity atoms from the surrounding solution to the new phase inclusions. The inverse process of transformation of a two-phase solution into the homogeneous state is associated with the dissolution of bcc phase inclusions, which also occurs as a result of transport processes.

In order to eliminate the effect of the first stage of phase transition associated with nucleation, the thermal cycling was carried out in the region of phase separation, so that the temperature at which cooling of the crystal was started was slightly lower than the equilibrium phase separation temperature. Thus, thermal cycling led to a partial homogenization of the separated phases in the solution. However, the growth and dissolution of the new phase inclusions during phase transition completely reflects the transport of matter in the crystal which is responsible for these processes.

Figure 1 shows a typical time dependence of the variation of the pressure in the sample with a molar volume

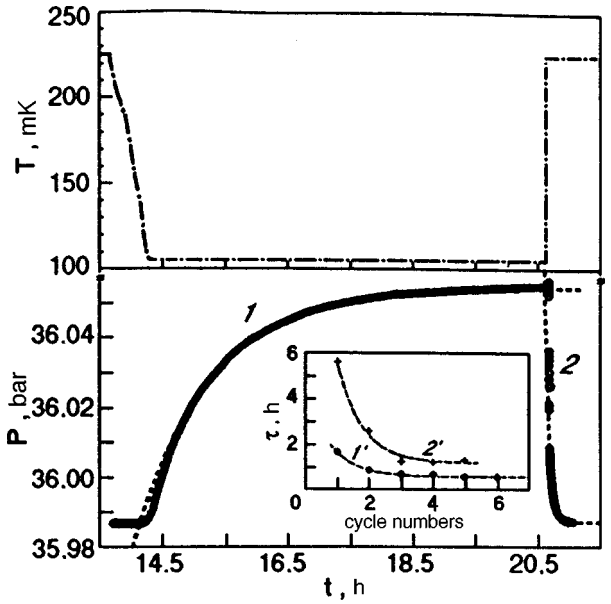

FIG. 1. Variation of temperature and the corresponding variation of crystal pressure during phase separation upon cooling from $T_i = 225$ mK to $T_f = 105$ mK (curve *1*), followed by homogenization during heating back to temperature T_i (molar volume 20.266 cm^3/mole) (curve *2*). The dashed line corresponds to the approximation described by formula *1*. The inset shows the dependence of the phase separation time on the number of cooling–heating cycle ($V = 20.266$ cm^3/mole, curve *2′*; $V = 20.435$ cm^3/mole, curve *1′*).

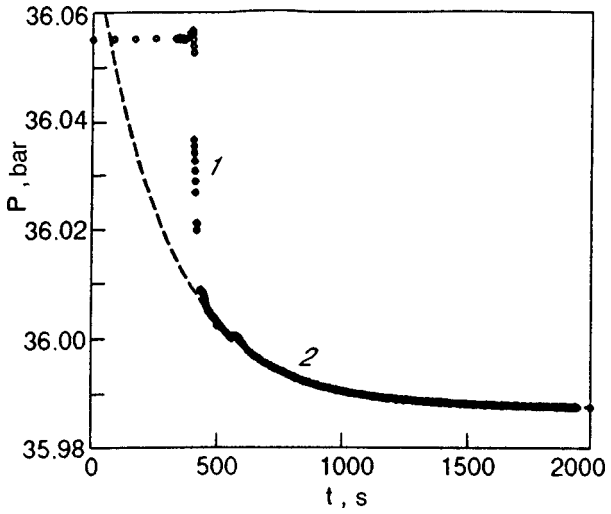

FIG. 2. Kinetics of phase transition of a separated two-phase solution into a homogeneous state (molar volume $V = 20.266$ cm^3/mole). Segments *1* and *2* corresponds to different homogenization regimes (see text). The dashed curve corresponds to the approximation described by formula *1* with a positive sign of the coefficient *A*.

20.266 cm^3/mole during both phase transitions, viz., phase separation and homogenization. An analysis shows that the increase in pressure during phase separation (curve *1*) can be described by the exponential law

$$P = P_0 - A \exp(-t/\tau), \tag{1}$$

where P_0 is the final equilibrium pressure, and A the difference in pressures after and before phase separation. The characteristic phase separation time was $\tau = 1.2$ h.

It was found that τ decreases during thermal cycling of the sample, as can be seen in the inset to Fig. 1 for two molar volumes. Starting from about the third cycle, the time constant of phase separation stops changing, which is apparently due to an improvement in the crystal quality after the first heatings and coolings. The kinetics of pressure variation shown in Fig. 1 corresponds to the fourth cooling-heating cycle.

It can be seen from Fig. 1 that the homogenization kinetics (curve *2*) differs sharply from the phase separation kinetics. The homogenization kinetics of a separated solution is shown in greater detail in Fig. 2. The obtained time variation of pressure cannot be approximated by a single exponential dependence. Two homogenization regimes can be singled out, viz., a rapid nonexponential decrease in pressure during the first 30 s after the onset of the phase transition (segment *1* in Fig. 2) followed by an exponential decrease of pressure with a characteristic time constant $\tau^* \sim 200$ s. The value of τ^* decreases during thermal cycling in the same way as during phase separation. Apparently, the rate of the first process is determined by the time of thermal relaxation of the sample associated with the Kapitza resistance. It can be assumed that, if the sample can be heated more rapidly by reducing the Kapitza resistance, the homogenization process would become still faster.

In order to find the possible reason behind such an anomalously rapid transport of matter during homogenization of a two-phase solution, let us evaluate the effective diffusion coefficient which can ensure such a fast transfer of ^{3}He atoms at the first segment of the curve in Fig. 2. Using the experimental data on separation kinetics obtained by us earlier during stepwise cooling,[12] it can be concluded that the variation of regimes shown in Fig. 2 corresponds to an equilibrium concentration of 1.6% ^{3}He. This means that 4.7×10^{20} of ^{3}He atoms were transported per cubic centimeter of the crystal during the first 30 seconds. For concentrated phase inclusions having a diameter 4.5 μm,[13] this corresponds to a density $\rho = 3.9 \times 10^{-8}$ cm^{-3}. In this case, the mean separation l between inclusions can be defined by the formula

$$l = \rho^{-1.3} = 13.7 \ \ \mu\text{m}. \tag{2}$$

Assuming that l is equal to the diffusion length, we obtain the effective diffusion coefficient

$$D_{\text{eff}} = l^2/\tau = 6.2 \times 10^{-8} \ \ \text{cm}^2/\text{s}, \tag{3}$$

which is several orders of magnitudes higher than the quantum diffusion coefficient measured in NMR experiments.[14,15] The value of the effective diffusion coefficient corresponding to the slower segment *2* in Fig. 2 is 10^{-8}–10^{-9} cm^2/s, which is also much higher than the available NMR data for samples of such density and concentration.

Note that the distribution of atoms was uniform and isotropic during NMR measurements in which the main experimental data on quantum diffusion of impurity excitations ^{3}He in ^{4}He were obtained. Hence the spin diffusion coefficient measured under such conditions can be identified with the self-diffusion coefficient for ^{3}He atoms.

An entirely different situation is realized during isotopic phase separation of solid solutions and their homogenization. Under these conditions, the movement of ^{3}He atoms occurs for quite high concentration gradients, which can significantly alter the nature of transport of matter in the crystal. Note that, in addition to the transport of ^{3}He atoms, the effect of transport of ^{4}He atoms from the surrounding matrix into the inclusions may also be quite significant. Since the diffusion length determined by the size of inclusions is quite small in this case while the molar volume of the inclusions is much larger than that of the matrix, this process may turn out to be quite effective.

On the other hand, we can estimate the lower limit of the time constant of the phase transition during ballistic motion of ^{3}He quasiparticles with a characteristic velocity[16]

$$v = a\Delta/h, \tag{4}$$

where a is the atomic spacing and Δ the bandwidth for ^{3}He impurity particles in solid ^{4}He and h Planck's constant. The velocity estimate obtained by using this formula is $v \sim 10^{-1}$ cm/s, which corresponds to the time constant $\tau^* \sim 10^{-2}$ s. The experimentally observed values of τ^* are higher than this lower limit.

The obtained results indicate that the transport of ^{3}He atoms cannot be diffusive, at least in the beginning of the homogenization process.

The possibility of hydrodynamic transport of ^{3}He quasiparticles under the conditions of our experiments cannot be ruled out.

The authors are grateful to V. N. Grigor'ev for fruitful discussions.

*)E-mail: rudavskii@ilt.kharkov.ua

[1] D. O. Edwards, A. S. McWilliams, and J. G. Daunt, Phys. Rev. Lett. **9**, 195 (1962).
[2] M. F. Panczyk, R. A. Scribner, J. R. Gorano, and E. D. Adams, Phys. Rev. Lett. **21**, 594 (1968).
[3] P. N. Henriksen, M. F. Panczyk, and E. D. Adams, Solid State Commun. **8**, 735 (1970).
[4] A. S. Greenberg, W. C. Thomlinson, and R. C. Richardson, J. Low Temp. Phys. **8**, 3 (1972).
[5] I. Iwasa and H. Suzuki, Proc. LT–17, North Holland Phys. Publ. **1**, 531 (1984).
[6] V. A. Mikheev, V. A. Maidanov, and N. P. Mikhin, Fiz. Nizk. Temp. **12**, 658 (1986) [Sov. J. Low Temp. Phys. **12**, 375 (1986)].
[7] V. A. Mikheev, V. A. Maidanov, N. P. Mikhin *et al.*, Fiz. Nizk. Temp. **14**, 563 (1988) [Sov. J. Low Temp. Phys. **14**, 309 (1988)].
[8] V. A. Mikheev, A. A. Golub' V. A. Goncharov *et al.*, Fiz. Nizk. Temp. **15**, 540 (1989) [Sov. J. Low Temp. Phys. **15**, 304 (1989)].
[9] R. Schrenk, O. Friz, Y. Fujii *et al.*, J. Low Temp. Phys. **84**, 133 (1991).
[10] S. C. J. Kingsley, I. Kosarev L. Roobol *et al.*, J. Low Temp. Phys. **110**, 359 (1998).
[11] V. A. Shvarts, N. P. Mikhin, E. Ya. Rudavskii *et al.*, Fiz. Nizk. Temp. **21**, 717 (1995) [Low Temp. Phys. **21**, 556 (1995)].
[12] A. N. Gan'shin, V. A. Maidanov, N. F. Omelaenko *et al.*, Fiz. Nizk. Temp. **24**, 815 (1998) [Low Temp. Phys. **24**, 611 (1998)].
[13] S. C. J. Kingsley, V. Maidanov, J. Saunders, and B. Cowan, J. Low Temp. Phys. **110**, (1998) [in press].
[14] A. R. Allen, M. G. Richards, and J. Schratten, J. Low Temp. Phys. **47**, 89 (1982).
[15] V. N. Grigor'ev, B. N. Esel'son, V. A. Mikheev *et al.*, Pis'ma Zh. Éksp. Teor. Fiz. **17**, 25 (1973) [JETP Lett. **17**, 16 (1973)] (see also V. N. Grigorev, Fiz. Nizk. Temp. **23**, 5 (1997) [Low Temp. Phys. **23**, 1 (1997)].
[16] A. F. Andreev and I. M. Lifshitz, Zh. Éksp. Teor. Fiz. **56**, 2057 (1969) [JETP **29**, 1107 (1969)].

Translated by R. S. Wadhwa

CHRONICLES

In memory of Sergei Vasil'evich Vonsovskii (1910–1998)

Fiz. Nizk. Temp. **24**, 1121 (November 1998) [S1063-777X(98)01311-5]

Sergei Vasil'evich Vonsovskii, Member of the Russian Academy of Sciences, founder and director of the Ural Research Center of the Russian Academy of Sciences for many years, an outstanding physicist and leading organizer of the research activity in Russia, expired on August 11, 1998.

The research activity of S. V. Vonsovskii and his school resulted in fundamental contribution to the foundation and development of a whole range of vital trends in modern theories of magnetism of solids and magnetic phase transitions. Many generations of physicists learned the subject of magnetism from his monographs. It is hard to overestimate the role played in the development of solid-state physics research by the Kourov scientific seminars organized and conducted regularly for several decades by Academician Vonsovskii. These meetings were always distinguished by persistent originality of topics, an excellent choice of qualified speakers, and high level of organization.

Sergei Vasil'evich was adored by everybody who had the pleasure of knowing him. His name will always remain in the history of science, and his colleagues and pupils will always cherish fond memories of him in their hearts.

Editorial Board

